UNIVERSITY OF TURIN

PhD Program in
Complex Systems for Life Sciences

XXXV Cycle
Academic Years: 2019-2022

Semaphorin 3A reprograms the tumor microenvironment "ecosystem" in pancreatic cancer

Tutor:
Prof. Enrico Giraudo

Candidate:
Carina Florina Cojocaru

ABSTRACT

Pancreatic Ductal Adenocarcinoma (PDAC) is considered a major public health concern globally due to its delayed diagnoses and to the almost absent repertoire of effective drugs for its treatment. Targeted or immune therapies, even though widely employed as an alternative and promising strategy to hamper the growth of many solid cancers, still represent a challenge for PDAC treatment. PDAC cancer cells represent less than the 20% of total tumor volume, while the remaining 80% is constituted by the desmoplastic stroma. Desmoplasia is a condition in which the tumor stroma is dense and stiff, cluttered with extracellular matrix and overactivated cancer-associated fibroblasts (CAFs). The interstitial pressure is elevated, and it causes the collapse and disruption of the vessel network. Furthermore, vessel abnormality is tightly coupled with immunosuppression.

We aimed to investigate the changes in the tumor microenvironment in an orthotopic PDAC model upon treatment with a member of the Semaphorin protein family, Semaphorin3A. Semaphorins and their cognate receptors Plexins are involved in the axonal navigation, immune regulation, organogenesis and angiogenesis. Lately, Semaphorins have been shown to play important roles in tumor progression and metastasis formation. Some Semaphorins have been reported to promote tumor growth and angiogenesis, while others have inhibiting roles on cancer dissemination and immune recruitment and activation. In particular, our laboratory demonstrated that a mutated form of Semaphorin3A (mut-Sema3A) was able to efficiently hamper tumor growth and metastatic dissemination in a mouse model of PDAC by promoting vessel normalization and reducing tumor hypoxia. In this study we performed single cell RNA-sequencing coupled with Visual transcriptomics to identify molecular changes induced by mut-Sema3A in the TME of PDAC. This analysis highlighted changes in different sub-populations of TME not previously identified, such as macrophages, neutrophils, lymphocytes and CAFs. Interestingly, we observed that mut-Sema3A treatment significantly reprogrammed CAFs toward a restraining anti-tumor phenotype. We therefore established a novel gene signature defining this unconventional class, called Sema-Associated Fibroblasts (SemAFs), that included up-regulated genes such as PDGFRA, ISLR, MMP2, CYGB, THBS2, CDH11. Many of them, such as Islr, coding for Meflin, have been correlated with improved survival and prognosis of PDAC patients. Notably, mut-Sema3A treatment of *ex-vivo* purified activated fibroblasts, enhanced the expression of several genes typically expressed in SemAFs and induced a strong inhibition of chemo-invasion of these cells. Among the genes that were up-regulated in fibroblasts, mut-Sema3A enhanced PlxnA4 expression, suggesting a feedforward mechanism of the ligand enhancing its own receptor. Remarkably, the SemAF gene signature, and in particular Isrl and PlxnA4, have been also identified by In Situ Hybridization and Visium Spatial Transcriptomics, in mut-Sema3A-treated tumor tissues.

Furtherly investigating the effect of mut-Sema3A on tumor vessels and immune cells, we first observed that it up-regulated the adhesion molecule VCAM-1 on normalized vasculature, shown to be involved in the recruitment of lymphocytes in tumor tissues. In line with these findings and with the scRNA-seq analysis, we observed a dramatic increase of $CD8^+$ T-cell in PDAC tumors treated with mut-Sema3A.

Based on these effects on T-lymphocytes, we performed several combinatorial treatments of mut-Sema3A with immunomodulatory agents, such as α-PD1, α-CTLA4 and α-CD40, unveiling that the most efficient combination in hampering PDAC growth was the "triple" combination of mut-Sema3A with α-CTLA4 and α-CD40. Starting to investigate the changes in the immune landscape of PDAC

in this particular triple combination treatment, we observed that along with the significant increase of $CD8^+$ T cells, mut-Sema3A enhanced the polarization of M1 anti-tumor macrophages.
Taken together these data suggest that mut-Sema3A is a novel agent able to re-program different cell populations of the PDAC ecosystem in a complementary manner, and that it may represent a good therapeutic candidate to be coupled with immunotherapies to more efficiently block PDAC progression.

TABLE OF CONTENTS

INTRODUCTION

1. Pancreatic Ductal Adenocarcinoma

1.1. Epidemiology

Despite the big accomplishments of the last years in the cancer therapeutic field, cancer still remains the second leading cause of death in the United States (1). Pancreatic cancer is the fourth leading cause of death in the US and it can be considered a major public health concern globally, since it ranks within the top 10 leading types of cancer death in over 130 countries. Both the incidence (by about 1% per year) and death rate (by 0.2% per year) have increased since 2000, and pancreatic cancer mortality is predicted to continue rising over the next few decades, with over 800.000 deaths expected by 2040 (2,3).

Based on its histogenesis, pancreatic cancer can arise from the epithelial or nonepithelial compartment: Pancreatic Ductal Adenocarcinoma (PDAC) constitutes the epithelial neoplasm which arises from the exocrine portion of the pancreas and represents the most common pancreatic malignancy accounting for more than the 90% of all pancreatic cancers (1,4,5). It is a highly lethal cancer with a 5-year survival rate of only 6% (6). Surgical resection remains the eligible remedy, however, only 20% of patients have resectable tumors when diagnosed. Furthermore, patients that undergo surgery, relapse in rapid recurrence, resulting in a 5-year relative survival of 39% (7).

The major challenges regarding this disease are represented by its delayed diagnoses, due to the lack of symptoms, and to the poor if not absent repertoire of effective drugs for its treatment. Chemotherapy remains the most used therapeutic approach, though its benefits are modest since most of the patients harbor or develop drug resistance (8,9). Nowadays there is a standard of care for PDAC that depends on the tumor staging: the most widely prescribed medication includes Gemcitabine alone or in combination with Nab-Paclitaxel and the multi-drug regimen FOLFIRINOX, although they show variable levels of toxicity (10,11).

Most of the solid cancers have effectively been attacked through the use of novel treatment regimens such as targeted or immune therapies in the last years (12,13) but PDAC treatment has not improved, and this pathology does not represent a good target for innovative agents due to its genetic and cellular variability and complexity (14). PDAC is characterized by considerable genetic heterogeneity not only among patients but also within a single primary tumor. It presents a variety of mutations that lead to cancer, and each mutation is present in a small percentage of patients (15). The persistence of multiple signaling pathway alterations could partially explain the presence of multiple resistance mechanisms. Although the underlying biology of PDAC has not been fully elucidated, key mutations of specific genes such as Kras, CDKN2A/p16, TP53 and SMAD4 and the concomitant activation of downstream signaling pathways appear to play an essential role in the resistance to treatments (16). In addition, a very strong barrier to PDAC treatment is represent by the desmoplastic reaction. PDAC is a peculiar tumor in which the cancer cells represent less than the 20% of total tumor volume, while the remaining 80% is constituted by the desmoplastic stroma (17,18). The dense stroma consists of several cellular components (i.e. fibroblasts, endothelial cells, immune cells) and acellular components (i.e. fibrin, collagen, hyaluronic acid, fibronectin), and all of these constituents are orchestrated by cytokines and growth factors that promote cancer progression thanks to favorable pH and hypoxic conditions (19–21).

1.2. PDAC Tumor Microenvironment (TME)

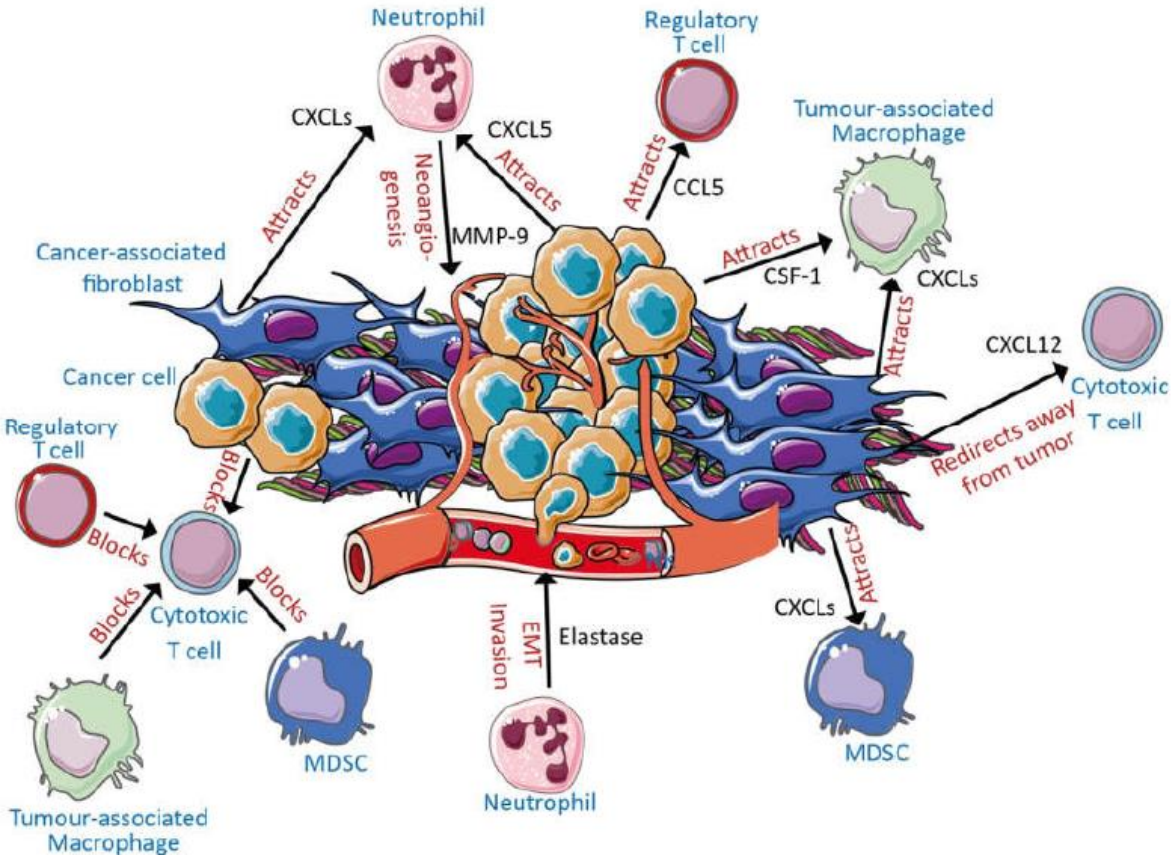

Figure 1. *The PDAC tumor microenvironment is orchestrated by a high grade of desmoplasia. Overactivated CAFs produce massive amounts of ECM leading to deregulation of the other stomal cells. ECM deposition causes impaired immune cell tumor infiltration and inefficient drug delivery, furthermore an immuno-suppressive niche is established by tumoral cells, CAFs and immune cells that are able of secreting cytokines, chemokines and growth factors. The vessel network is affected since it is compressed, twisted and at the same time stimulated by pro-angiogenic factors, indeed it results in poor pericyte coverage and subsequent vessel leakage. The immune compartment that populates the TME is constituted by GN, TAMs, MDSC and Tregs, all characterized by a tumor-permissive and immune suppressive phenotype* (22).

The Tumor Microenvironment (TME) of PDAC (**Fig. 1**) is the niche created by the tumoral cells themselves in which they orchestrate and take control of normal cellular components located nearby and that can be eventually recruited through chemical stimuli. The PDAC TME is composed of several cell types, but its most abundant constituent is an acellular element: the Extracellular Matrix (ECM). The ECM is a physiological component contained in every type of tissue that provides physical scaffolding and biochemical and biomechanical cues to the surrounding cellular elements. It consists of water, proteins, glycoproteins and proteoglycans, and its composition may be regulated based on the needs of the adjacent microenvironment. There are mostly two types of ECM: an interstitial matrix in which the ECM is a three-dimensional lattice providing support to the enclosed stromal cells or a basement membrane in which the ECM is a layer that separates epithelial and stromal cells (23–25).

Since the ECM represents a great proportion of the stroma, it naturally interacts with stromal cells and engages a huge number of links, bindings, and a dense crosstalk with the surrounding ecosystem. It considerably impacts malignant cell transformation and metastasis, and, on the other way around, it is affected by tumor progression and consequently influences stromal-cell behaviors, such as angiogenesis and inflammation, and can enhance formation of a tumorigenic microenvironment (26–28). Over 90% of the ECM mass is produced by stromal cells, and among the secreted proteins there are several types of collagens, laminin, elastin, fibronectin, glycoproteins such as Tenascin C and Thrombospondin and proteoglycans such as Lumican, Byglican and Decorin (27).

In the early phases of PDAC progression, pro-inflammatory cytokines secreted by neoplastic cells stimulate quiescent pancreatic stellate cells (PSCs) to produce extracellular matrix (ECM) and to increase fibrotic stromal deposition (29,30). The solid stress generated by the dense stroma produces lymphatic obstruction and subsequently causes intratumoral interstitial fluid pressure increase, which leads to vascular compression, tissue perfusion reduction, and a hypoxic microenvironment establishment (31,32). In fact, approximately 80% of the intratumoral blood vessels are abnormal and dysfunctional, poorly fenestrated and lacking proper pericyte coverage, which hinder the effective delivery and accumulation of chemotherapeutic agents (33,34). Furthermore, the fibrotic microenvironment of PDAC results in an inhibitory effect on both the innate and adaptive immune system, reducing cytotoxic T cells and increasing M2 immuno-suppressive macrophages, N2 immuno-suppressive neutrophils, and T-regulatory cells at tumor sites. Growth factors and cytokines secreted by PSCs also promote the formation of a tumor immunosuppressive microenvironment (35,36).

The tumor stroma has often been portrayed as a contributor to the development of the disease and tumor progression. However, several recent preclinical and clinical studies have shown that stroma-depletion can lead to a more aggressive disease (27,37–40). In patients and PDAC mouse models, it has been found that increased stroma correlates with improved survival and that stroma content at solid organ metastases is decreased (41,42). Furthermore, acting on the Hedgehog signaling, strongly involved in stroma modulation and ECM deposition, has led to worse tumor progression dynamics (38,40), and the reduction of ECM through lysyl oxidase (LOX) inhibition in mouse models led to accelerated tumor growth (23).

The tumor suppressive properties of the PDAC stroma have been revealed gradually, and several studies, using genetic or pharmacological approaches to eliminate the PDAC stroma in preclinical models, showed that stromal depletion promoted tumor cell proliferation, invasion, and metastasis and reduced survival (38,40). PDAC tumor cells in the primary lesion showed loss of differentiation, epithelial-to-mesenchymal transition (EMT), and enhanced cancer stem cell-like phenotypes after stromal ablative treatment. In addition, severe weight loss, acidosis, and cachexia were observed in PDAC mouse models (37,43).

These findings suggest that stroma depletion might activate dormant neoplastic cells and induce their metastatic potential, thereby promoting PDAC progression (17).

1.2.1. Cancer Associated Fibroblasts

Among the various PDAC stromal cell types, the Cancer-Associated Fibroblasts (CAFs) are the most abundant. The CAF population is highly heterogeneous and presents a multitude of functions, presumably due to the variegated origins of these cells (44). Indeed, they can originate from tissue-

resident fibroblasts that are activated under the control of growth factors such as TGF-β or following genetic mutations such as TP53 or PTEN (45).
Another cellular origin of CAFs, and probably the most frequent one, is constituted by the Pancreatic Stellate Cells (PSCs) that are CAFs progenitors (46). PSC activation occurs following pancreatic injury, or upon PDGF or TGF-β stimulation, and leads to morphological changes from a star-like cellular shape into spindle-like cells, loss of retinoic acid storage capability and increased nuclear volume (29,47,48) (**Fig. 2 A**).
CAFs may also derive from the recruitment and differentiation of bone marrow-derived mesenchymal stem cells or from the trans-differentiation of non-fibroblastic lineages such as adipocytes, pericytes, monocytes, epithelial or endothelial cells (40,49–51) (**Fig. 2 B, C, D, E, F**).

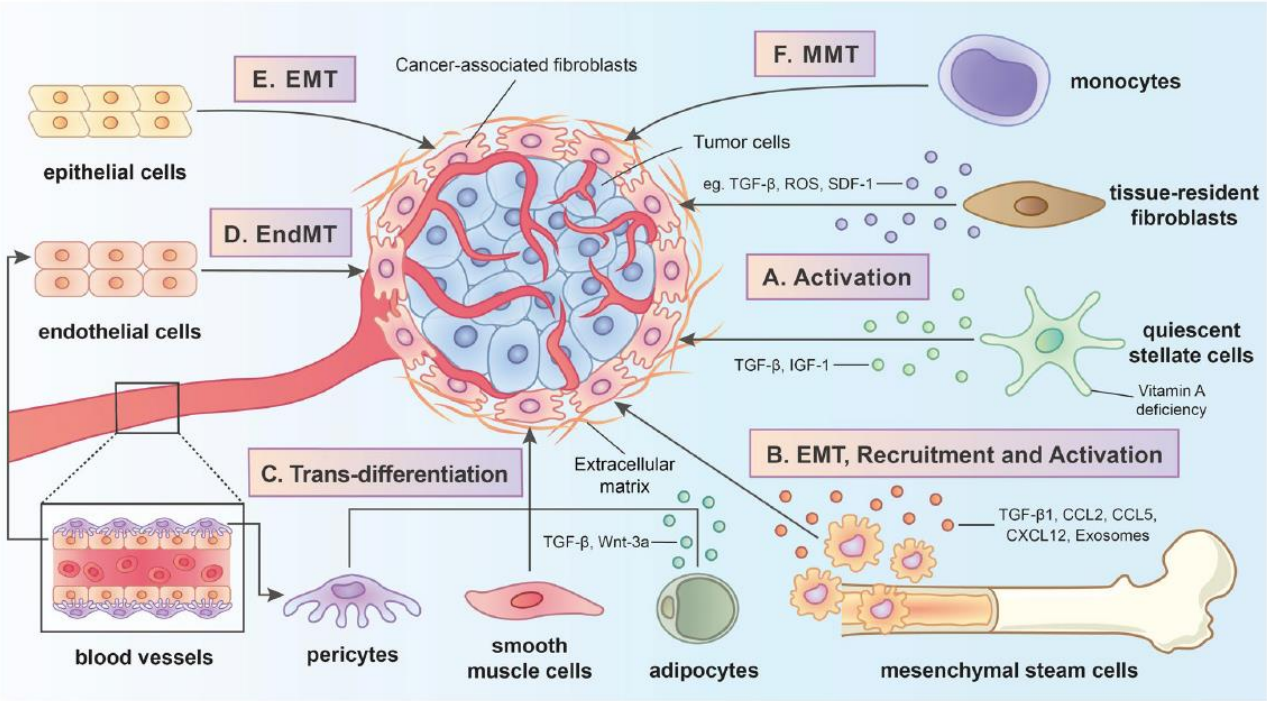

Figure 2. *The origins and differentiation pathways of cancer-associated fibroblasts (CAFs) in the tumor microenvironment (TME).* ***A)*** *CAFs can derive from activation of quiescent stellate cells (qSCs) or tissue resident fibroblasts through stimulation with transforming growth factor-beta (TGF-β), insulin-like growth factor-1 (IGF-1), stromal derived factor-1 (SDF-1), hepatocyte growth factor (HGF), reactive oxygen species (ROS) or vitamin A deficiency.* ***B)*** *CAF can be recruited through tumor derived cues and undergo trans-differentiation from mesenchymal stem cells thanks to the action of TGF-β, C–C chemokine ligand 2 (CCL2), C–C chemokine ligand 5 (CCL5), C-X-C chemokine ligand 12 (CXCL12) and tumor-derived exosomes.* ***C)*** *CAF can arise through trans-differentiation from pericytes, smooth muscle cells or adipocytes, or can undergo Mesenchymal Transition starting from* ***D)*** *endothelial,* ***E)*** *epithelial cells or* ***F)*** *monocytes* (52).

The healthy pancreas contains two populations of fibrogenic progenitors: they are both periacinar cells but, unlike pancreatic stellate cells (PSCs), resident fibroblasts (FBs) do not have the ability of storing lipid droplets. Moreover, FBs are characterized by the presence of markers such as S100A4, cytoglobin and vinculin while they lack adipophilin, which is instead a marker of PSCs together with cytoglobin and vinculin (53).
PSCs derive from bone marrow mesenchymal stem cells and play a critical function in providing a homeostatic response to tissue injuries caused by pancreatitis or partial pancreatectomy (54,55).

In the normal human pancreas, they comprise approximately 4% to 7% of the parenchymal cells and are found in an inactive state, in which they lack proliferative or secretory activity. During pancreatitis and PDAC, they enter an active state, resulting in loss of vitamin A droplets and gaining the ability to express the cytoskeletal protein α-smooth muscle actin (α-SMA), acquiring a myofibroblast-like phenotype and the potential of producing, depositing, and remodeling components of the ECM (56–60). The main cue that shapes the activation of quiescent PSCs is the TGF-β signaling, that plays a key role through both autocrine and paracrine signaling mechanisms, since it derives primarily from pancreatic cancer cells (61). Moreover, PSCs contribute to tumor immunosuppression secreting proinflammatory cytokines such as IL-6, thus promoting the expansion and function of myeloid-derived suppressor cells (MDSCs) (62). PSCs were also found to sequester $CD8^+$ T-cells through the expression of the chemoattractant CXCL12 and preventing them from entering the tumor (63). Interestingly, PDAC patients have higher expression of the receptor for CXCL12 and CXCR4 on the tumor infiltrating T-cells compared to healthy volunteers (64). Indeed, blocking the CXCL12/CXCR4 axis reduced tumor burden in preclinical models when used in combination with anti-PD-L1 (65). However, clinical trials combining a CXCR4 antagonist with pembrolizumab (anti-PD-L1) failed to reduce patients' tumor burden during treatment (66,67).

Several markers can be used to identify the activated components deriving from PSCs, that are generally addressed to as Cancer Associated Fibroblasts (CAFs). PDGF-receptor α and β (PDGFRα/β), α-SMA, FAP, and S100A4 (FSP1) are considered pan-markers to distinguish CAFs, but none of them is exclusively expressed by PDAC fibroblasts, further highlighting CAF heterogeneity (50,68). Among the CAFs typical features, their principal ability is to deposit an enormous amount of dense stroma, that can function as a physical barrier towards the infiltration of immune cells and to the delivery of therapeutic agents, but also serves as a structural scaffold for cell interactions. CAFs also secrete Matrix Metallo Proteinases (MMPs), which ensure ECM degradation and the subsequent release of various factors leading to the recruitment of specific cells and/or cell dissemination. Additionally, CAFs also produce many growth factors and proinflammatory cytokines such as TGF-β, vascular endothelial growth factor (VEGF), interleukin-6 (IL-6) and CXC-chemokine ligand 12 (CXCL12), thereby promoting tumor growth, angiogenesis and recruitment of immunosuppressive cells into the TME to assist in immune evasion (49,69).

During the last years, genome-wide studies have demonstrated that depending on the distance of PSCs from the source of TGF-β, and on the surrounding cells, they can assume slightly different phenotypes and three subtypes of CAFs have been revealed up to now in PDAC: "inflammatory," "myofibroblastic" and "antigen-presenting" CAFs (51,70,71) (**Fig. 3**). The myofibroblastic CAFs (myCAFs) depend tightly on TGF-β signaling, they are characterized by high α-SMA expression and are considered profoundly involved in the ECM deposition and remodeling. They are located near to the tumor cells and faithfully recapitulate the model of activated PSCs (70,72). The cancer-promoting function might belong to the inflammatory CAFs (iCAFs) that are located further away from tumor cells. iCAFs are characterized by the expression of CXCL12 and IL-6, and they act on immune modulation via NF-kB signaling. The reprograming of CAFs into the $CXCL12^+$ $IL\text{-}6^+$ phenotype is induced by IL-1α via the activation of JAK-STAT3 signaling (73). Notably, CAF subtypes show a dynamic cellular identity and are able to interconvert at least in the *ex vivo* model. Changing culture conditions from an organoid-conditioned medium into monolayer culture shifts iCAFs into the myCAF phenotype (59,70). The most recently identified CAF subtype represents the antigen-presenting CAFs (apCAFs) which have a high expression of MHC-II molecules and

CD25 but low level of costimulatory genes such as CD40, CD80, CD86 (71). While the MHC-II is essential to interact with $CD4^+$ T cells, the lack of costimulatory molecules needed for $CD4^+$ T cell clonal expansion may inhibit T cell-mediated anti-tumor immunity (59,74).

Undeniably, CAFs exert a strong cancer-promoting action throughout the TME, which they implement through ECM deposition and release of growth factors and signaling molecules. Some subpopulations seem to be more cancer-permissive than others, indeed inhibition of Il-6, secreted by iCAFs, leads to a significant improvement in the efficacy of anti-PD-L1 checkpoint inhibitor in PDAC. Furthermore, in a mouse model of PDAC treated with a JAK inhibitor, iCAFs were reprogrammed to express myCAF features, therefore increasing the ECM deposition and restraining tumor growth (73). However, the targeting of other CAF subpopulations, induced a tumor-progressing output: the genetic deletion of Hedgehog resulted in the reduction of stroma deposition and myofibroblastic CAFs, inducing more aggressive and de-differentiated tumor phenotypes (40). Similarly, genetic ablation of myofibroblastic CAFs directly targeting α-SMA^+ CAFs, through chimeric antigen receptor T-cell (CAR-T) therapy, or small inhibitors targeting FAP^+ cells, induced more aggressive PDAC tumor phenotypes, manifested by Epithelial to Mesenchymal Transition (EMT), cancer stemness, chemotherapy resistance, and tumor immune evasion (38,75).

This observation may be explained by the fact that stromal cells naturally restrain tumor growth but are recruited and re-programmed during neoplastic processes to support tumor cells. These findings suggest that CAF and ECM targeted therapies must be finely tuned since inflammatory CAFs might be a potential therapeutic target, while myofibroblastic CAFs may support tumor suppression in PDAC (17,59).

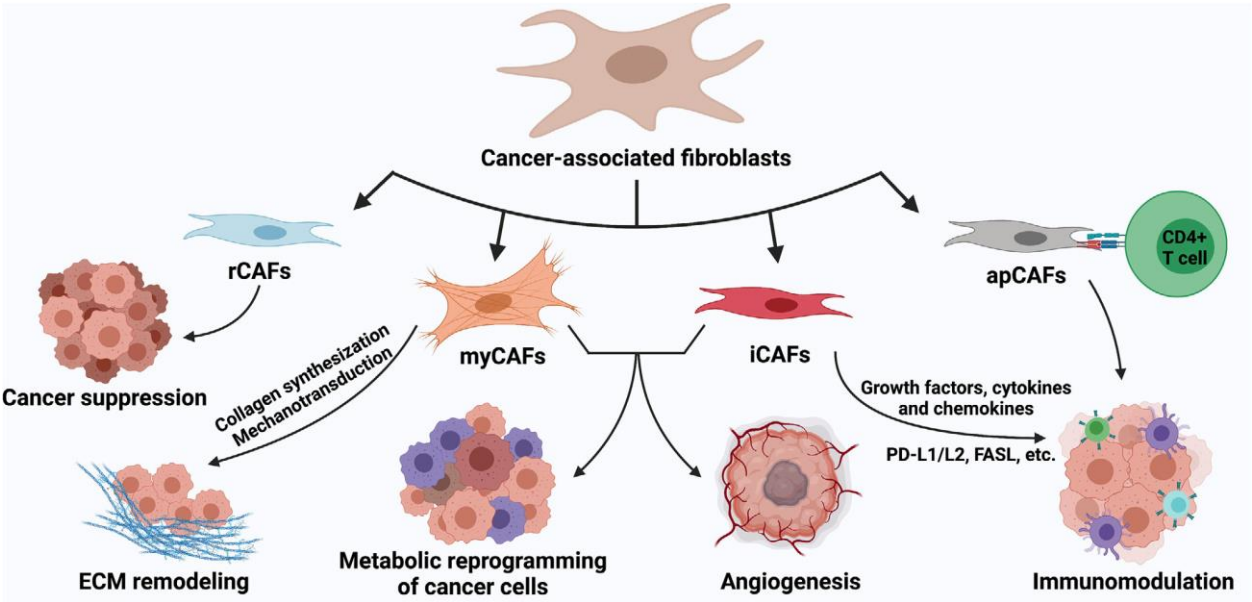

Figure 3. *CAF subpopulations in PDAC. Among the several CAF subpopulations identified in PDAC myCAFs better represent the activated form of PSCs, displaying contractile features and a remarkable ECM production, deposition and remodeling capability. iCAFs are the counterpart that more deeply shape the inflammatory environment promoting immune evasion and enhancing immune suppression. apCAFs exhibit antigen presenting features but lack co-stimulatory molecules therefore they do not exert an effective immune activation. Finally, cancer restraining CAFs are still poorly characterized but their prevalence throughout the PDAC tissue has been correlated with good patient prognosis* (76).

1.2.2. Immune cells

Like all types of cancer, the formation of PDAC is allowed to progress in time thanks to the tolerance of the immune system that gradually switches from a step of elimination of the neoplastic cells, to an equilibrium state and finally to an immune-evasion condition, in which cancer cells are not kept under control but are free to proliferate and orchestrate stromal cells and increase immune-suppression. In fact, during tumor progression, malignant cells evolve mechanisms to avoid immune recognition, indeed the absence of anti-tumor immunity in PDAC is partly caused by the lack of antigen-presentation to the immune system (77).

The immune infiltrate in PDAC comprises both the innate and the adaptive immune compartment. The innate immune cells of the myeloid lineage, including granulocytes, monocytes, macrophages, and dendritic cells, play an important role in cancer cell recognition, initiation of inflammation, and antitumor responses (78) (**Fig. 4**). Tumor cells, however, often develop mechanisms to evade immune surveillance, and persistent inflammation has been shown to be a driver of tumor progression in many malignancies, including pancreatic cancer (79). Myeloid cells thus play a dual role in cancer, on one hand initiating antitumor responses, but also promoting local inflammation leading to chronic cancer-associated inflammation (80,81).

On the other side, PDAC may have variable degrees of adaptive immune cell infiltration, comprising distinct T-cell subpopulations and B lymphocytes (82–84). The accumulation of $CD8^+$ cytotoxic T lymphocytes (CTLs) in proximity of cancer cells correlates with increased patient survival, while high levels of infiltrated regulatory T cells (Tregs) produce the opposite outcome. The differential effects of T cells in PDAC are dependent on the spatial distribution, type of subpopulation involved, and relative macrophage infiltration (85,86).

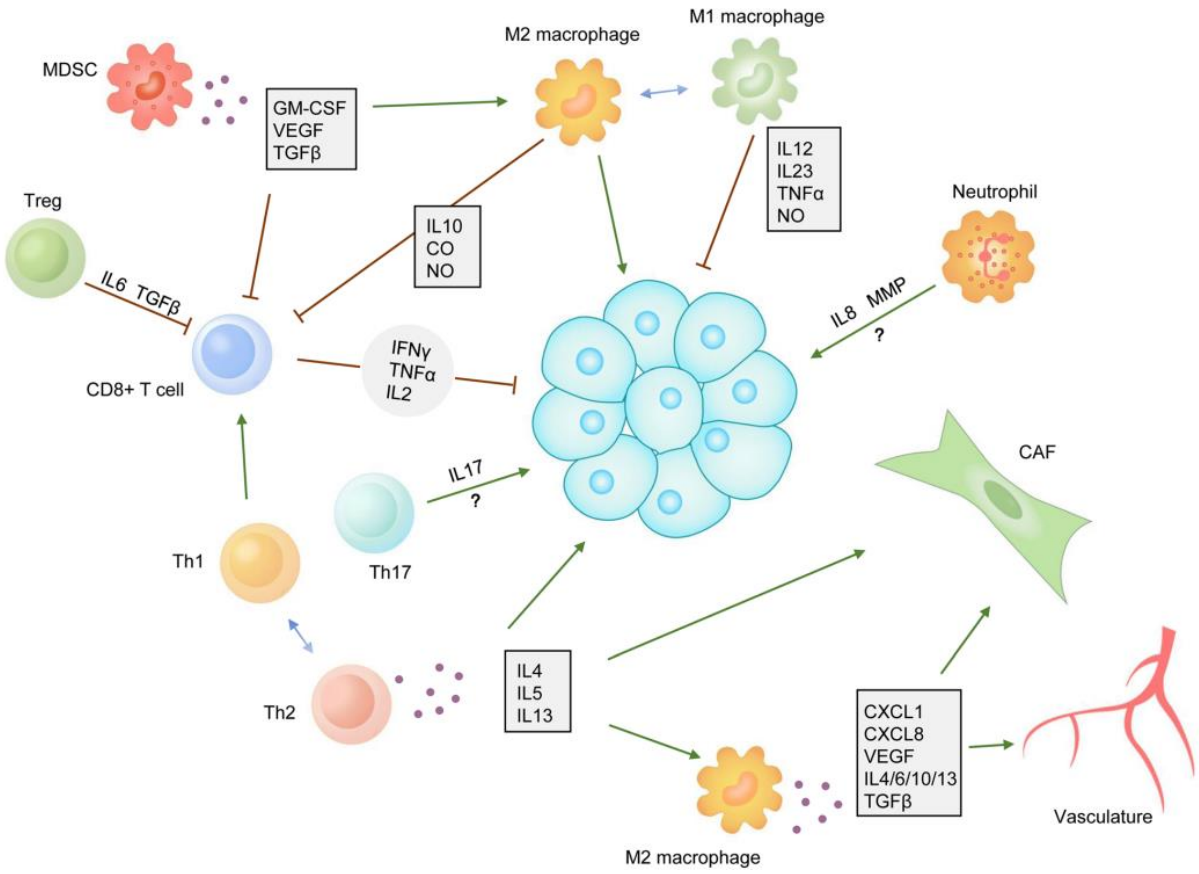

Figure 4. *Immune infiltration affects PDAC progression. PDAC cancer cells markedly interact with several immune cell subpopulations, mainly shaping them towards an anti-tumoral behavior. Among the scarce anti-tumoral immune cells CD8$^+$ T lymphocytes fight cancer cells through the secretion of interferon-γ (IFN-γ), tumor necrosis factor-α (TNF-α), perforin and granzymes. CD4$^+$ T lymphocytes, instead, can polarize towards the Th1 or Th2 subtype, therefore supporting anti-tumor immunity or driving cancer cell growth, fibroblast activation and macrophage transition towards the pro-tumoral phenotype. Regulatory T cells (Tregs) are able of mitigating the cytotoxic function of CD8$^+$ T lymphocytes via interleukin-6 (IL-6) and tumor growth factor-β (TGF-β). Myeloid derived suppressor cells (MDSC) and M2 polarized macrophages have pro-tumoral functions and suppress anti-tumor immunity, while M1 anti-tumoral macrophages exert pro-inflammatory actions releasing TNF-α, interleukin-12 (IL-12), interleukin-23 (IL-23) and nitric oxide (NO). The role of Th17 T cells and neutrophils are still under debate but they are thought to have pro-tumoral effects acting through interleukin-17 (IL-17), interleukin-8 (IL-8) and matrix metalloproteinases (MMPs)* (87).

1.2.2.1. Myeloid-Derived Suppressor Cells

Myeloid-Derived Suppressor Cells (MDSCs) are a mixture of immature myeloid cells that are recruited from the bone marrow during inflammatory and tumorigenic processes. MDSCs comprise two types of cells: polymorphonuclear granulocytic MDSCs (PMN-MDSC, neutrophil-like) and mononuclear monocytic MDSCs (M-MDSC, monocyte-like). Although their identification remains difficult because of the lack of defining surface markers, they can be pointed out through flow cytometry since murine PMN-MDSC express high levels of Ly6G and a medium level of Ly6C, while M-MDSC show high levels of Ly6C and are Ly6G$^-$.

Tumor cells producing granulocyte-macrophage colony-stimulating factor (GM-CSF) attract immature myeloid cells from the bone marrow, and drive differentiation towards MDSCs. Indeed, MDSCs can be detected in very early lesions and, during tumor development, they strongly increase in number both in the circulation and in the TME. Their circulating levels have been correlated to a more advanced stage in human PDAC patients (88), in fact, together with tumor-associated macrophages (TAMs), and regulatory T cells (Tregs), MDSCs contribute to establishing an immunosuppressive TME (89).

In genetically engineered mouse models (GEMM) and orthotopic mouse models of PDAC, the preponderant immune cell type are myeloid cells, that are comprised of MDSCs and TAMs, accounting for 5–10% and 15–20% of total tumor mass, respectively (59,90,91). Typically PMN-MDSCs represent more than 80% of all tumor-associated MDSCs (92).

The main outcome of MDSCs action is to suppress both CD4$^+$ and CD8$^+$ T cells, mitigating the CD8$^+$ T-cell immune surveillance, and allowing the expansion of immunosuppressive regulatory T cells (Tregs) (93). MDSCs affect CD4$^+$ and CD8$^+$ T tumor infiltration through direct cell-cell contact with lymphocytes, which leads to the upregulation of programmed death-ligand 1 (PD-L1) on MDSCs membrane. The PD-L1/PD-1 interaction, in turn, leads to the suppression of T-cell activation and promotes self-tolerance establishment (94). In addition, MDSCs have also been shown to stimulate the expansion of Tregs through the IL-10-dependent secretion of TGF-β and IFN-γ again, resulting in suppression of the T cell function (95,96). Besides their role in blunting the anti-tumor response of the adaptive immune system, MDSCs also have the ability to attenuate innate anti-tumor immunity through a variety of mechanisms: they have been shown to inhibit natural killer cell (NK cell) cytotoxicity and to promote the conversion of macrophages towards an M2 phenotype (86,97–99).

Targeted depletion of MDSCs in GEMMs has been demonstrated to activate an effective endogenous antitumor T cell response in established tumors and to significantly impair KrasG12D-

driven pancreatic cancer initiation when induced at early stages (100,101). Thus, the inhibition of MDSCs is a potential therapeutic target in PDAC (60,100).

1.2.2.2. Tumor-Associated Macrophages

The majority of macrophages in healthy and inflamed tissues differentiate from bone marrow-derived monocytes in the peripheral blood circulation (102). Thanks to the action of chemokines, cytokines, and other secreted factors (e.g., GM-CSF, CSF-1, IL-3, CXCL12, and CCL2), as well as other environmental clues, such as local hypoxia and high levels of lactic acid, circulating monocytic cells are recruited to the tumor microenvironment and become tumor-associated macrophages (TAMs) (103,104).

TAMs display different functional states, termed polarization states, during tumor initiation, progression, and therapeutic intervention. They are commonly broadly divided into classically activated M1 and alternatively activated M2 macrophages to characterize the opposite extremes of a dynamic spectrum of polarization states. Generally, M1 macrophages have been described to secrete pro-inflammatory cytokines with predominantly anti-neoplastic effects, while M2 macrophages produce anti-inflammatory signals which may facilitate tumor progression (105–107). TAMs mostly recapitulate M2 macrophage features and exhibit pro-tumor activity, indeed they are associated with poor prognosis due to their overall density in the tumor (108).

M1 macrophages are activated through various signals like interferon-γ (IFNγ) and bacterial lipopolysaccharides (LPS), they detect and clear tumor cells, pathogens and also present antigens to T cells. They are reservoirs of pro-inflammatory cytokines like IL-23, TNF-α, IL-6, and IL-12 and are involved in Th1 responses to infection. On the other hand, IL-4, IL-13, IL-10, CSF-1 and TGF-β activate M2 macrophages, which in turn, produce IL-10 and IL-1b, which suppress Th1-mediated inflammation and induce a Th2 response. While CSF-1 promotes the M2 polarization, GM-CSF is able of reversing their phenotype towards the M1 status (109).

During the neoplastic transformation, tumor cells start expressing C-C motif chemokine ligand 2 (CCL2), which is the major chemoattractant of monocytes and macrophages. Apart from CCL2, other chemokine attractants secreted by tumor cells such as CCL5, CXCL8, CCL7 and CXCL12 and cytokines like VEGF and M-CSF enrich the tumor milieu. Since the TME is IFN-γ and bacterial components deprived, upon arrival of the circulating monocytes, these factors shape the maturation of cells to become full-fledged M2-macrophages (110–112). Except from tumor cells, Tregs and fibroblasts secrete factors like TGF-β, IL-10 and hypoxia-inducible factor-2α (HIF2α) which enhance M2 polarization and TAMs themselves can secrete CCL2 to nourish this feedforward loop (113).

In contrast, macrophages also express colony stimulating factor 1 receptor (CSF-1R) and focal adhesion kinase (FAK) that mediate signaling cascades to promote MDSC, TAM, and Treg infiltration and are under investigation as therapeutic targets for the treatment of PDAC (114,115).

M2 macrophages promote wound healing and tissue remodeling by secreting matrix metalloproteinases which digest extracellular matrix. They can also exude vascular endothelial growth factor (VEGF) which promotes vascularization and angiogenesis and foster cancer invasiveness (116).

TAMs are capable of inhibiting anti-tumor responses of NK and T effector cells by expressing non-classical MHC-1 and ligands of co-inhibitory receptor PD-1 and CTLA-4 (117). Macrophage-induced IL-6 also promotes malignant progression via the JAK-STAT3 signaling pathway in early lesions (118–120).

Concerning drug resistance, TAMs have been shown to influence the activity of cytidine deaminase (CDA), which is a key metabolizer of gemcitabine, thereby driving resistance to gemcitabine-based chemotherapy in *in-vivo* PDAC models (121). Moreover, TAMs impair the

efficacy of therapeutic irradiation and targeted antiangiogenic treatment by promoting angiogenic escape mechanisms. CCR2 inhibition has been demonstrated to improve the efficacy of chemotherapy, inhibit metastasis, enhance the efficacy of radiotherapy, and increase T cell immune infiltration by blocking monocyte recruitment to the tumor microenvironment in mouse models of PDAC.
TAMs can thus be effectively targeted for therapeutic benefit in preclinical PDAC models, making them potential targets for novel therapeutic strategies in human PDAC (86,90,122–124).

1.2.2.3. Tumor-Associated Neutrophils

As previously described, the tumor microenvironment in PDAC is naturally rich of immune components and accumulation of tumor-associated neutrophils has been reported in pre-neoplastic lesions of PDAC, although their precise impact on carcinogenesis is not clear yet (125). Pancreatic tumor cells secrete pro-inflammatory factors, such as TNF-α and IL-12, that recruit a relevant amount of polymorphonuclear (PMN) cells (also called granulocytic neutrophils) into the tumor site. Due to the tumor permissive milieu that they are enrolled in, PMNs fail to mount an effective anti-tumor immune response and are thought instead to promote tumor progression since high neutrophil counts correlate with poor patient prognoses.
PMNs secrete a number of chemokines, such as CCL2, CCL3, CCL19, and CCL20 (126) to attract monocytes and dendritic cells to the TME. As neutrophils secure the survival of the host by resolving inflammation, in physiological conditions, their role in inflammation-driven tumorigenesis is indubitable. PMNs participate in close crosstalk with the TME and, consequently, their activation/polarization state is affected by the molecular cues with which they are confronted, therefore constituting a population of Tumor-Associated Neutrophils (TANs). TANs are a major source of pro-inflammatory cytokines, including IL-12, TNF-α, and GM-CSF, as well as chemokines, including CCL-3, CXCL-8, and CXCL-10. These factors affect the migration of cancer cells, as well as other immune cells such as lymphocytes. By specifically releasing IL-10 and TNF-α, TANs reduce the number of lymphocytes and even lead to their dysfunction, such that the outcome of this signaling is a suppressed immunologic reaction at the tumor site.
TGF-β is able of polarizing TANs into the N1 phenotype, while Interferon-α (type I IFN) and Treg-derived IL-35 are able of driving TANs polarization towards a N2 state (127–129). The tumor associated neutrophil N1 and N2 subpopulations are thought to have different functions in cancer. N1 neutrophils release pro-inflammatory or immunostimulatory cytokines, such as interleukin (IL)-12, tumor necrosis factor (TNF)-α, CCL3, CXCL9, and CXCL10, which facilitates the recruitment and activation of $CD8^+$ T cells (130). In contrast, N2 neutrophils have strong immunosuppressive and tumor-promoting activity, including the enhancement of tumor angiogenesis, invasion, and metastases via various factors, such as hepatocyte growth factor (HGF), oncostatin M, reactive oxygen species (ROS), reactive nitrogen species (RNS), matrix metalloproteinases (MMPs), and neutrophil elastase (NE) (131–133).
TANs were shown to localize at the margin of tumor sites in early-stage cancer, but they can massively infiltrate into the center of the tumor mass at later neoplastic stages. Following the recruitment of TANs to the tumor tissue, thanks to the action of cytokines and chemokines, they are promptly activated based on a process depending on their specific antigen CD177, a key factor for neutrophil activation. CD177 has been demonstrated to be negatively correlated with the survival of PDAC patients (134).
A peculiar characteristic of neutrophils is their cytoplasmic granules content, that is the mean through which they exert their immune functions. In fact, they are easily recognizable owing to the diverse type of granules they contain. Tertiary granules are the major constituents in shaping the TME of PDAC and proteins localized into these granules can be highly mobilized. For instance,

they contain a high amount of matrix metalloproteinase-9 (MMP-9) that, when released extracellularly, exerts its catalytic activity in the TME, leading to an enhanced invasion of tumor and immune cells following the cleavage of ECM proteins (collagens, laminin, and fibronectin), and also leads to enhanced tumor angiogenesis by mobilizing Vascular Endothelial Growth Factor (VEGF) from the ECM (135). With regard to immunosuppression, tertiary granules can release arginase-1 (ARG-1) that induces suppression of CD3-mediated T cell activation and proliferation (136,137). Recently, a study reporting the effects of IL-17 on the TME, has identified neutrophil recruitment and NETosis as the main outcome of this cytokine in the contest of PDAC. Neutrophil Extracellular Traps (NETs) are intricated networks of DNA filaments and proteolytic enzymes able to trap and attack pathogens, and they are set up by neutrophils that release chromatin and carry out degranulation (138). As a result of neutrophil recruitment and NETosis, $CD8^+$ T cells remained excluded from tumors, thereby IL-17 mediates the resistance of PDAC to the checkpoint inhibitors PD-1 and CTLA-4 (139,140).

Furthermore, neutrophils are very relevant in metastasis formation thanks to their potency to enter the tissue from the circulatory system. When they are located in the bloodstream, neutrophils can escort circulating tumor cells that are disseminated from the primary tumor site (141). During the extravasation process and after infiltration into metastatic sites, neutrophils undergo apoptosis and NETosis, so that their cargo proteins are released and create a pro-tumorigenic microenvironment. This includes the release of ARG-1 to create an immune-suppressed environment; MMP-9 to promote the infiltration of tumor cells and tumor angiogenesis; and other potent serine proteases, e.g., neutrophil elastase (NE), Cathepsin G, and human proteinase 3 that can shape the TME at the metastatic site. Other proteins released from neutrophils are lipocalin-2, heparanase, CD11 and CD18, and S100/A9. For instance, through the release of lipocalin-2, neutrophils can activate tumor cells via the phosphorylation of PI3K/Akt, causing the downstream expression of VEGF and HIF-1, which are important factors for tumor progression, angiogenesis, and chemoresistance (142).

Mouse models of PDAC treated with Lorlatinib (a kinase inhibitor) demonstrated a reduction in tumor progression mediated by inhibition of neutrophil development and mobilization. Treatment with Lorlatinib improved response to anti-PD-1 immunotherapy and promoted activation of $CD8^+$ T cells (143).

Given their biological characteristics and short lifespan, there is more evidence for a tumor-promoting than tumor-suppressing effect of neutrophils in PDAC. Due to the instant release of proteins associated with the infiltration of tumor cells and suppression of the immune response, recent data point towards a more active role in the TME, in which neutrophils affect the activation states of other cell types in the immune landscape, such as CAFs and T cells (59,86,115).

1.2.2.4. Dendritic cells

Dendritic cells are part of the innate immune system and represent the main cell type in charge of processing and presenting antigens to adaptive immune cells to mediate their polarization into effector cells. However, once located inside of carcinomas, tumor-associated dendritic cells (DCs) start to display tolerogenic properties. Such properties include low expression of costimulatory molecules, low ability to process and present antigens and low production of proinflammatory cytokines (144,145). The accumulation of tolerogenic tumor-associated DCs has been attributed to tumor- and TME-derived immunosuppressive factors such as VEGF, interleukin-10 (IL-10), transforming growth factor β (TGF-β), and PGE2 that modulate DC maturation and favor

tolerogenic DC differentiation (146,147). The tolerogenic nature of DCs, that are recruited to the pancreatic TME, is also indicated by their expression of indoleamine 2,3-dioxygenase (IDO), a heme enzyme that catalyzes the first and rate-limiting step in tryptophan catabolism. Since IDO action leads to a reduction of tryptophan levels with consequent accumulation of tryptophan catabolites, it has been shown to inhibit T cell proliferation and T cell cytotoxicity (148). IDO-expressing DCs have been found at the tumor site and in tumor-draining LNs. They have been implicated in suppressing anti-tumor T cell responses and in promoting immune tolerance (115,149) therefore a growing body of evidence is indicating that DCs as well can be shaped by intratumoral factors to become tumor permissive.

1.2.2.5. T regulatory cells

$CD4^+$ $Foxp3^+$ T regulatory cells (Tregs) are crucial for the maintenance of immunological self-tolerance and have the ability to actively impede the anti-tumor immune response in a variety of cancer types (150). Tregs are detected in the TME during PDAC development from pre-neoplastic lesions. With the disease progression, there is a marked increase in the Treg/$CD8^+$ T cell ratio that is correlated with poor prognosis (151). A low abundance of Tregs is instead associated with a better outcome and increased prevalence of beneficial CTLs (cytotoxic T lymphocytes) (152). Accordingly, tumor infiltration with low numbers of Tregs and high numbers of M1 macrophages and $CD8^+$ T-cells significantly correlated with longer survival in the invasive stages of the disease (65,151).

A variety of mechanisms for Treg mediated immune suppression have been proposed, including direct elimination of effector T cells and competition with effector T cells for access to antigen-presenting dendritic cells (DCs) (144,150). Indeed, PDAC intratumor Tregs have been found to express a higher level of CTLA-4 and PD-1 than Tregs in pancreatic or peripheral lymph nodes, therefore displaying a higher capability of inducing co-inhibitory stimuli in previously activated T cells (153). Moreover, Treg cells have also been shown to suppress DC immunogenicity in *in vitro* co-culture systems (153–155). Treg cell ablation resulted in the expansion and activation of tumor infiltrating $CD4^+$ and $CD8^+$ T cells at the tumor level. Treg cell depletion in combination with conventional PDAC treatment strategies has been shown to enhance cancer-specific T cell activation in preclinical studies (156,157). Co-depletion of Tregs with either $CD4^+$ and $CD8^+$ T cells indicate that Treg cells may promote pancreatic neoplasia through the suppression of IFN-γ-producing activated $CD8^+$ T cells, while $CD4^+$ cells are dispensable for the neoplastic process (153). Intratumoral Treg cells engage in prolonged interactions with tumor-associated $CD11c^+$ DCs and reduce their expression of T cell activation fundamental molecules. Treg cell ablation leads to the restoration of immunogenic tumor-associated $CD11c^+$ DCs and increases $CD8^+$ T cell activation. Thus, the targeting of Treg cells in PDAC may facilitate anti-tumor immunity by harnessing the immune-stimulatory potential of tumor-associated DCs (153). These results suggest that the cytotoxic $CD8^+$ T cell activation and effector activity observed in the setting of Treg cell ablation might be mediated by the functional maturation of tumor-associated $CD11c^+$ DCs. Additionally, Tregs show potential plasticity toward Th17 ($Foxp3^+ROR\gamma^+$) and induce the production of IL-17, IL-23, and TGF-β which promote cancer growth and evasion (158).

Nonetheless, some studies highlighted instead the anti-tumoral properties of Tregs. Indeed, it has been shown that Treg depletion resulted in the induction of tumor-promoting inflammatory cancer-associated fibroblasts (iCAFs) instead of tumor-restraining myofibroblastic CAFs (myCAFs), which were dependent on TGFβ secreted by Tregs. Moreover, Treg depletion induced the

expression of CCL3, CCL6, and CCL8 chemokines by epithelial cells and fibroblasts, which recruited myeloid cells in a CCR1-dependent manner thereby promoting immune suppression (158) (153). Similarly, the genetic depletion of Tregs during the onset and progression of murine PDAC caused disease acceleration by modulating the cellular components of the tumor microenvironment (159). Accordingly to these controversial findings, a recent report revealed an increased intra-tumoral presence of Treg cells and $CD8^+$ T cells (CTLs), while decreased numbers of $CD4^+$ T cells in tumors of long-term survivors compared to short-term PDAC survivors (84) .
Taken together, these results suggest that Tregs display multifaceted roles in pancreatic cancer dependently on the tumor stage and environment. On one hand, they can promote tumorigenesis by suppressing T cell activity via immunomodulatory effects on DCs or by plasticity towards Th17 cells. On the other hand, they can restrain tumor growth by promoting myCAFs formation and balancing the suppressive myeloid compartment (86).

1.2.2.6. Cytotoxic T lymphocytes

The stroma of PDAC contains a considerable amount of $CD3^+$ T lymphocytes, of which the major components are $CD4^+$ T helper (Th) cells, $CD8^+$ T cells, and $CD4^+CD25^+$forkhead box P3 ($FoxP3^+$) regulatory T cells (160).
Among the tumor-infiltrating lymphocytes (TILs), cytotoxic T lymphocytes (CTLs) are a subset of $CD8^+$ T cells that generally inhibit tumor growth by diverse mechanisms such as: i) Cytotoxicity through granzymes and perforin degranulation; ii) Cell apoptosis induction through the Fas-FasL system; iii) Cytotoxicity through IFNγ and TNFα secretion (161). $CD8^+$ T cells are also able of forming a long-term existing memory, thereby establishing protection from cancer recurrence. In pancreatic cancer, an increased accumulation of $CD8^+$ T cells in the tumor tissue and close proximity to tumor cells correlates with better survival (84).
However, the tumor microenvironment often induces a dysfunctional state in CTLs, termed *exhaustion*, which is characterized by an impairment of the effector function, reduced survival, and increased expression of inhibitory receptors. In their late stages of activation, $CD8^+$ T cells express inhibitory receptors to avoid an excessive immune response and to promote a correct immune homeostasis. These inhibitory molecules are named *immune checkpoints,* and their most representative members are PD-1, CTLA-4, TIM-3, LAG-3 and TIGIT. T-cell immunoreceptor with Ig and ITIM domains (TIGIT) is a receptor that interacts with dendritic cells and macrophages inducing the expression of anti-inflammatory cytokines that interferes with the ability of CTLs to mitigate PDAC progression. Programmed cell death 1 (PD-1) instead, by binding to its ligands PD-L1 and PD-L2, inhibits the T cell receptor (TCR) downstream signaling and subsequently T cell biological functions, including proliferation, cytokine secretion, cytotoxic activity, finally leading to T cell apoptosis. Cytotoxic T-lymphocyte-associated protein 4 (CTLA-4) mediates immunosuppression by indirectly diminishing signaling through the co-stimulatory receptor CD28. Both CD28 and CTLA-4 bind to CD80 and CD86 to exert their actions, but CTLA-4 does so with much higher affinity, effectively outcompeting CD28 and therefore propagating its inhibitory signals (159,162,163). Targeting immune checkpoints has been established as a novel therapeutic strategy against tumor in the last years. The checkpoint blockade has led to durable responses in multiple cancers, such as melanoma, non-small cell lung carcinoma, head-and-neck cancer, and urothelial carcinoma (162). The application of checkpoint inhibitors as monotherapy has been unsuccessful in PDAC so far, and better understanding of the mechanisms regulating

$CD8^+$ infiltration inside tumors is fundamental for designing more effective combination immunotherapies (86).

1.2.2.7. $CD4^+$ T helper cells

$CD4^+$ T cells represent the major TIL portion inside of PDAC and they may differentiate into diverse phenotypes. One of them is constituted by the Th17 $CD4^+$ cells that have been shown to promote early PDAC lesions formation and KRAS-driven PDAC development by secreting IL-17, a potent cytokine that establishes a chronic inflammatory status that promotes carcinogenesis (164). Furthermore, $CD4^+$ T cells can also differentiate towards the Th1 or Th2 subtype: Th1 $CD4^+$ T cells ($T\text{-}BET^+$) secrete IL-2, TNF-α and interferon-γ, responsible for the cell-mediated immune response. Indeed they promote the anti-tumoral immune response through the priming, activation, and recruitment of CTLs, M1 macrophages, and NK cells (165). Th2 $CD4^+$ T cells ($GATA3^+$) secrete IL-4, IL-5, IL-6, IL-9, IL-10, and IL-13 and are involved in the humoral immune response also driving the induction of M2 macrophages and promoting ECM deposition and collagen synthesis (166).
There is a reciprocal relationship between Th1 and Th2 development, in which Th1 inhibits Th2 differentiation and vice versa. Elevated Th2/Th1 ratios within the tumor-infiltrating cells are a negative survival marker in patients with stage IIB/III pancreatic cancer, in fact Th2 $CD4^+$ T cells, are more abundant in PDAC, and exert a tumor promoting effect due to their prevalent anti-inflammatory action (60,167). Indeed IL-4 secretion by Th2 $CD4^+$ T cells promotes pancreatic cancer cell proliferation and enhances the activation of STAT3, AKT, and MAPK pathways, suggesting direct tumor-promoting activity (168). Furthermore, the polarization and accumulation of Th2 $CD4^+$ T cells in the tumor microenvironment are driven by thymic stromal lymphopoietin (TSLP)-activated myeloid dendritic cells (DCs) expressing the receptor for TSLP (167). TSLP is a cytokine produced mostly by non-hematopoietic cells that regulates the activation and maturation of both myeloid and lymphoid cells. In turn, TSLP is secreted by cancer-associated fibroblasts activated by IL-1α and IL-1β (iCAFs), produced by cancer cells and M2 macrophages (169).
Inhibition of the pathways that induce Th2 polarization leads to a shift towards protective Th1 responses accompanied by the activation of M1 macrophages and CTLs restricting tumor progression (59,86).

2. Tumor vasculature in PDAC

Angiogenesis is the process through which new capillaries are formed starting from pre-existing blood vessels. It is crucial for tumor development and progression since actively proliferating cells have high oxygen and nutrient requirements, and it also plays a key role in metastatic dissemination (170,171). Angiogenesis is activated when an imbalance between pro- and anti-angiogenic molecules is established, with a predomination of pro-angiogenic factors. This event is called *angiogenic switch* when it occurs at a tumoral level (172). The key mediator promoting the angiogenic switch is vascular endothelial growth factor A (VEGF-A), that functions as a mitogen for vascular endothelial cells and enhances endothelial cell survival. Angiopoietin-2 is a pro-angiogenic factor as well and it facilitates VEGF-dependent angiogenesis. VEGF-A is able of increasing vascular permeability and amplifying the mobilization of bone marrow-derived endothelial precursor cells and it mediates its pro-angiogenic effects interacting with vascular

endothelial growth factor receptor 1 and 2 (VEGFR-1 and VEGFR-2) and their co-receptors neuropilin-1 and 2 (NRP-1 and NRP-2) (173,174).

2.1. Pathways of vessel formation in pancreatic cancer

Angiogenesis can occur through different mechanisms: i) sprouting angiogenesis consists in a sprout arising from a pre-existing blood vessel, that elongates until it forms a new vessel. This is a physiological event that can be induced by cancer cells including PDAC cells (175). ii) intussusceptive angiogenesis is an alternative pattern for neovascularization that consists in the formation of an intraluminal pillar, in a pre-existing blood vessel, that increases in size until it splits the initial vessel forming two new vessels. This process does not depend directly on endothelial cell proliferation, therefore is a rapid mechanism for generating new vessels and increasing microvessel density (176). iii) vessel cooption is a process in which tumoral cells parasitize pre-existing vessels of the host organs and use them for the blood supply and to move along them (177). iv) vascular mimicry consists in cancer cells mimicking endothelial cells and forming vessel-like fluid-conducting channels. This mechanism is typical of highly aggressive and genetically dysregulated cancer cells and in PDAC it is correlated with poor tumor differentiation, late clinical stage, lymph node metastasis and bad prognosis (178). v) vasculogenesis instead is the spontaneous formation of new blood vessels mediated by bone marrow derived endothelial progenitor cells (EPCs). The amount of EPC in PDAC is significantly higher when compared with normal pancreatic tissue, indeed this cellular type is strongly correlated with shorter survival in PDAC patients (179,180).

2.2. Tumor and stromal cells – endothelial cells cross-talk in pancreatic cancer

Considering the multiple mechanisms allowing vessel formation in PDAC, and the establishment of a pro-angiogenic microenvironment, it is conceivable that pancreatic cancer is characterized by a high microvascular density. Furthermore, the desmoplastic reaction initiated by CAFs, causes abnormally elevated stromal pressure that impairs the correct functioning of the vascular network. Indeed, PDAC blood vessels are poorly perfused, collapsed, poorly covered with pericytes and their integrity is affected, therefore blood flow is dramatically diminished, drug delivery is inefficient and hypoxia shapes cell polarization throughout the tumor ecosystem (181,182).
Since high microvascular density is a hallmark of pancreatic cancer, anti-angiogenic therapy should represent a valid approach for targeting such a tumor. Multiple trials employing monoclonal antibodies against VEGF or its receptors have been proposed, but their outcome resulted to be disappointing (183).
Considering that anti-angiogenic therapy aims at decreasing the intra-tumor vessel network to devoid tumoral cells from oxygen and nutrient delivery, it was unexpected that following treatment many trials resulted in increased invasive tumors and distant metastasis formation. The mechanism underlying these events is plausibly ruled by tumor hypoxia, leading to the selection of hypoxia-tolerant tumor cells that actively escape the hypoxic TME, hastening the epithelial to mesenchymal transition (EMT) and consequently an impairing drug delivery due to the decreased vascular distribution (170,184).
Beyond microvessel density, another important parameter to take into consideration when dealing with tumor vasculature is microvessel integrity. Microvessel integrity is an indicator of vessel quality, and it is strictly correlated with pericyte presence in the PDAC TME. Pericytes are mural

cells of the microcirculation that wrap around the endothelial cells that line capillaries. They serve several fundamental functions such as regulation of the endothelial cell growth, microvessel maturation, and microvessel remodeling. In PDAC it is well stablished that blood vessels are poorly covered by pericytes, and therefore they result to be leaking and poorly perfused. Vessel normalization consists in increasing the pericyte coverage of endothelial vessels in order to improve microvessel integrity, vessel perfusion, drug delivery efficiency and to decrease vessel leakage and tumor hypoxia. In contrast to anti-angiogenic treatments, vessel normalization has been proposed as an effective mechanism to undermine PDAC progression (185–191).
Vessel normalization has an impact on the whole tumor microenvironment, indeed it is often accompanied by stromal normalization (**Fig. 5**). Once tumoral blood vessels acquire a physiological architecture and are correctly covered with pericytes, the cross-talk between these cells and other components of the TME switches towards an anti-tumoral approach. Endothelial cells start overexpressing higher amounts of adhesion molecules that facilitate the tissue transmigration of anti-tumoral immune cells, thus repopulating the TME with effector immune cells. Endothelial cells also upregulate CD40 expression promoting the activation of macrophages and antigen presenting cells, and through the secretion of chemokines they recruit pro-inflammatory immune cells. All these mechanisms lead to the reprogramming of the whole immune compartment of the TME, therefore co-operating with the normalized vessels in hampering tumor progression (192) (**Fig. 5**).

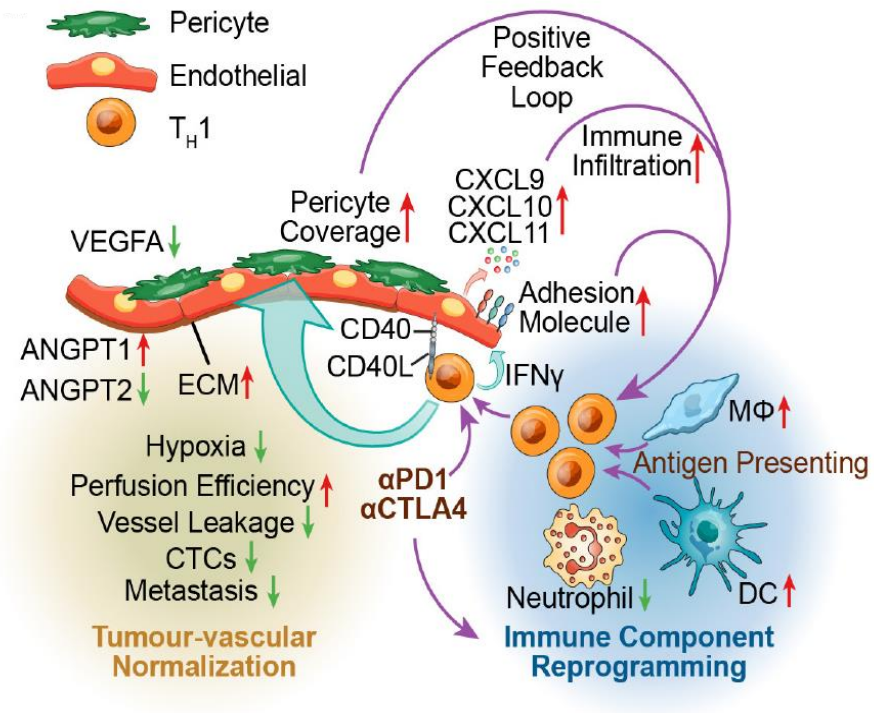

Figure 5. *Vessel normalization induces stromal normalization. Subsequently to vessel normalization the immune compartment undergoes reprogramming. Since endothelial cells and pericytes change their transcriptomic profiles, upregulating molecules involved in the crosstalk with the immune compartment, the immune infiltration at a tumor level is subjected to a switch towards an anti-tumoral phenotype. Chemokines such as CXCL9, CXCL10 and CXCL11 attract pro-inflammatory macrophages at the tumor site, increased adhesion molecule exposure on endothelial cells facilitates leukocyte transmigration into the tumor tissue and augmented CD40 and IFN-γ production promotes the activation of several immune subpopulations, improving the overall immune response against the tumor* (192).

3. Semaphorins

Semaphorins are a large family of evolutionary conserved proteins that were initially identified as signaling cues in axonal guidance and synapse formation during embryogenesis. During the last decades new knowledge has unveiled their multiple roles in adult tissues and outside of the nervous system. These molecules are now known to be expressed in a multitude of adult tissues and have pleiotropic effects in both health and disease (193). The members of this family represent more than 20 secreted, transmembrane and GPI-linked glycoproteins (**Fig. 6 A**). The structure of these proteins shows a highly conserved N-terminal sema domain of about 500 amino acids, a plexin–semaphorin–integrin domain and distinct protein domains that further define semaphorins, including immunoglobulin-like, thrombospondin, and basic C-terminal domains (194). The semaphorin family is divided into eight classes: class 1-2 are constituted by invertebrate semaphorins, class 3-7 comprise the vertebrate semaphorins and class 8 contains the viral semaphorins.To exert their action, they require signaling through their cognate receptors constituted by plexins and neuropilins (**Fig. 6 A**).

Plexins are divided into invertebrate plexins (classes A and B) and vertebrate plexins (classes A-D), containing 2 and 9 proteins respectively. Plexins are composed of an extracellular portion typically formed by 10 domains, including a sema domain, which differs from that of semaphorins for the lack of ability to dimerize, a membrane-spanning region and a cytoplasmic segment, which interacts with intracellular signaling molecules transducing the downstream signal (195).

A shorter intracellular domain, containing a PSD95/Dlg/ZO-1 (PDZ) binding motif, characterizes the other class of receptors, composed of neuropilin − 1 and − 2. In the extracellular segment of neuropilins, there are different domains and among these there is also the binding site for vascular endothelial growth factor (VEGF), hepatocyte growth factor (HGF), fibroblast growth factor-2 (FGF-2), platelet-derived growth factor-β (PDGF-β), transforming growth factor-β (TGF-β) and other ligands (196–198).

Semaphorins and their receptors are involved in multiple physiological and pathological processes as they participate in immune regulation, extracellular matrix remodeling, organogenesis, bone homeostasis, angiogenesis and pathways such as apoptosis, autophagy and senescence (**Fig. 6 B**). Several human diseases including immunopathological, neurodegenerative and cardiovascular diseases show aberrant expression of semaphorins, furthermore, their signaling can also play a major role in tumor progression and metastatic dissemination (199–201). More specifically, by participating to the crosstalk between cancer cells and stromal cells in the TME (i.e. fibroblasts, immune and endothelial cells), semaphorins are involved in various aspects of tumor development, sometimes defining tumor-restraining effects. Several semaphorins have been reported to reduce tumor growth and angiogenesis, others are found to promote tumor growth or metastasis (202) (**Fig. 6 B**).

Some semaphorins have also been demonstrated to play a role in vessel normalization and their action as potential therapeutic targets has been evidenced (191,203,204). Similar to their function in axonal guidance, semaphorins are able of driving endothelial cells towards vessel formation and remodeling. In fact, they are able of shaping the balance between other pro- or anti-angiogenic factors in the tumor microenvironment. Pro-angiogenic semaphorins include Sema3C, Sema4A, Sema4D, Sema6D, and Sema7A, while angiostatic semaphorins include Sema3A, Sema3B, Sema3D, Sema3E, and Sema3F (205) (**Fig. 6 B**).

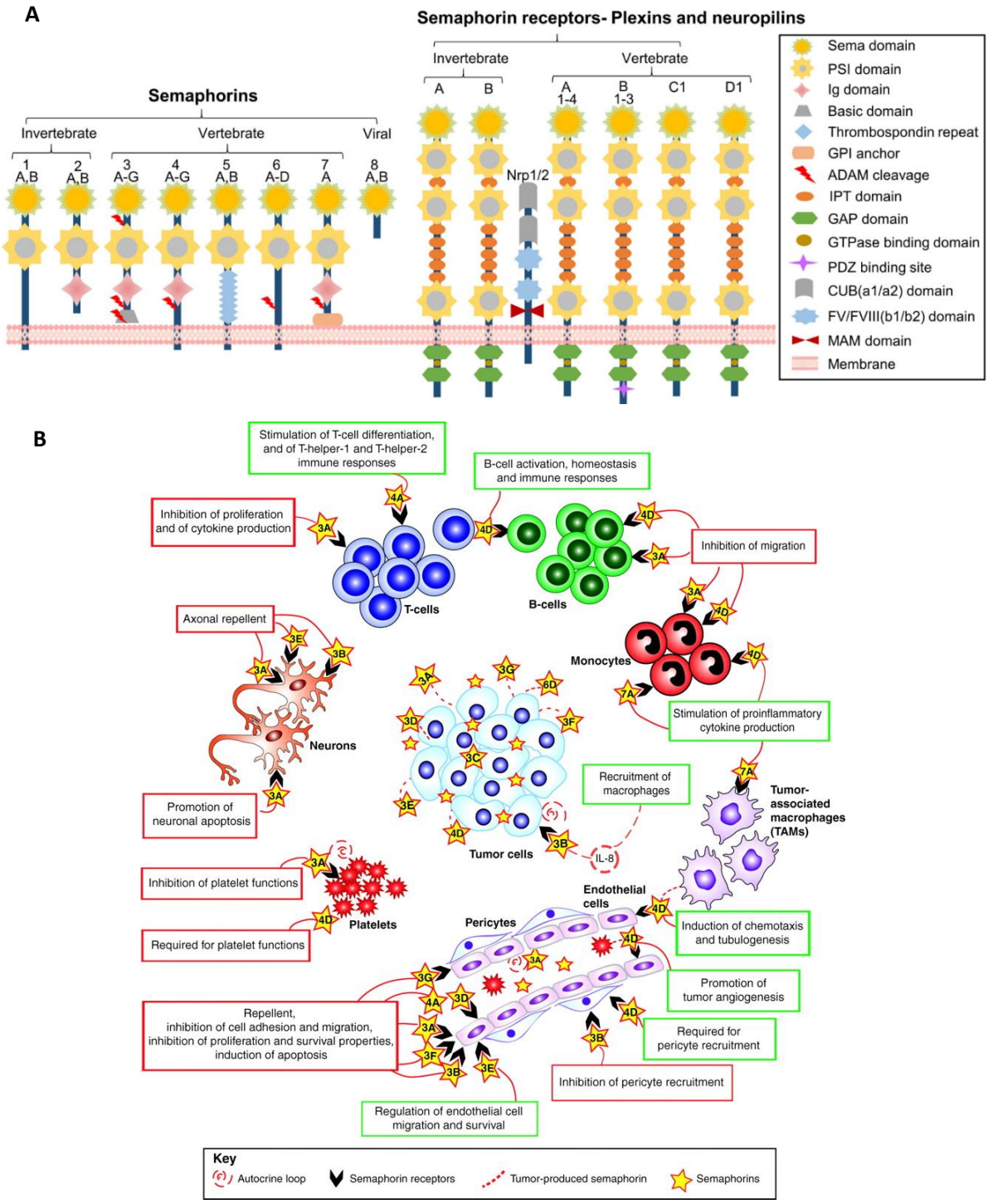

Figure 6. A) *Schematic representation of semaphorins and their receptors. The semaphorin family can be classified based on structural and sequence similarity in eight classes. Among vertebrate semaphorins, class 3 consists of secreted members, while class 4 to 7 semaphorins are membrane bound proteins. Plexins, the semaphorin receptors, are categorized in four subfamilies on similarity bases. In vertebrates, nine plexins have been identified so far. However, most class 3 semaphorins require binding to co-receptors of the neuropilin family, NRP1 and NRP2, and cannot bind directly to plexins* (206). ***B)*** *Semaphorin activity on cancer cells or on components of the TME. Diverse tumor types are able of producing several semaphorins depending on tumor staging. Many of them resulted to have tumor promoting effects while others are able of exerting tumor restraining actions and stromal normalizing activities* (207)

3.1. Semaphorin 3A

Class 3 semaphorins are secreted proteins that require binding to neuropilins and cannot bind directly to plexins for transducing their signal. Thanks to their binding to neuropilin-1, -2 (NRP-1, NRP-2) and vascular endothelial growth factor (VEGF) receptor family they are able of exerting anti-angiogenic effects. Sema3A indeed is a potent inhibitor of developmental angiogenesis and has also been shown to impair neovascularization and tumor progression in various types of cancer. Since endothelial cells express both plexin and neuropilin receptors, prolonged stimulation with Sema3A is able of inducing endothelial cell apoptosis, suggesting that this mechanism of cell death is the mean through which Sema3A negatively regulates the angiogenic switch.
Moreover, *in vitro* and *in vivo* studies using pancreatic neuroendocrine and PDAC mouse models demonstrated that Sema3A exerts a vessel normalizing activity. Indeed, Sema3A was shown to counteract the activation of HIF-1α improving tumor tissue oxygenation and decreasing tumor hypoxia, it showed a significant enhancement of the microvascular integrity thanks to improved pericyte coverage of endothelial vessels, it led to improved chemotherapeutic delivery and vessel perfusion and finally it synergized with chemotherapeutic regimens in reducing tumor progression (185,190,191).
Semaphorins Sema3A, Sema3E, Sema4A, Sema4D, Sema5A, Sema6D, and Sema7A may be considered as “immune semaphorins” since they are involved in physiological and pathological immune responses and regulate immune homeostasis and tissue inflammation (208).
Interestingly, Sema3A produced by tumor cells is able to recruit bone marrow derived cells that contribute to the stabilization and normalization of the tumor vessels. Moreover, neuropilins are important for the primary immune response since it mediates the contact between DCs and T cells in the immunological synapse (209).
Sema3A is a potent immunoregulatory molecule and has been shown to suppress the over-activity of T and B lymphocytes (210).
Activation of naïve T cells requires an immunological synapse with dendritic cells in the secondary lymphoid organs. The immunosuppressive role of Sema3A on T cell proliferation was first described (211).
Lepelletier et al. found that the high levels of Sema3A produced in the later stage of DC-T cells co-cultures inhibited T cell proliferation. Thus, the induced Sema3A expression by both DCs and T cells during the latter part of the immune response could be regulating this response (211,212).

3.2. Mutant Sema3A

Normally, Sema3A can be found as a stable homodimer, due to the interactions that form between the sema domain and the basic stretch, but in order to bind to Nrp1, the furin processing resulting in the exposal of a C-terminal arginine is essential to allow the interaction with the b1 domain of Nrp1 (213). It has also been demonstrated that furin-like protease is fundamental to end the Sema3a-Nrp1 bond, due to its ability to cleave the PSI/sema domain, permitting its dissociation from the Ig-like domain/basic tail.

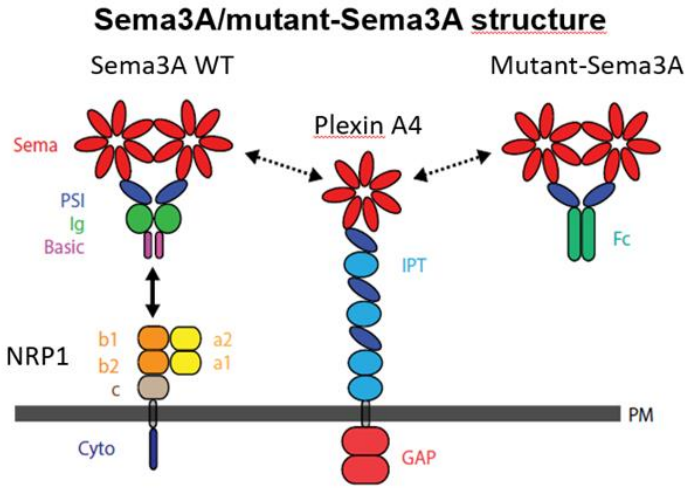

Figure 7. *Sema3A WT binds to the b1 domain of NRP1 through its C-terminal basic stretch and this helps keeping Sema3A WT close to PLXNA4. NRP1 acts therefore as a co-receptor and allows the sema domain-sema domain interaction between Sema3A WT and PLXNA4 that leads to the activation of PLXNA4 GTPase activating protein domain. In the Sema3A ΔIg-b deletion mutant the high-affinity NRP1- binding stretch was removed and substituted with the mouse IgG1 constant fragment, making the mutant Sema3A stably dimeric.*

However, along the years, several studies have brought to light how the activation of the Sema3a-Nrp1 pathway can lead to numerous side effects, such as tumor progression (through the recruitment of TAMs into hypoxic niches) (214), inhibition of VEGF-induced angiogenesis and induction of vascular permeability in mice (215), induction of vasogenic edema in diabetic retinopathy (216). For these reasons, it has been generated a Nrp1-independent mutant Sema3a that is able to bind to PlxnA4 with high affinity, allowing the normalization of tumor blood vessels and the inhibition of metastatization (185).

Initially, wild-type Sema3a was modified by removing the Ig-like domain and the basic tail and, later, the remaining C-terminal portion was fused with the constant fragment of the mouse IgG1, generating the Fc-tagged SEMA3A_ΔIg-b. Compared to the WT Sema3a, the rationally engineered Sema did not interact with Nrp1, therefore preventing the internalization of active integrins in the extracellular matrix adhesion and the endothelial cells collapse. In addition, by lacking the C-terminal tail, SEMA3A_ΔIg-b could not interact with the Nrp1 b1 domain, thus impeding endothelial cells internalization and vascular leakage (217) (**Fig. 7**).

On the other hand, it was demonstrated that Nrp1 binding is not essential for haptotactic EC migration nor was it proven to be fundamental for the antitumor effects of Sema3a, as these activities did not depend on the activation of the Sema3a-Nrp1 pathway, but are more likely mediated by other signaling receptors, such as PlxnA4.

Even though Sema3a anticancer response does not directly rely on the interaction with Nrp1, studies showed that SEMA3A_ΔIg-b was less efficient in impairing tumor progression, probably due to its low affinity for PlxnAs (185). For this reason, another modification realized on Sema3a through rationally designed mutagenesis, consisted in altering the electrostatic charges in the sema domain by introducing a positive charge (A106K) in the extrusion 1 of Sema3a. The generation of a SEMA3A_A106K_ΔIg-b, with a positively charged Lysine instead of a non-polar Alanine, led to an increased affinity of Sema3a for PlxnA4 and, consequently, to an improvement in the previously described biological functions of the modified Sema both on ECs and on cancer, in particular in PDAC. In addition, it was demonstrated that SEMA3A_A106K_ΔIg-b, similarly to WT Sema3a, could also normalize tumor vasculature, increase pericytes coverage and reduce

tumor hypoxia, even in a more efficient manner than its wild type counterpart. Moreover, the normalisation of the blood vessels caused by SEMA3A_A106K_ΔIg-b allowed an enhanced delivery of anticancer drugs, such as gemcitabine, improving the efficacy of anticancer therapies. In conclusion, SEMA3A_A106K_ΔIg-b was proven to be more effective than WT Sema3a in binding Plxn4A and, as a result, in inhibiting tumor growth and metastatization, without triggering the sides effects normally caused by the interaction of Sema3a with Nrp (185).

AIMS

Considering the challenges concerning pancreatic ductal adenocarcinoma treatment, we sought to improve the knowledge about the complexity of this disease that depends on the multitude of non-tumoral cells that are hijacked to become tumor-permissive and to promote tumor progression. The following study was designed to elucidate the complex interactions that occur between the heterogeneous populations of the tumor ecosystem and how these interplays are shaped following administration of exogenous Semaphorin3A. More specifically, one of our aims was to unveil how the different cell types interact with each other, and how this cross-talk is modified following treatment. For doing this we took advantage of several approaches:

1. To perform single cell RNA-sequencing on control and mut-Sema3A treated samples and to analyze the changes in cell populations composing the tumor microenvironment in the two treatment groups. Moreover, we sought to identify specific gene signatures in the TME induced by mut-Sema3A.
2. To employ the Visium Spatial Gene Expression and In Situ Hybridization technologies to confirm the transcriptomic changes identified through scRNAseq at a tissue level and to determine the localization of specific cell populations highlighted from the scRNAseq analysis.
3. To investigate the changes in the immune landscape in PDAC treated by mut-Sema3A and to investigate the molecular mechanisms underlying immune cell recruitment through normalized tumoral vessels.
4. To assess the effect of mut-Sema3A on other TME components, such as the activated cancer-associated fibroblasts (CAFs) and their functional role in vivo and ex-vivo models.

MATERIAL AND METHODS

Single cell separation and cDNA sequencing

In order to analyze transcriptome 3' gene expression at single cell resolution, samples have been processed with Chromium Next GEM Single Cell 3′ Reagent Kits v3.1 Dual Index and Chromium Controller instrument (10X Genomics, Inc; Pleasanton, CA, US) following manufacturer's instructions. Briefly, single cell suspensions obtained from control and treated samples by means of Fluorescence-Activated Cell Sorting (FACS) were brought to a concentration of 500 and 350 cells/µl respectively, and the proper volume of cell suspensions (based on 10X Genomics user guide) to achieve 7.000 targeted cell recovery has been used. For the cDNA amplification step, 12 cycles have been identified as the optimal number in our condition, while the index PCR has been performed with 14 cycles of amplification. Final libraries were quantified by means of Qubit dsDNA HS Assay Kit (Thermo Fisher Scientific, Waltham, MA, USA) and their fragment distribution was evaluated thanks to High-Sensitivity DNA assay kit (Agilent Technologies, Santa Clara, CA). Equal amounts of DNA libraries were pooled and sequenced using Illumina NextSeq500 sequencer (Illumina Inc., San Diego, CA, USA), thus generating sequencing data as required by manufacturer's instructions (read1 28bp, read2 90bp, double index 10bp).
The estimated number of sequenced cells was of 3623 and 3392 cells for control and mut-Sema3A treated respectively, with a sequencing depth of 45.688 and 52.173 reads per cell. The median sequenced genes per cell was of 1432 genes in the control and 942 genes in the treated samples.

Single-cell RNA-sequencing data processing

The count matrix was generated using 10XGenomics Cell Ranger software, using the implementation of the version 5 of the software implemented in rCASC analysis package (218)
Sc-RNA-Sequencing low-quality cells were identified using the Ribo/Mito scoring, described in rCASC analysis package (218). Specifically, cells showing more that 10% of the total counts associated with mitochondrial genes were removed. Furthermore, only cells characterized by the detection of at least 250 genes were retained. We defined a gene called detected, based on the definition suggested in rCASC paper (i.e., a gene is called detected in a cell, if it is supported by at least 3 UMIs).
Hou and coworkers (219) showed that scRNA-seq imputation methods outperform no imputation in recovering gene expression observed in bulk RNA-seq.
Furthermore, they showed that, in scRNAseq imputation, MAGIC, kNN-smoothing, and SAVER tools outperform other methods most consistently (219).
In this manuscript, scRNAseq counts matrices were imputed using SAVER (220).
ScRNAseq clustering was performed using Louvain modularity method implemented in Seurat (221), embedded in rCASC package (218). The number of clusters was defined based on the level of cluster stability, defined by the Cell Stability Score (CSS), implemented in rCASC. (218).

10X Genomics Visium Gene Expression tissue sampling

RNA quality of OCT embedded tissues (control and treated) was estimated before the placement of the tissue sections on the slide for Visium experiments. RNA was extracted from 10 sections (each of 10 μm thickness) using Qiagen RNeasy mini kit (Qiagen).
RNA quality was evaluated using Agilent bioanalyzer with Agilent RNA 6000 Nano kits.
Tissues with high quality RNA were removed from the –80°C storage and cryo-sectioned in a cryostat to generate appropriately sized sections to place within the frames of capture areas on Visium Spatial slides (10X Genomics). The Visium Spatial Tissue Optimization Slide & Reagent kit (10x Genomics) was used to optimize permeabilization conditions. Tissue permeabilization was performed for 18 minutes. Spatially barcoded full-length cDNA was generated using the Visium Spatial Gene Expression Slide & Reagent kit (10x Genomics). RT Master Mix, containing reverse transcription reagent was added to the permeabilizated tissue section to obtain spatially barcoded, full-length cDNA from poly-adenylated mRNA on the slide. Second strand mix was added to the tissue sections on the slide to synthetize second strand cDNA. The cDNA from each capture area was denaturated and transferred in a new tube for amplification and library construction.
cDNA amplification was conducted using 12 PCR cycles for tissue control and 16 PCR cycle for treated tissue. Cycles number was identified by qPCR, using KAPA SYBR fast qPCR Master Mix 2X (KAPA Biosystem), as recommended by 10X Genomics.
10 μl of cDNA were used for the 10xGenomics Visium library preparation followed manufacturer's instructions and using 16 PCR cycles for tissue control and 9 PCR cycles for treated tissue.
Enzymatic fragmentation, end repair, A-tailing, adaptors ligation and PCR are done using reagents from Visium Spatial Gene Expression Slide & Reagent kit (10x Genomics). Size selection and clean-up are performed using SPRIselect reagent (Beckman Coulter). Final Visium spatial gene expression library was composed of standard Illumina P5, i5 index, spatial barcode, 12 bp UMI, cDNA fragment, i7 index and standard Illumina P7. 1 ul of each library was run on Agilent DNA High sensitivity chip for quality control. Libraries were quantified with Qubit DNA HS (Life Technologies). Pools of 4 libraries was sequenced on a NextSeq 500 sequencer (Illumina) loading 1.8 pM of the pool with 1% PhiX (Illumina), as recommended by 10X Genomics, with the following run parameters: 28 cycles for read 1, 90 cycles for read 2, 10 cycles for i7 index and 10 cycles for i5 index.

10X Genomics Visium Gene Expression data processing

The count matrix was generated using 10XGenomics Cell Ranger software, version 6. The count matrix was generated using only the spots assigned to slide areas covered by tissue.
Visium Spatial Gene Expression low quality spots were identified using the Ribo/Mito scoring, described in rCASC analysis package (218). Specifically, spots showing more that 10% of the total counts associated to mitochondrial genes were removed. Furthermore, only pots characterized by the detection of at least 250 genes were retained. We defined a gene called detected, based on the definition suggested in rCASC paper (i.e., a gene is called detected in a cell, if it is supported by at least 3 UMIs).
Visium Spatial Gene Expression counts matrices were imputed using SAVER (220).

Visium Spatial Gene Expression clustering was performed using Louvain modularity method implemented in Seurat (221), embedded in rCASC package. The number of clusters was defined based on the level of cluster stability, defined by the Cell Stability Score (CSS), implemented in rCASC (218).

Mouse model and *in vivo* treatments

PDAC model (mPDAC) has been previously described(185,222). Briefly, FVB/n females of 5-6 weeks were inoculated with 1500 murine PDAC cells (p48^{cre}, Kras^{LSL_G12D}, p53$^{R172H/+}$, Ink4a/Arf$^{flox/+}$) in the pancreas tail. The treatments started one week following tumor cell injection. mPDAC has been treated three times a week with 10mg/kg mutant-Sema3A (via intravenous injection). After the 3-week treatment mice were euthanized according to the animal facility regulations.
For the combinatorial trials, mPDAC mice were treated with immunotherapeutic drugs using the following schedule: one day prior to mut-Sema3A administration, α-CD40 antibody (BioXcell Ref. BE0016-2) was administered twice: at day 6 and day 13 following PDAC cell inoculation at 200 µg/mouse via intraperitoneal injection. α-CTLA4 (BioXcell Ref. BE0164) and αPD1 (BioXcell Ref. BE0146) were administered twice a week for three weeks (**Fig. 8**) at 250 µg/mouse via intraperitoneal injection. Mut-Sema3A was administered three times a week at 250 µg/mouse via intraperitoneal injection to avoid cross-reactivity due to the intravenous administration together with multiple inoculated agents.

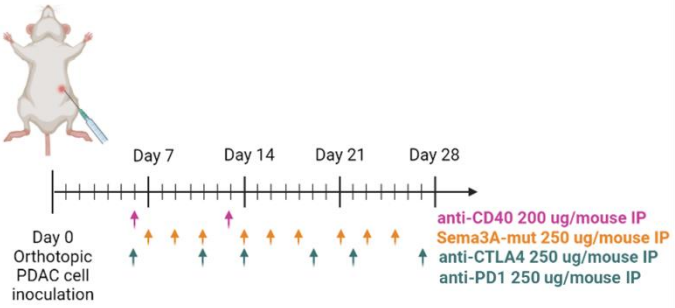

Figure 8. *Treatment schedule of the mPDAC mouse model with combination therapy. The therapeutic regimen started one week following tumor cell inoculation and lasted for 3 weeks. Mut-Sema3A was administered at 250 µg/mouse via intraperitoneal injection three times a week; αCTLA4 and αPD1 were administered at 250 µg/mouse via intraperitoneal injection two times a week; αCD40 was administered at day 6 and day 13 following tumor cell inoculation at 200 µg/mouse via intraperitoneal injection.*

Pancreatic Stellate Cells isolation

Healthy pancreata were harvested from 5-6 weeks FVB/n females. They were processed according to the following protocol (70), in brief: pancreata were minced and digested with a buffer containing Gey's Balanced Salt Solution (GBSS) (Sigma-Aldrich Ref. G9779), 0.05% Collagenase P (Sigma-Aldrich Ref. 11213857001) and 0.01% DNase I (Sigma-Aldrich Ref. D5025) for 45 minutes at 37°C under rotation. Subsequently the cell suspension was filtered through a 100 µm nylon mesh and centrifuged at 1000 RPM for 5 minutes. Supernatant was discarded and the cell pellet was resuspended in 9.5 mL of GBSS containing 43.75%

weight/volume Histodenz powder (Sigma-Aldrich Ref. D2158) and 0.3% BSA. The cell suspension was then carefully layered with 6 mL GBSS containing 0.3% BSA and the tube was centrifuged for 20 minutes at 1400 G without breaks. The cells forming the ring at the interface were harvested, washed with PBS and used for further applications.

Immunofluorescence

Tumor tissues were fresh frozen in OCT and 10-µm-thick frozen sections were serially cut using a Leica 2135 cryostat. Dried tumor slices were fixed with Zn fixative for 10 minutes and permeabilized with Triton 0,1% PBS solution. After saturation with DAKO protein block (Agilent Ref. X0909) at room temperature for 1 hour, tumor slices were incubated overnight with optimized primary antibody dilution, washed and incubated with Alexa Fluor secondary antibody for 45 minutes. After staining with DAPI, tumor slices were mounted and images acquired with SPEII DM5500 CSQ Leica confocal microscope using Leica LAS AF software. Images were analyzed using ImageJ software (NIH). For IF staining the following primary antibodies were used (see Table 1). Secondary antibodies were used to amplify the fluorescent signal (Alexa fluor™-488, Alexa fluor™ -555, Alexa fluor™ -647 Thermo Fisher Scientific).

RNA extraction and qRT-PCR

Whole tumor RNA was harvested by embedding in RNA later Tissue Storage Reagent (Sigma-Aldrich Ref. R0901). RNA was extracted with Maxwell® RSC miRNA Tissue Kit (Ref. AS4500). cDNA preparation was performed according to standard procedures with High-Capacity cDNA Reverse Transcription Kit (Applied Biosystems™ Ref. 4368814). PCR was performed by applying the following Taqman probes (see Table 2).

Sample preparation for sc-RNA sequencing

Tumors were harvested and immediately processed for obtaining the single cell suspension. In brief, tumors were first finely minced with a scalpel, then digested for 45 minutes at 37°C while rotating in a RPMI buffer containing 1.5 mg/mL Collagenase IV (Worthington Ref. LS004186) and 0.1 mg/mL DNase I (Sigma-Aldrich Ref. D5025), complemented with 2% FBS. Subsequently the cell suspension was filtered through a 70 µm nylon mesh and stained with DAPI and Epcam-PE (BioLegend Ref. 118206) for undergoing Fluorescence Activated Cell Sorting. Sorting and cloning was carried out on MoFlo ASTRIOS EQ ™ Cell Sorter (Beckman Coulter, Brea,CA). Dead cells, doublets, and higher order clumps were excluded. Sorted cells were then singularly barcoded and further isolated through Chromium Controller 10X Genomics.

Magnetic activated cell sorting

Following tumor digestion cells were incubated with microbeads following manufacturer's instructions. The following isolation Miltenyi Biotec kits were used: Dead Cell Removal Kit (Ref.

130-090-101), Debris Removal Solution (Ref. 130-109-398), CD326 (EpCAM) Microbeads Isolation Kit (Ref. 130-105-958).

Flow cytometry

Mouse tumors were cut into small pieces, disaggregated with Collagenase IV (Worthington Ref. LS004186) (1.5 mg/ml) and DNase I (Sigma-Aldrich Ref. D5025) (100 µg/ml) and filtered through strainers. $1x10^6$ cells were stained with specific antibodies (see table 1) incubating for 1h at 4°C. Cell death and apoptosis was evaluated through staining with DAPI and Annexin V-APC (Bender MedSystems Ref. BMS306APC). Cytofluorimetric analysis was carried out on a CyAn ADP ™ (Beckman Coulter, Brea, CA) flow cytometer and analyzed with FlowJo software.

Graph plotting and statistical analysis

Graphs and statistical analysis were performed with GraphPad Prism version 8.0. Bar plots were represented as mean and SD. Statistical significance was evaluated through Student t-test or one-way ANOVA. Heatmaps and dot-plots were plotted with Morpheus https://software.broadinstitute.org/morpheus.

Western Blot

Proteins were isolated using cell lysis buffer (50 mmol/l Tris-HCl, 150 mmol/l NaCl, 5 mmol/l Na3VO4, 1 mmol/l PMSF, 0.01 mmol/l ZnCl2, protease inhibitors, and 1% Triton X-100) and quantified with BCA (Thermo Scientific). Equal amounts of proteins (30 µg) were separated by 4-12% Bolt Bis-Tris Plus gel (Invitrogen) and transferred to nitrocellulose membrane (Invitrogen). Membrane was first blocked with 10% BSA in TBS-Tween (TBS-T) and incubated under gentile agitation for 1 hour at RT, then primary antibodies were added and (see Table 1) membrane was incubated overnight under agitation at 4°C. Thereafter, membrane was washed several times in TBST, and HRP-conjugated secondary Ab was added. After incubation at RT for 1 h, proteins were visualized by ECL system (Western Lightning Plus, Perkin-Elmer).

Hematoxylin and Eosin

10 µm tumor sections were fixed with Zinc fixing solution. Subsequently, they were stained for 4 minutes with Hematoxylin solution, then washed with tap water and stained with Eosin solution for 30 seconds. Finally, the slides were dehydrated for 5 minutes each in 50%, 70% and 90% ethanol, and twice for 10 minutes in xylene.

Cell viability assay

Pancreatic *ex vivo* CAFs were seeded at 2500 cells/well into 96-well plates and treated with different concentrations of the mut-Sema3A (0, 200, 400, 600, 800 ng/mL). After 24h, 48h and 72h medium was removed and cell viability was quantified by adding 100 µL of CellTiter-Glo®

reagent (Promega Ref. G7570) to each well. 96-well plates were gently mixed through a plate shaker at 150 rpm for 15 minutes at room temperature. 150 µL of volume was transferred from each well to a 96-well plate suitable for use with the plate reader. Luminescence was measured at 560 nm using VICTOR® X4 multilabel plate reader (Perkin Elmer).

Transwell invasion assay

40 µL of the diluted Corning® Matrigel® Matrix coating solution (1 µg/µL in PBS) were added into each polycarbonate 8-µm porous Transwell membrane (Corning Ref. 3342) with avoidance of air bubble formation while pipetting. Transwell membranes were incubated 1 h at 37°C. CAF suspension of 10^5 cells/mL in DMEM/F12 supplemented with 0.5% FBS was prepared and seeded in 100 µL volumes into the Transwell inserts (10^4 cells/insert), in presence or absence of 800 ng/mL mut-Sema3A. Lower wells were loaded with 500 µL DMEM/F12 supplemented with 1% FBS, in presence or absence of 800 ng/mL mut-Sema3A. After incubating for 72h the Transwell inserts were washed with PBS and fixed with 2.5% glutaraldehyde and stained with 0.1% crystal violet for 15 minutes, respectively. Pictures of the stained cells on the bottom side of the membrane were taken with Olympus BX60F-3 microscope using a 2.5X original magnification.

RNA In Situ Hybridization - RNAscope assay

mRNA expression of target genes was evaluated on OCT embedded samples using RNAScope Multiplex Fluorescent V2 Assay (Ref. 323100 Advanced Cell Diagnostics - a Bio-Techne brand®). Target genes are listed in Table 3. Sequences of target probes, preamplifier, amplifier, and label probe are proprietary (Advanced Cell Diagnostics, Hayward, CA).
The sections, 10 µm thickness, were fixed in 10% NBF at 4°C for 15 minutes and then dehydrated with alcohol scale. After pretreatment at room temperature with hydrogen peroxide (10 minutes) and protease IV (30 minutes), the samples were incubated for 2 hours at 40°C with appropriate probes. The signal was amplified and detected with OPAL dyes according to the ACDbio protocol and assigning OPAL570 at channel 1, OPAL690 at channel 2 and OPAL520 at channel 3.
Images of fixed tissues were acquired with Leica TCS SPE II confocal microscope, 40X of magnification, 1.5 of digital zoom and were analysed with NIH ImageJ (W. Rasband, NIH) software.
10 randomly chosen fields per slide were acquired to calculate the number of target RNA in individual cells identified by DAPI staining: we statistically estimated the average of spots each cell calculated as the number of total specific RNA spot/number of total cells each field.
To have an indication about the presence of more different RNA spots in the same cell, we utilized the Coste's method (223), via "Coloc2" tool of NIH ImageJ (PSF 1.5, 200 randomizations), in which comparing 2 different spot masks, if the p-value for the true colocation has the probability of 95% of confidence level, give as result "1".

Table 1. Antibodies used for immunofluorescence, western blot and flow cytometry.

	Brand	Ref.	Dilution	Assay
CD68	BIORAD	MCA1957	1:100	Immunofluorescence
CD8	EBioscience	14008182	1:100	Immunofluorescence
GZMB	Abcam	AMab4059	1:100	Immunofluorescence
MRC1	R&D	FAB2535G	1:100	Immunofluorescence
CD11c	BIORAD	MCA1369	1:100	Immunofluorescence
CD45	BD Miltenyi Biotec	550539 130-110-802	1:100 1 ug/10^6cells	Immunofluorescence Flow Cytometry
CK19	Novus Biologicals	nb100-687	1:100	Immunofluorescence
α-SMA	Sigma	A5228	1:100	Immunofluorescence
E-cadherin	Invitrogen Invitrogen R&D	14-3249-82 14-3249-82 FAB7481A	1:100 1:1000 1 ug/10^6cells	Immunofluorescence Western Blot Flow Cytometry
EpCAM	Abcam Biolegend	AMab71916 118206	1:100 1 ug/10^6cells	Immunofluorescence Flow Cytometry
β-Tubulin	Santa Cruz	SC9104	1:1000	Western Blot
CD4	BD	550539	1:100	Immunofluorescence
FoxP3	EBioscience	17S77382	1:100	Immunofluorescence
CD3	NOVUS BIOLOGICALS	NB600-1441	1:50	Immunofluorescence

Table 2. Gene probes used for rtq-PCR experiments.

	Brand	Ref.
GAPDH	Thermo Fisher	MM99999915_G1
ACTB	Thermo Fisher	MM01205647_G1
ACTA2	Thermo Fisher	MM00725412_S1
COL1A1	Thermo Fisher	MM00801654_G1
ISLR	Thermo Fisher	MM01700423_M1
CXCL12	Thermo Fisher	MM00445552_M1
DCN	Thermo Fisher	MM03003496_S1
PDGFRA	Thermo Fisher	MM00440701_M1
PLXNA4	Thermo Fisher	MM00558881_M1
VIM	Thermo Fisher	MM01333430_M1
BGN	Thermo Fisher	MM01191753_M1
IL6	Thermo Fisher	MM00446190_M1
S100A4	Thermo Fisher	MM00803372_G1
HSPA1A	Thermo Fisher	MM01159846_S1
PLXNA4	Thermo Fisher	MM00558881_M1
MMP2	Thermo Fisher	MM00439498_M1
CDH11	Thermo Fisher	MM00515466_M1
THBS2	Thermo Fisher	MM01279240_M1
CYGB	Thermo Fisher	MM00446071_M1
HSPA1B	Thermo Fisher	MM03038954_S1

Table 3. RNA-probes used for in situ hybridization experiments.

	Brand	Ref.
Mm-Islr-O1-C1	Advanced Cell Diagnostics	453321
Mm-Acta2-C2	Advanced Cell Diagnostics	319531-C2
Mm-Plxna4-C2	Advanced Cell Diagnostics	515491-C2
Mm-Dcn-C3	Advanced Cell Diagnostics	413281-C3
Mm-Cygb-C3	Advanced Cell Diagnostics	1113911-C3

RESULTS

1. Study design and experimental setting

1.1. Orthotopic PDAC model

Based on our previous findings describing an anti-tumor and anti-metastatic effect of a mutant form of Semaphorin 3A (mut-Sema3A) in a mouse model of PDAC (185,190,191) we sought to further investigate the molecular changes in the tumor microenvironment (TME) and the key cell subpopulations mainly affected by the treatment. We treated PDAC mice with mut-Sema3A for three weeks as previously described (185) (**Fig. 9**) and we observed a significant reduction of the tumor volume (by 53% and 48% respectively) (**Fig. 10 A, B**) (see also Methods).

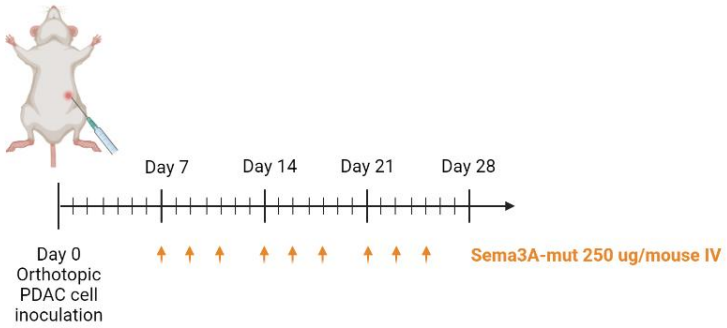

Figure 9. *Mice treatment schedule with intravenous administration of Mutant-Sema3A. Mice were inoculated with 1500 PDAC cells/mouse directly into the pancreas. One week post inoculation we started the treatment with Mutant-Sema3A 250 µg/mouse. Mice were treated three times a week for a total of three weeks.*

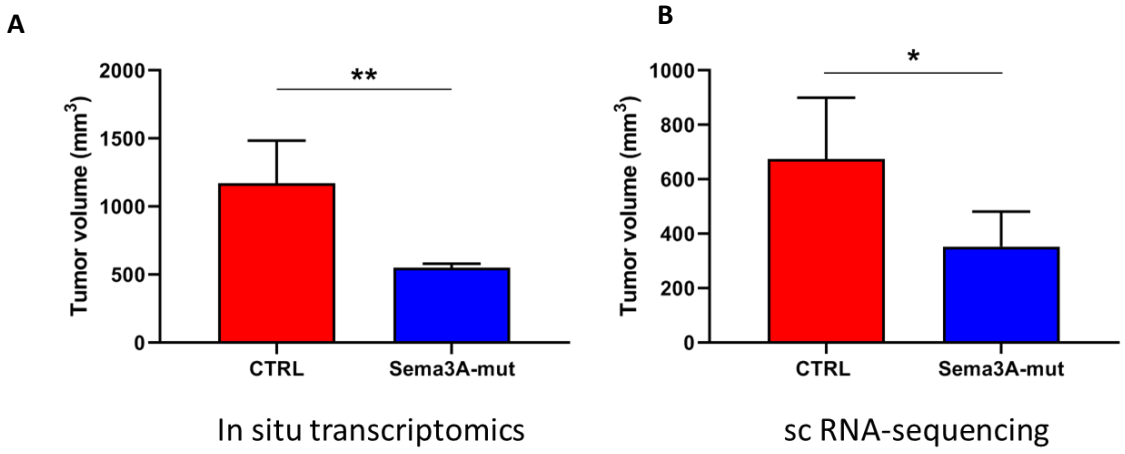

Figure 10*. Tumor volume evaluation following mut-Sema3A treatment of PDAC bearing mice. The decrease is of about 50% following three weeks of treatment.* ***A)*** *Treatment group employed for the In Situ Transcriptomics experiments. 7 control and 5 Mut-Sema3A replicates were plotted with GraphPad Prism 8. Statistics was implemented in GraphPad Prism 8 and analysis through the Student T-test highlighted a p-value of 0.0014. The decrease in tumor volume is of about the 53%.* ***B)*** *Treatment group employed for the of sc-RNA sequencing experiments. 5 control and 4 Mut-Sema3A replicates were plotted with GraphPad Prism 8. Statistics was implemented in GraphPad Prism 8 and analysis through the Student T-test highlighted a p-value of 0.04. The decrease in tumor volume is of about the 48%.*

In order to have an initial overview of the main TME components in the PDAC tissues derived from our treatment groups, we performed a characterization, by means of Immunofluorescence (IF) and confocal microscopy (CM), of the tumor and TME populations, such as immune cells ($CD45^+$), epithelial tumor cells ($EpCAM^+$, $CK19^+$, $E\text{-}Cad^+$) and fibroblasts ($\alpha\text{-}SMA^+$) (**Fig. 11**). The percentage of $CD45^+$- immune cells clearly outnumbers the total amount of $CK19^+$- tumoral cells, confirming the suitability of our mPDAC model in recapitulating human PDAC. Moreover, α-SMA defined a fibroblast subset (**Fig. 11 middle panel**), that were found to be often enriched in the tumor-edges, and pericytes (**Fig. 11 right panel**). We further analyzed the levels of epithelial tumor cells with EpCAM and E-Cad, and we confirmed the paucity of tumor cells in this model and we observed the preponderance of EpCAM over E-Cad in characterizing PDAC cells (**Fig. 11 right panel**).

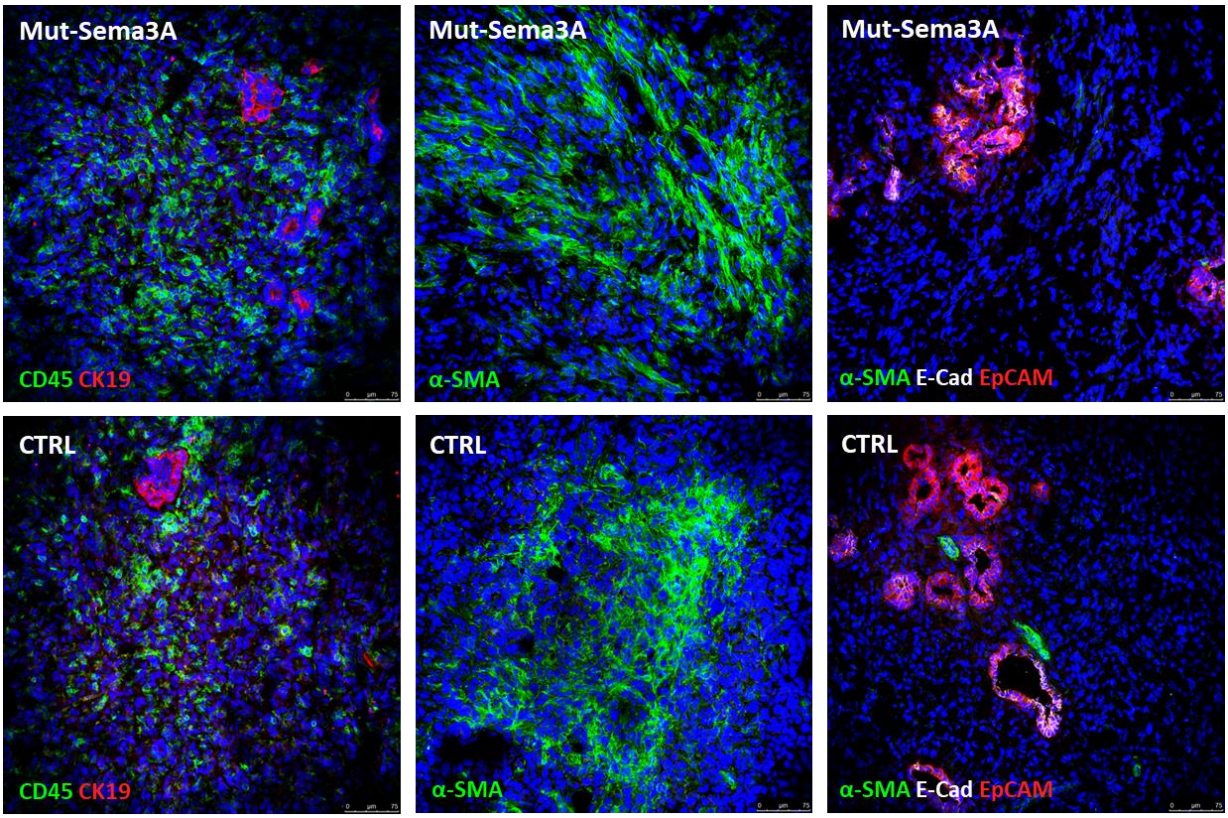

Figure 11. *PDAC tumor characterization with known tumor and TME markers. To visualize the principal components of our PDAC mouse model we performed immunofluorescence staining with markers identifying epithelial tumor cells characterized by CK19, E-Cad and EpCAM expression, $\alpha\text{-}SMA^+$- cells (fibroblasts and pericytes) and $CD45^+$- immune cells. No substantial changes were evident between the control and the Mut-Sema3A treated tumors. Pictures are representative of five fields acquired for every sample, for a total of 7 control samples and 5 mut-Sema3A treated samples.*

Since our initial aim was to undercover the mechanisms lying under the complex crosstalk among tumor cells and stromal cells in this murine PDAC model, we carried out single cell (sc) RNA-sequencing analysis (*10x Genomics* Chromium Controller) (**Fig. 12**) coupled with Spatial Transcriptomics (*10x Genomics* Visium Spatial gene expression) using RNA samples derived from mut-Sema3A-treated and control (untreated) PDAC tumors.

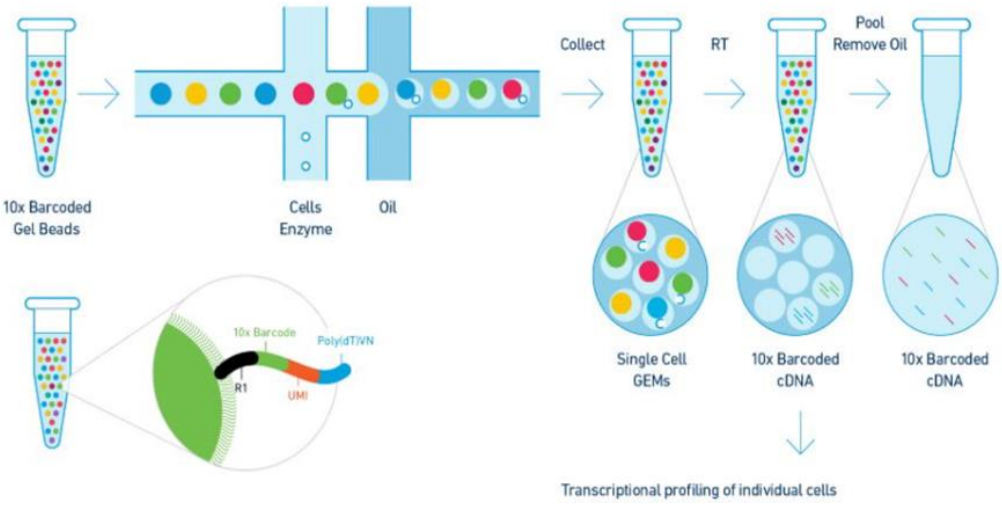

Figure 12. *10x Genomics Chromium Controller single cell RNA-sequencing. In order to perform transcriptome sequencing on single cells, the Chromium Controller separates cells into single-cell gel droplets, each of them has a unique barcode identifier. Through reverse transcription a barcoded cDNA library is created in each droplet, and it is sequenced. The procedure has been performed with Chromium Next GEM Single Cell 3' Reagent Kits v3.1 Dual Index and Chromium Controller instrument (10X Genomics, Inc; Pleasanton, CA, US).*

Considering the strong decrease in tumor volume following treatment, we analyzed 2 control samples and 4 mut-Sema3A-treated samples for the sc-RNA-sequencing analysis (**Fig. 10B**). On the other hand, one control and one treated tumor were used for the Spatial Transcriptomics experiment (**Fig. 10A**). The sc-RNA-sequencing and the Visium Spatial gene expression employed tumors deriving from 2 independent treatments in which we maintained the same dose and treatment schedule. We chose not to use samples arising from the same experiment to strengthen our findings to a greater extent.
Although we observed that tumoral cells represent the minority of the cells in this tumor model, which faithfully recapitulates human PDAC (**Fig. 11**), to analyze more selectively the TME, we decided to sort out PDAC cancer cells from the tumor mass of mPDAC mice, to enrich the samples with stromal cells, before proceeding with the single cell sequencing.

1.2. Protocol setting for tumor epithelial cell depletion

To obtain a viable cell suspension mostly enriched in TME cells, we decided to eliminate epithelial PDAC cells from our cell suspension, optimizing and adapting published protocols (71,224,225). In order to obtain the standard quality sufficient to undergo single cell RNA-sequencing, we evaluated several parameters characterizing the cells, such as: cell viability, apoptotic state, doublet percentage and epithelial markers expression. First, we assessed cell viability following enzymatic tumor dissociation (**Fig. 13**) through trypan blue and flow cytometry (FC), to check the level of mortality of the cells after the digestion process.
Disappointingly, both with trypan blue and through FC analysis, cell viability resulted to be very low (less than the 10% of total live cells) (**Fig. 14 left panel**). We decided therefore to perform a Magnetic Associated Cell Sorting step to enrich live cells. We used the Dead Cell Removal kit from Miltenyi (see methods) to devoid the mix from dead cells (**Fig. 14**), but unexpectedly,

although the total number of live cells was doubled, it was still under the 15% (**Fig. 14 right panel**).

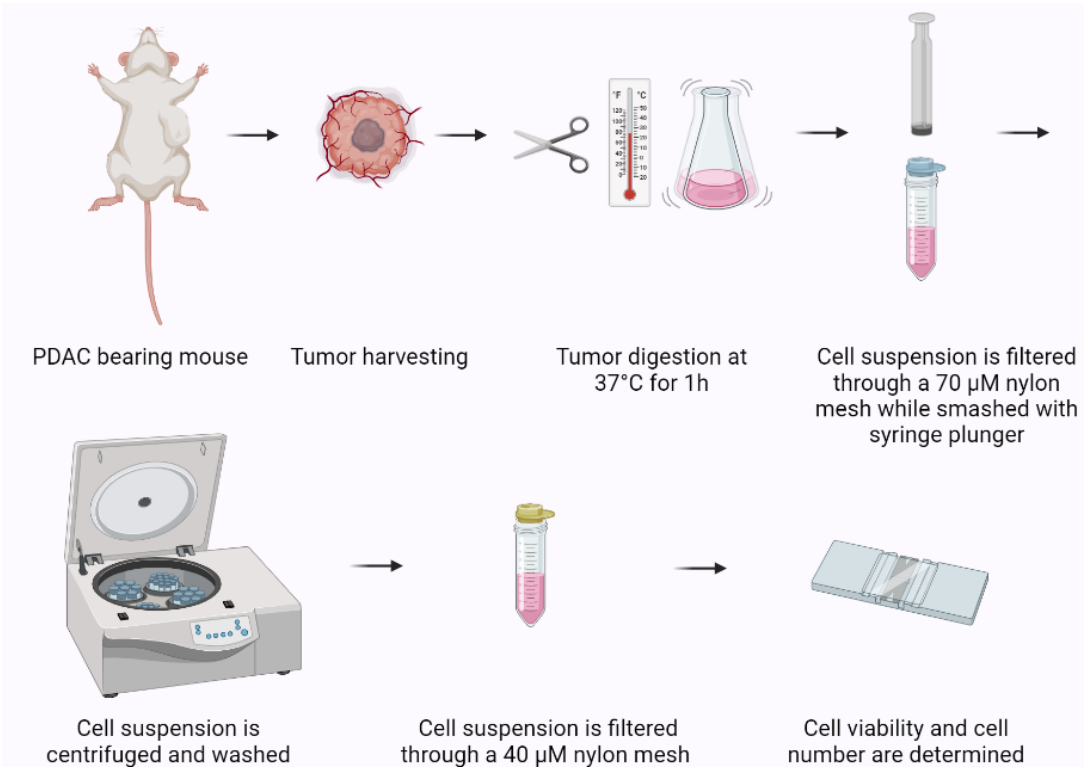

Figure 13. *Enzymatic PDAC tumor dissociation. Tumor masses are harvested from mice and immediately processed. First, they are finely minced with scissors and scalpels, then they are incubated with a digestion cocktail made of collagenase IV and DNase I and kept on rotation at 37° for 1h. Following these steps, the mix is filtered through a 70 µM nylon mesh while smashed with a syringe plunger. After some washing and centrifugation steps cell number and viability is determined through trypan blue counting.*

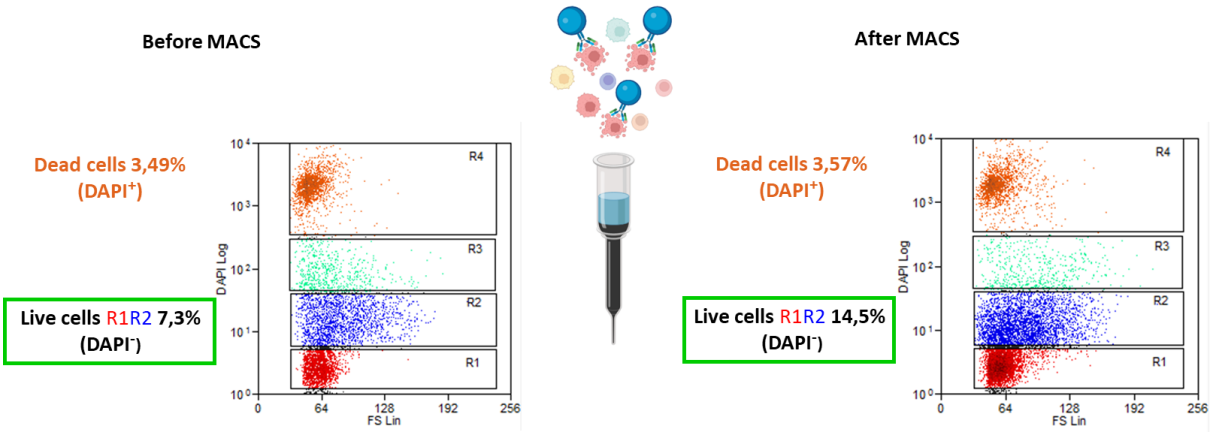

Figure 14. *Cell viability is assessed through flow cytometry following MACS of live cells with the Dead Cell Removal kit. Prior to dead cell removal, the cell suspension was in great part composed by debris, dead cells and doublets, while live cells represented the 7,3% of the total events. Following MACS, the number of live cells grows up to 14,5%, but it is still too low to proceed with sc-sequencing.*

To further solve this issue, we decided to process our samples through the Fluorescence Activated Cell Sorter after staining the cellular mix with DAPI. Finally, we obtained a cellular suspension of 82.4% live cells, DAPI$^-$ (**Fig. 15**).

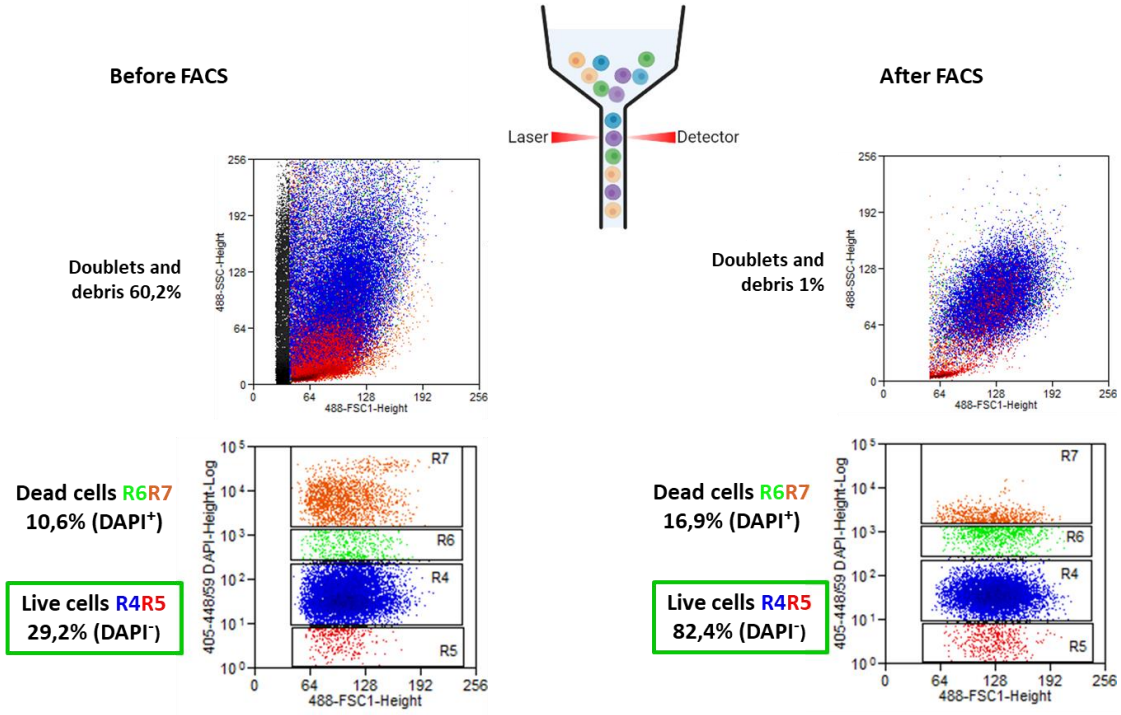

***Figure 15**. Cell viability assessment through flow cytometry following FACS, reveals that DAPI$^-$ live cells hugely increase: from 29,2% of total live cells we reach the 82,4% cell viability after selection with DAPI. This represents a good cell suspension quality for downstream analysis.*

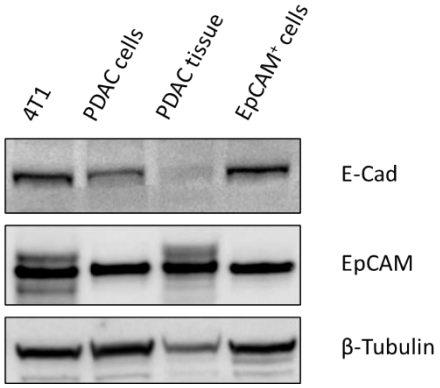

***Figure 16**. Western Blot displaying the expression levels of E-Cadherin and EpCAM. The tested samples consisted in 20 µg protein loading and included Triple Negative Breast Cancer 4T1 cells as a positive control, PDAC cells in 2D cultures, PDAC tissue from murine tumors and EpCAM$^+$-cells deriving from MACS EpCAM selection. Normalization on β-tubulin highlights a higher level of EpCAM in PDAC tissue lysates respect to PDAC 2D cultures. Importantly these data confirm EpCAM expression on PDAC cells and its relevance in epithelial cancer cell depletion from the tumor-dissociated cell suspension.*

Based on our main aim to purify TME from epithelial tumor cells, we first checked the expression of tumoral markers into the tumor-harvested cells. We observed that tumoral cells in our PDAC model expressed Epithelial Cell Adhesion Molecule (EpCAM) and Epithelial-Cadherin (E-Cad) (**Fig. 11**).
We confirmed the overexpression of these markers in PDAC cells, by means of Western Blot (WB) (**Fig. 16**) and quantitative Real-Time PCR (qRT-PCR).

Importantly, EpCAM represented a more expressed molecule in PDAC derived tissues, respect to E-Cad, that further corroborated our initial hypothesis based on published data (71) in which colleagues purified PDAC cell suspensions through $EpCAM^+$-cell depletion. Moreover, we performed flow cytometry on freshly dissociated PDAC tumors (see methods) in order to evaluate the percentage of $E\text{-}Cad^+$-cells, $EpCAM^+$-cells and $CD45^+$-cells (immune cells) (**Fig. 18, 19**).
Motivated by previous findings (71,226) and by our preliminary results showing that the staining for E-Cad did not represent a large cell portion throughout the tumor slice (**Fig. 11, 16**), we decided to eliminate epithelial tumoral cells from the cell suspension through the exclusion of $EpCAM^+$-cells. We employed the MACS technique, using anti-EpCAM microbeads (**Fig. 17**).

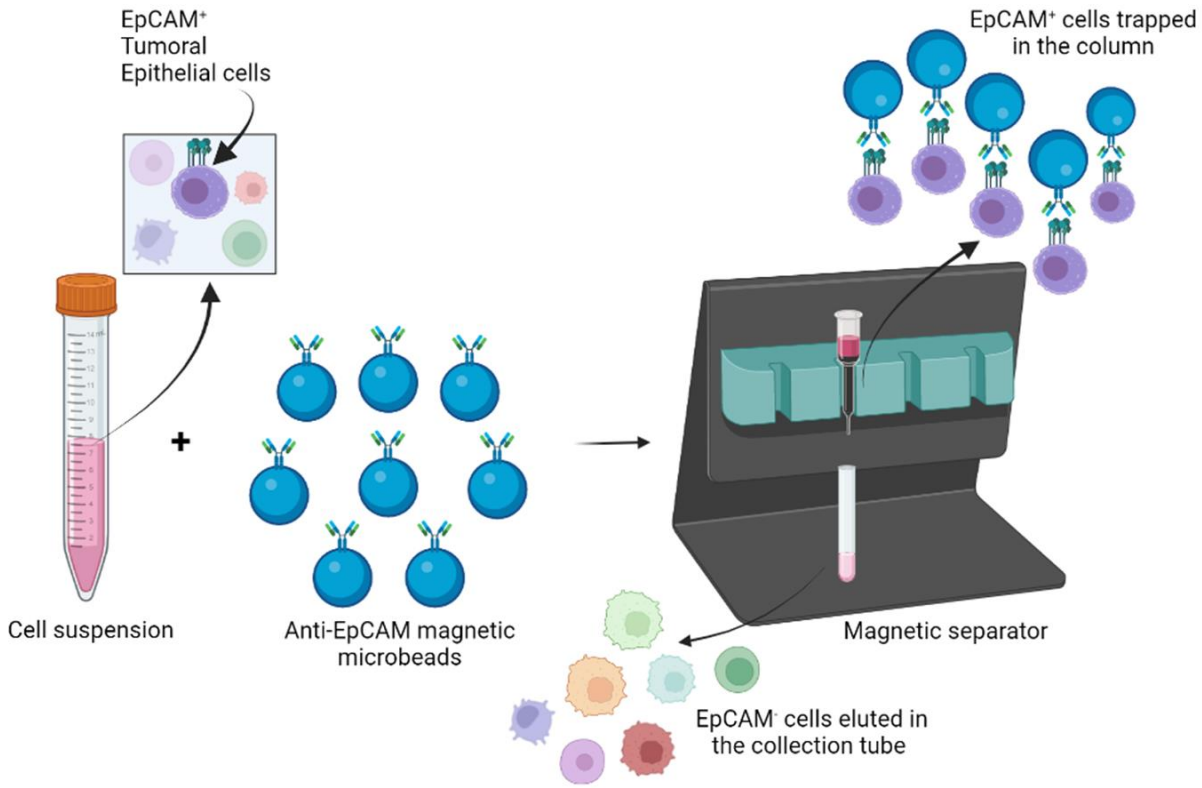

Figure 17. *$EpCAM^+$-cells exclusion through magnetic microbeads isolation. Following digestion, the cell suspension is incubated with EpCAM magnetic microbeads according to manufacturer instructions. After the incubation, the cell suspension is eluted into a LS column (Miltenyi): $EpCAM^+$-cells bound to magnetic microbeads will remain trapped inside the column, while $EpCAM^-$-cells will flow through it, and will be harvested in a clean tube.*

To evaluate its efficacy, we performed Flow Cytometry on freshly dissociated cells, on cells eluted following MACS with EpCAM microbeads and on cells bound to the magnetic column ($EpCAM^+$-cells hypothetically). The flow cytometry (FC) analysis showed that about the 57% of total live

cells were positive for E-Cad (**Fig. 18 A**), while the 48% were positive for CD45 (**Fig. 18 A**), meaning that there was a partial overlapping of these two markers. On the other hand, the 28% of cells resulted positive for EpCAM (**Fig. 19**). It is conceivable that a portion of the tumoral epithelial cells were double positive for E-Cad and EpCAM. Unfortunately, we could not appreciate an EpCAM^{+}-cells depletion in the whole mix (**Fig. 18 B**) or an EpCAM^{+}-cell enrichment in the column-trapped cells (**Fig. 18 C**). Considering the unsuccess of the MACS technique, we opted again for FACS to obtain a cellular mix depleted of epithelial tumor cells. In order to devoid the cellular mix from dead and EpCAM^{+}-cells, while keeping live EpCAM^{-} cells, we used the negative selection, staining the cellular mix with the anti-EpCAM antibody and DAPI.

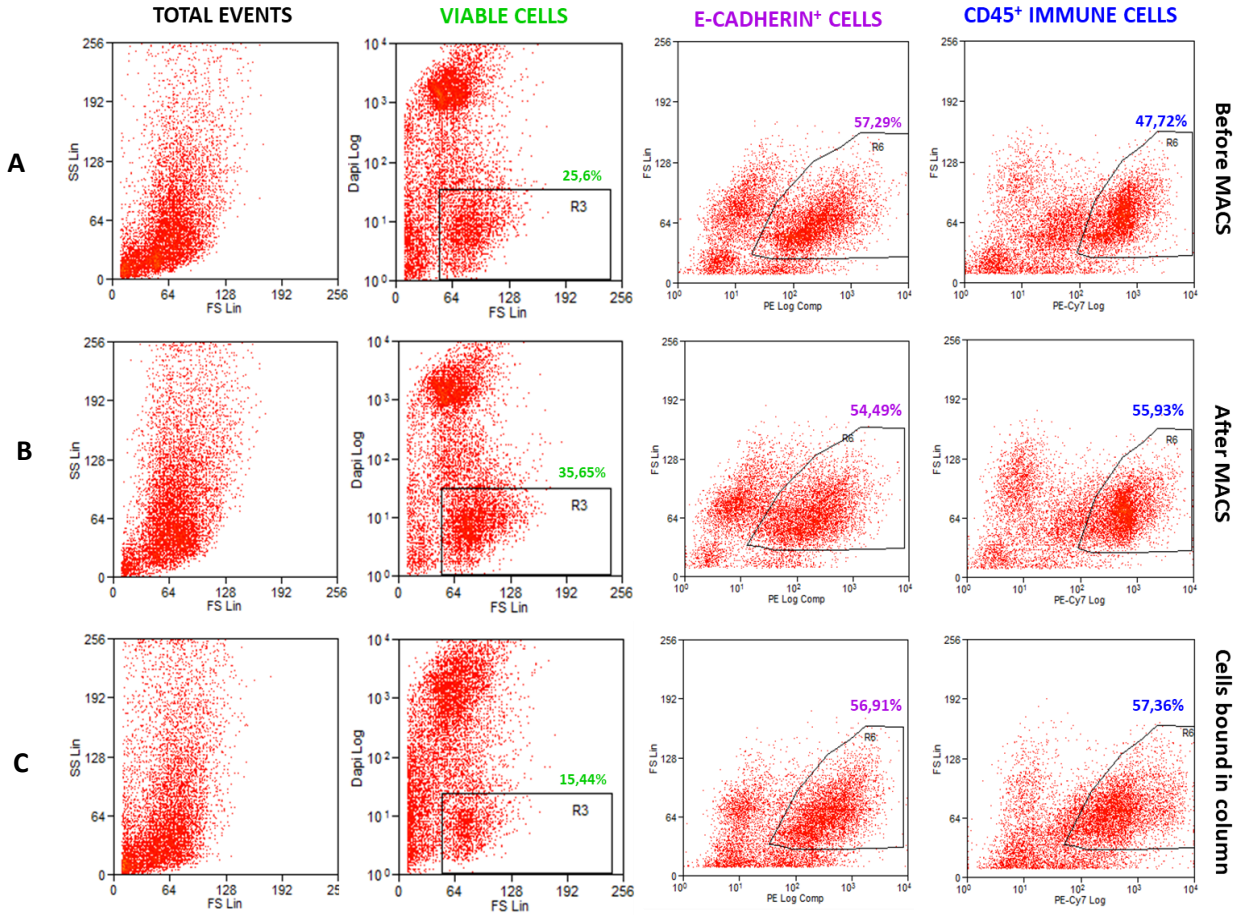

***Figure 18**. Fluorescent staining of PDAC deriving cells for E-cad and CD45 shows the cell type percentage before, after the MACS and bound to the magnetic columns. Cells were isolated through anti-EpCAM magnetic microbeads. A depletion of EpCAM^{+}-epithelial cells was expected, but the percentage of E-Cad^{+}-cells remains nearly unvaried when we compare the whole cell suspension (before MACS), the EpCAM^{+}-depleted (after MACS) and the EpCAM^{+}-enriched (cell bound in column). The same can be noticed for what it concerns CD45^{+}-immune cells: the EpCAM^{+}-cells bound to the column should specifically be epithelial tumoral cells, and not be constituted by the 57,36% of immune cells. This brings us to the conclusion that EpCAM-magnetic beads are not efficient enough for the needed applications.*

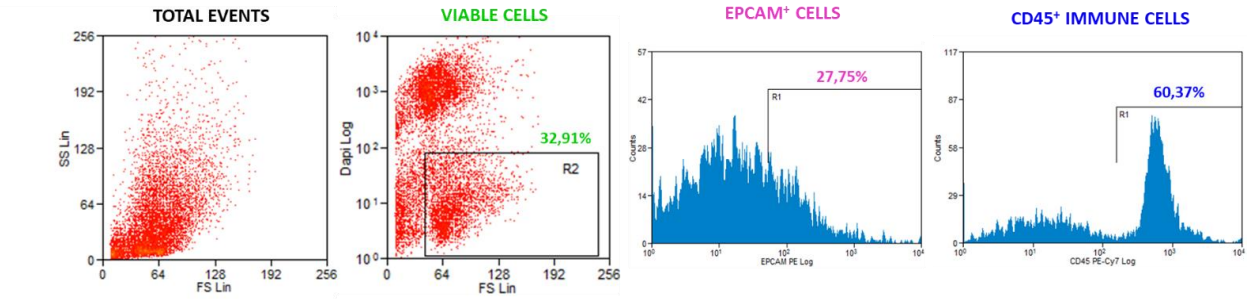

Figure 19. *Fluorescent labeling of PDAC deriving cells for EpCAM and CD45 markers. About the 28% of total live cells is composed by EpCAM$^+$ epithelial tumor cells, while the 60% represents CD45$^+$ immune cells.*

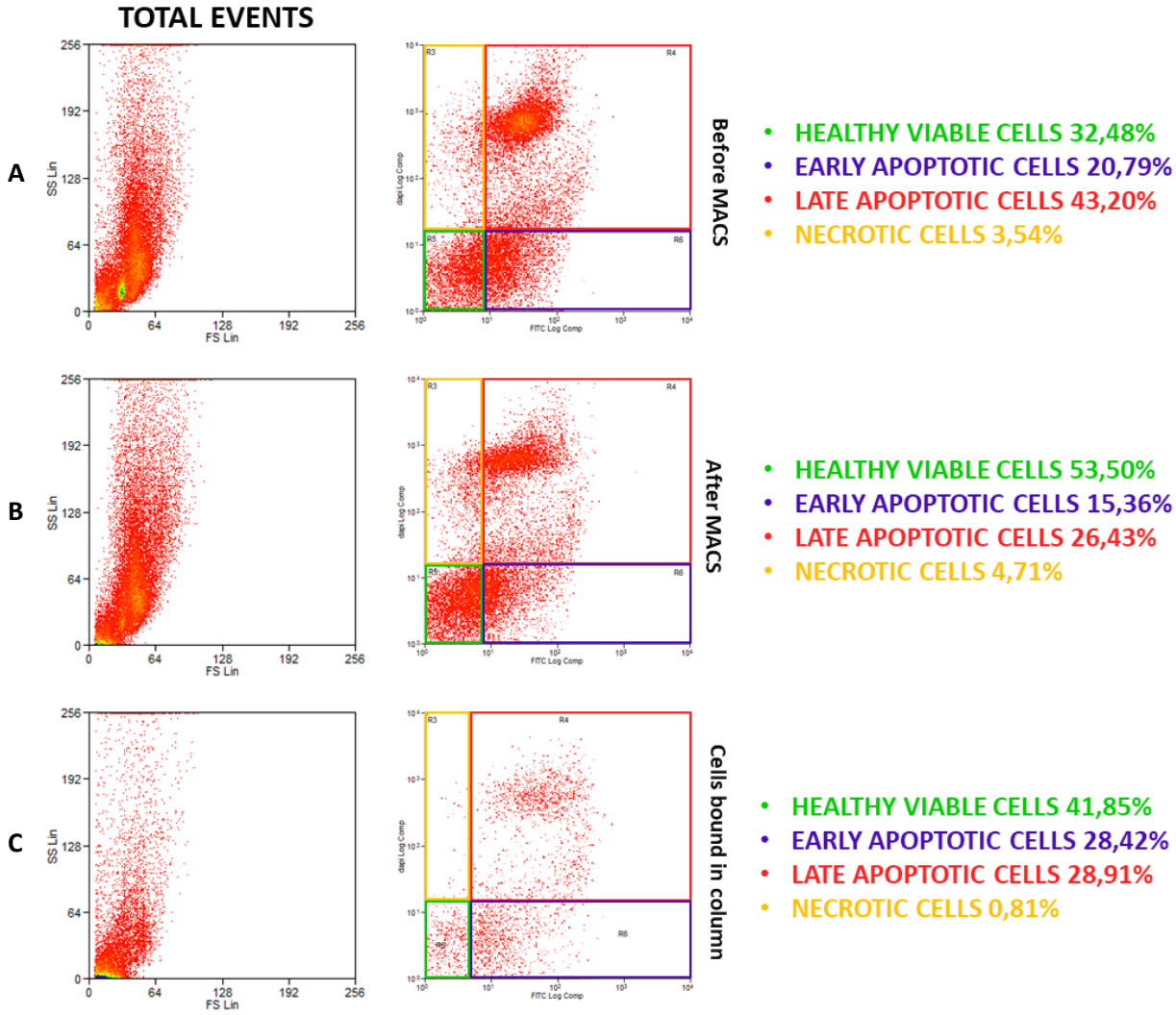

Figure 20. *Fluorescent labeling of PDAC deriving cells with Annexin V and DAPI to evaluate cell viability (DAPI$^-$ and Annexin V$^-$), necrotic cells (DAPI$^+$ and Annexin V$^-$), early apoptotic cells (Annexin V$^+$), late apoptotic cells (DAPI$^+$ and Annexin V$^+$). Panels A and B represent samples prior or following MACS with EpCAM, panel C represents cells bound to the column (EpCAM$^+$-cells).*

Before proceeding with the FACS, we checked the apoptotic state of the cells. To this aim we used the Annexin V-DAPI staining. Annexin V is a molecule used to recognize apoptotic cells due to its ability of binding to phosphatidylserine, a phospholipid exposed on the outer leaflet of the plasma membrane by apoptotic cells. This allowed us to assess the percentage of cells that were in early apoptosis and that could not be identified with DAPI. In this case we found about the 21% of cells in an early apoptotic state (**Fig. 20 A**) and about the 32% of healthy viable cells. This allowed us to conclude that the percentage of cells in early apoptosis was within the standard of FACS and the single cell-sequencing analysis.
Finally, since the cell suspension quality was appropriate for proceeding with the subsequent analysis, we proceeded with labeling it with DAPI and EpCAM, and selected cells that were negative for both these parameters (**Fig. 21**). In conclusion, through FC we confirmed that the cells isolated through FACS were largely negative for EpCAM and DAPI, successfully achieving the 96-97% of live and EpCAM$^-$ cells, in both control and treated samples (**Fig. 22**).
T

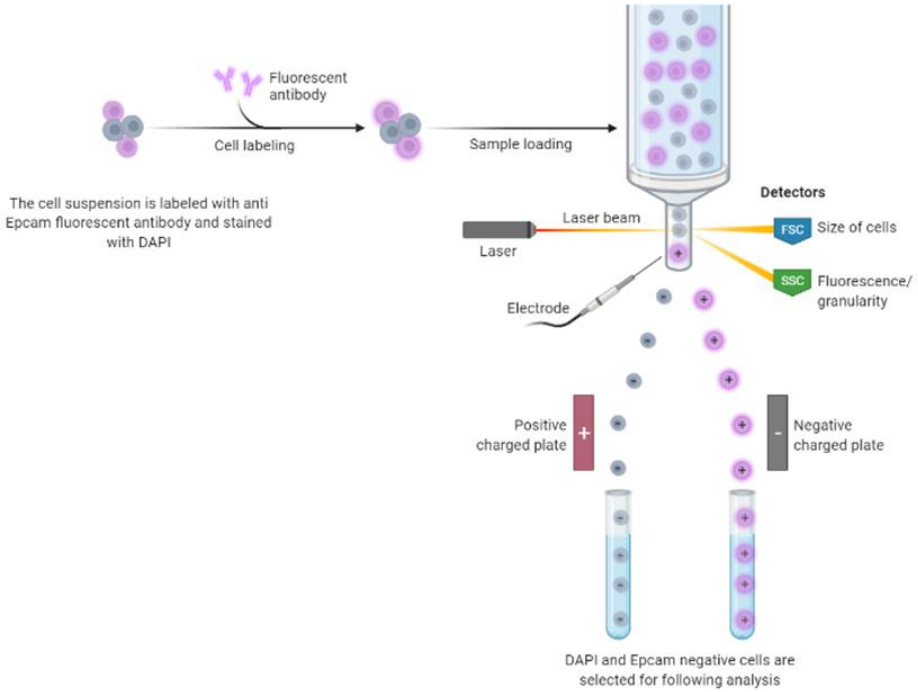

Figure 21. *FACS of fluorescent labeled cells with DAPI dye and EpCAM antibody for negative isolation. The cell suspension is stained for DAPI and EpCAM: cells will pass through a laser that will excite the fluorophores at given wavelengths, and subsequently the detectors will discard the cells that are positive for the chosen parameters.*

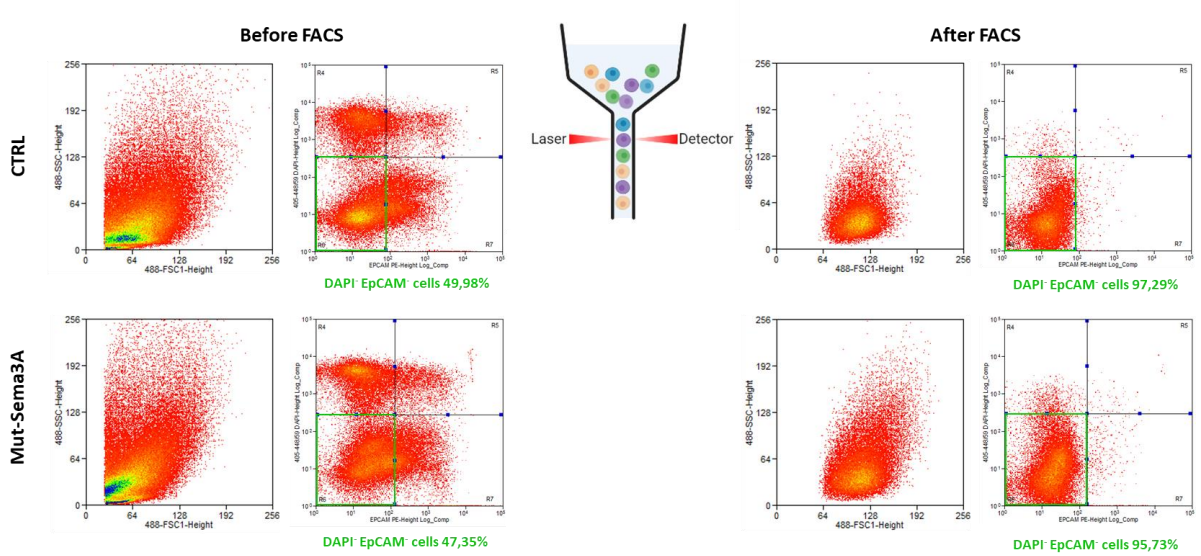

Figure 22. *Flow cytometry analysis to evaluate the amount of DAPI$^-$ and EpCAM$^-$ cells following FACS. After performing FACS for excluding dead and EpCAM$^+$-cells, we managed to obtain a highly pure cellular mix almost devoid by tumor cells and dead cells: we achieved the 97% of purity for the control and the 96% of purity for the treated sample.*

2. Semaphorin 3A induces gene-reprogramming in the PDAC TME

2.3. Single cell analysis of mPDAC and cluster annotation

The complex and stepwise experimental procedures that we set up, allowed us to find the best possible conditions in order to obtain high quality data from our single cell RNA-sequencing. Following the FACS negative selection 4,8 x 10^5 and 4,2 x 10^5 cells were respectively harvested from control and mut-Sema3A-treated tumors. The totality of cells was processed in the single cell RNA-sequencing facility (at IRCCS-FPO) at a dilution of 500 and 350 cells/µl respectively, and the proper volume of cell suspension (based on the 10X Genomics user guide) was used to achieve 7.000 targeted cell recovery.

Subsequently to the single cell separation, a total number of 3623 and 3392 EpCAM$^-$ and DAPI$^-$ cells for control and mut-Sema3A-treated, respectively, were sequenced with the Illumina NextSeq500 sequencer. These cells underwent quality control concerning their cell cycle status, their transcript number and the number of reads per transcript, and high-quality cells were selected for further analysis.

Single cell RNA-sequencing and unsupervised clustering of 1645 and 1376 cells for control and Mut-Sema3A treated samples revealed 11 clusters in control and 8 cluster in Mut-Sema3A treated samples respectively. Clustering was performed using Louvain modularity method implemented in Seurat, embedded in rCASC package. The number of clusters was defined based on the level of cluster stability, determined by the Cell Stability Score (CSS), implemented in rCASC (see methods) (**Fig. 23**).

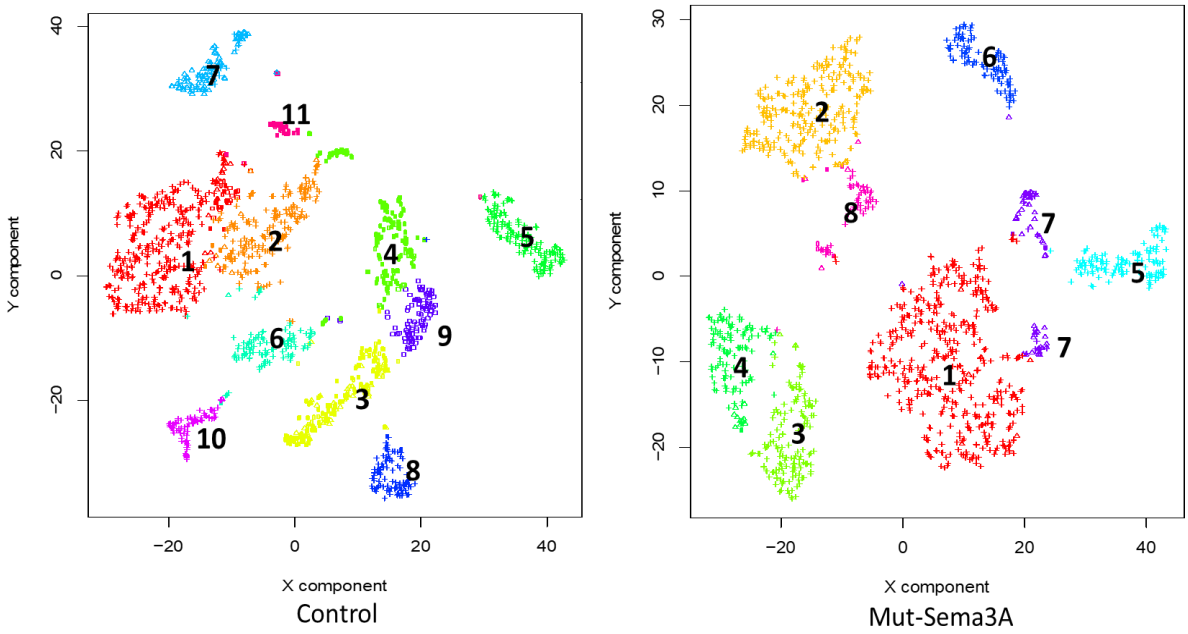

Figure 23*. Unsupervised clustering of 1645 and 1376 cells for control and Mut-Sema3A treated samples reveals 11 clusters in control and 8 cluster in Mut-Sema3A. Clustering was performed using Louvain modularity method implemented in Seurat, embedded in rCASC package. The number of clusters was defined based on the level of cluster stability, determined by the Cell Stability Score (CSS), implemented in rCASC. The clusters of the control are in order: macrophages I, macrophages II, neutrophils I, neutrophils II, fibroblasts, dendritic cells, PDAC cells, B lymphocytes, neutrophils III, T lymphocytes, macrophages III. The clusters of the mut-Sema3A are in order: macrophages, macrophages II, PDAC cells, fibroblasts I, fibroblasts II, T lymphocytes, neutrophils I, neutrophils II, pericytes.*

Cluster identification was assessed based on previous findings (224) and clusters were further manually annotated through known markers from published data and Enrichr (https://maayanlab.cloud/Enrichr/). We annotated one CAF cluster in the control (cluster 5) and two distinct CAF clusters in the Mut-Sema3A (clusters 3 and 4). In addition, we detected: i) 3 macrophage clusters in the control (clusters 1, 2 and 11) and one macrophage cluster in the treated sample (cluster 1); ii) 3 neutrophil clusters in the control (clusters 3, 4 and 9) and 2 in the treated sample (clusters 3 and 7); iii) one T lymphocyte cluster in each sample (cluster 10 control and cluster 5 Mut-Sema3A); iv) one B lymphocyte cluster and one dendritic cell cluster present in controls (cluster 8 and cluster 6 respectively), but absent in treated samples ; v) one pericyte cluster in the treated sample (cluster 8), that was absent in the controls; vi) one PDAC cell cluster both on controls and mut-Sema3A samples (cluster 7 control and cluster 2 Mut-Sema3A) (**Fig. 24, 25**). It is conceivable that this PDAC cell cluster still present in the samples after the negative selection described above (**Fig. 18, 19, 21, 22**) was due to the fact that not all epithelial tumoral cells homogeneously express EpCAM, and, therefore, some tumors cells expressing other markers were not depleted from the tumor mass. In any case, the proportion of these unselected cancer cells is very low, compared to the other TME cells, and did not interfere significantly with the analysis.
Next, we wanted to estimate the cell amount in each cluster and to compare the corresponding percentage of controls with mut-Sema3A-treated tumors. Notably, cluster composition clearly differed between control and mut-Sema3A treatment: first, the number of fibroblasts doubled in the treated sample (20,71%) respect to the controls (9,06%) (**Fig. 24**).

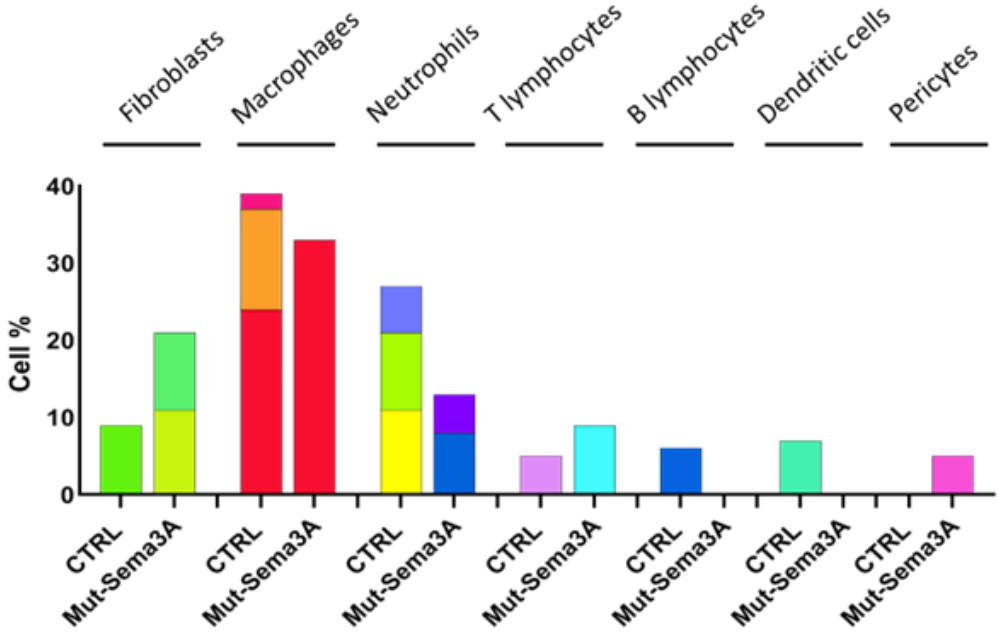

Figure 24. *Graphical representation of cell clusters as percentages, calculated on the entire amount of sequenced cells. Graph was performed with GraphPAD Prism 8. The clusters identified in the control were composed by: one fibroblast cluster (9,06%), 3 macrophage clusters (23,65%, 13,19%, 2,31%), 3 neutrophil clusters (10,76%, 10,27%, 5,65%), one T-lymphocyte cluster (5,11%), one B lymphocyte cluster (6,02%) and one dendritic cell cluster (7,05%). The clusters in the mut-Sema3A instead comprised: 2 fibroblast clusters (11,12% and 9,59%), one macrophage cluster (33,28%), 2 neutrophil clusters (7,63% and 4,94%), one T-lymphocyte cluster (9,38%) and one pericyte cluster (4,65%).*

Macrophages and neutrophils decreased in the Mut-Sema3A from 39,15% to 33,28% and from 26,88% to 16,06% respectively (**Fig. 24**). T lymphocytes increased in the treated samples, almost doubling their amount and switching from the 5,11% in the control to reach the 9,38% in the Mut-Sema3A (**Fig. 24**). This event is consistent with our findings showing increased amounts of $CD8^+$-T cells in PDAC tumors after Sema3A treatments (see chapter 4). On the other hand, B lymphocytes and dendritic cells were only identified in the control condition, in a percentage of 6,02% and 7,05% respectively, while pericytes were found solely in the Mut-Sema3A and comprised the 4,65% of the total cells (**Fig. 24**). This last finding, demonstrating the enhanced amount of pericytes, is again consistent with previous data of our laboratory in which a significantly improved vessel normalization and pericyte coverage following murine PDAC treatment with mut-Sema3A has been demonstrated (185,190,191).

To additionally confirm the nature of the clusters we annotated, we plotted the sc-RNA-seq expression data into a dot-plot, visualizing the expression level of well-established markers showing the lineage of clusters (**Fig. 25**).

Macrophages showed high expression levels of Aif1, CD68, CSF1R, CCR2. The genes that were present in the fibroblast clusters were Lum, Col1a1, Dcn, Dpt, Pdgfra. T cells were instead characterized by several subunits of the T-cell receptor and by CD4 and CD28, while neutrophils showed peculiar expression of markers such as Mmp9, Elane, Ly6G, Mpo, Csf3R, all mostly known as pro-tumoral neutrophil markers. B cells displayed clearly specific markers including CD19, Pax5, CD79A, Ms4a1 and dendritic cells expressed high levels of Itgax, H2-aa, H2-ab1

and CD80. The pericyte population, identified in the treated condition only, was showing differentially high levels of Angpt2, Kdr and Cdh5, but they were also positive for some epithelial markers, therefore we believe they do not constitute a highly pure population. Finally, the remaining PDAC cells that were not excluded trough FACS, were expectedly expressing epithelial genes such as Cdh1, Krt19, Krt7 and Krt9, but they were missing high expression of EpCAM (**Fig. 25**).

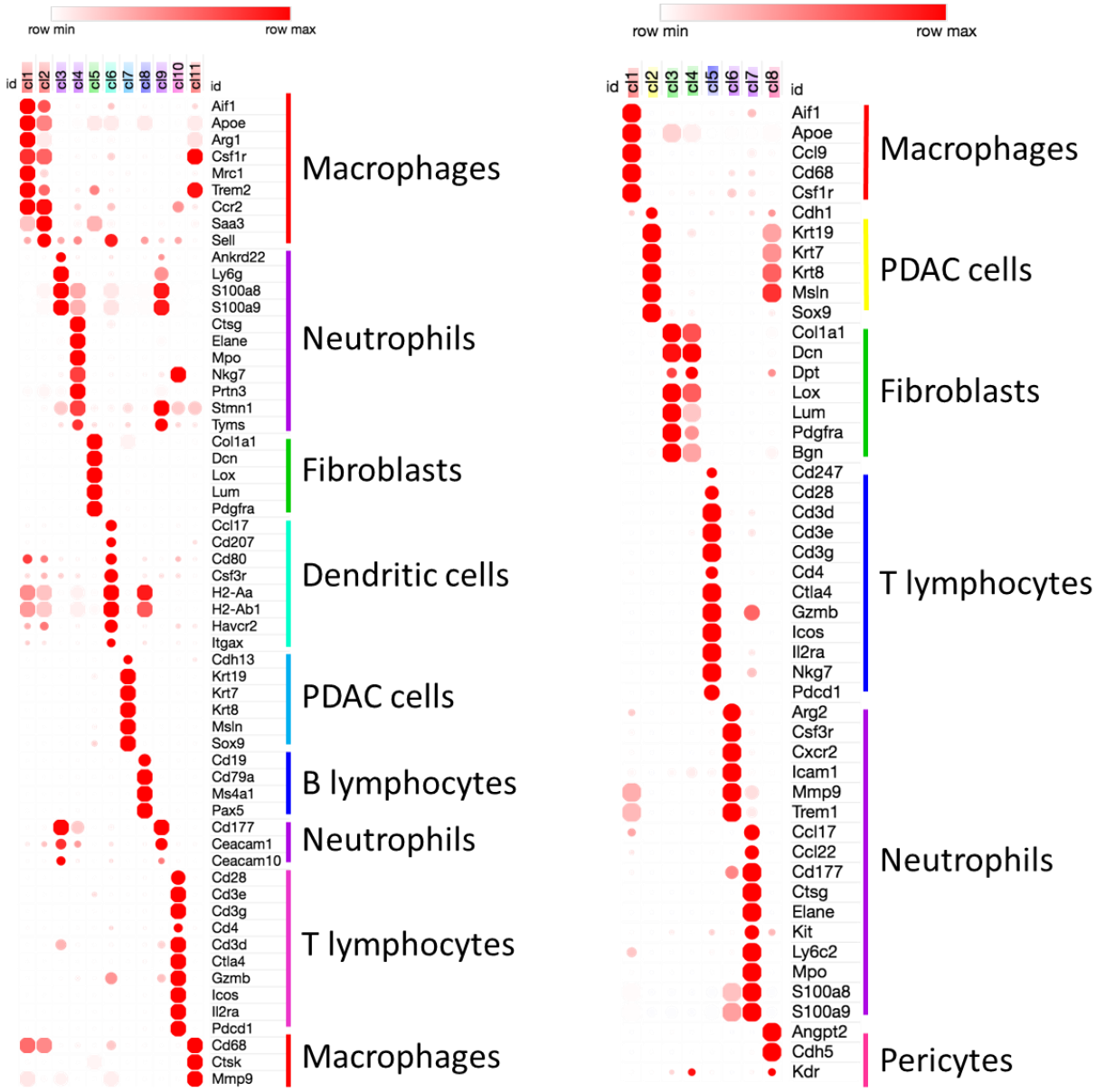

Figure 25. *Dot-plot representing the expression level of well-established markers across all clusters in control and mut-Sema3A treated samples. 11 clusters were defined in the control condition: 3 of them were annotated as macrophages and 3 of them were constituted by neutrophils; the other 5 clusters were described as T lymphocytes, B lymphocytes, dendritic cells, fibroblasts and PDAC cells. The treated sample instead was made of 8 clusters among which there were 2 neutrophil and 2 fibroblast clusters, one macrophage cluster, one T lymphocyte, one pericyte and one PDAC cluster.*

2.4. Fibroblasts are reprogrammed into two distinct subpopulations when tumors undergo mut-Sema3A treatment

Unexpectedly, among the different populations of the TME, the most distinctly defined cells were cancer-associated fibroblasts (CAFs), represented by cluster 5 in the control, and by clusters 3 and 4 in the mut-Sema3A treated sample. Surprisingly, cluster annotation highlighted that mut-Sema3A was able to induce the appearance of two populations of fibroblasts in the treated tumors compared to the control (**Fig. 23, 24, 25, 26, 27**). First, by assessing the expression of known fibroblast markers in these populations, we corroborated the fact that cluster 5 control, and clusters 3 and 4 of the mut-Sema3A were *bona fide* fibroblasts, with distinct different transcriptomic profiles respect to the rest of the other clusters (**Fig. 26**).

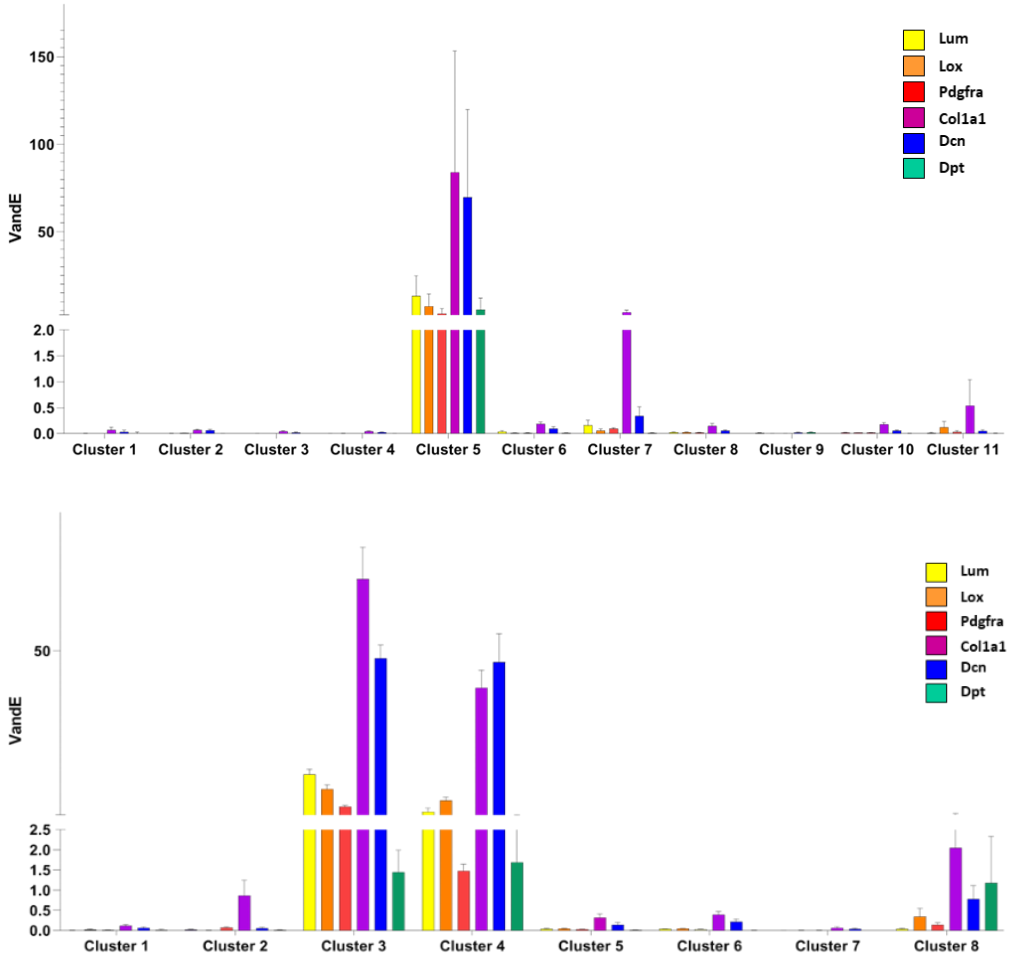

Figure 26. *Histogram plot representing 5 of the most characteristic fibroblast genes sequenced in our sc-RNA-sequencing experiment: Lum, Dcn, Col1a1, Dpt, Lox and Pdgfra are specifically upregulated in cluster 5 control and clusters 3 and 4 of the treated sample confirming their specificity and the fibroblastic nature of those clusters. Plot was implemented in GraphPAD Prism 8.*

Then we calculated the percentage of CAFs on the total cell number and surprisingly we found out that it was more than doubled in the mut-Sema3A-treated samples compared to controls (9.06%

CAFs in cluster 5 control and 11.12% and 9.59% CAFs in cluster 3 and 4 of the mut-Sema3A treated tumors respectively, **Fig. 24**).

To understand the potential differences of the expression profile in control CAFs compared to mut-Sema3A-treated CAFs, we performed Venn diagram crossing between the differential expressed genes of every fibroblast cluster. Both cluster 3 and cluster 4 of the mut-Sema3A share only 50% of gene similarity with control CAFs, indicating that their transcriptome was reprogrammed towards different fibroblastic phenotypes.

Based on previous findings describing CAF subtype signatures in pancreatic cancer (71,227,228) we started to better identify the CAF subtypes in our fibroblast clusters. Notably, while the CAF cluster of the control recapitulated faithfully the three CAF subpopulations (consisting of 25% apCAFs, 43% iCAFs and 32% myCAFs) from Elyada et al. (**Fig. 27 A**), the two clusters of the treated tumors displayed different, non-perfectly overlapping gene signatures (**Fig. 27 C, D**). In the treated sample cluster 4 we could still recognize the 3 subpopulations, although there was a switch between the percentage of iCAFs (17%) and apCAFs (57%), while myCAFs accounted for the 24% (**Fig. 27 B, C**). Remarkably, we were able to identify a very small percentage of cells corresponding to the iCAFs (5%) and apCAFs (13%) signatures in the treated sample cluster 3, (**Fig. 27 B, D**), while the great majority of cells (82%) were not falling into one of those 3 categories. Therefore, we defined a novel CAFs subtype (from now on Sema-Associated-Fibroblasts, SemAFs) (**Fig. 27 D**), based on their differential gene profile.

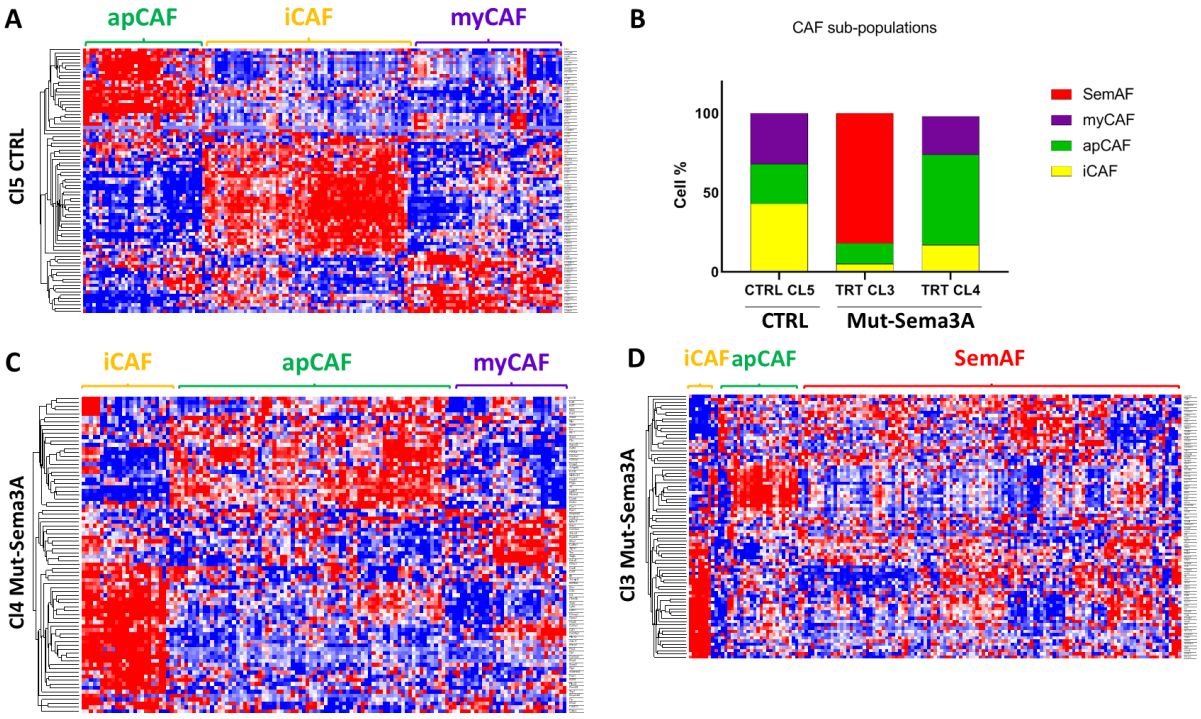

Figure 27. A) *Heatmap showing the distribution of control fibroblast according to the classification of myCAFs, iCAFs and apCAfs.* ***B)*** *Bar plot representing the percentual distribution of CAF sobpopulations in the three identified fibroblast clusters.* ***C)*** *Heatmap showing the distribution of cluster 4 fibroblasts (mut-Sema3A) according to the classification of myCAFs, iCAFs and apCAfs. It is less defined respect to control fibroblasts.* ***D)*** *Heatmap showing the distribution of cluster 3 fibroblasts (Mut-Sema3A) according to the classification of myCAFs, iCAFs and apCAfs. Strikingly the only subpopulations that remain clearly visible are iCAFs and apCAFs, while the gene signature for myCAFs is not present anymore and a new fibroblast class emerges.*

2.5. Sema3A-induced a tumor-restraining CAF gene signature

Since CAFs are an extremely heterogenous population, deriving from several sources, showing different or opposite phenotypes or differentiation subtypes, (229–231), we further investigated the specific gene signature identifying our new SemAF population. We considered the fibroblasts from cluster 3 mut-Sema3A and selected the 82% of these cells that constituted the SemAF subpopulation. Then we ranked their differentially expressed genes and among those genes we identified a portion that was significantly up-regulated in SemAFs respect to control CAFs and treated cluster 4 CAFs. The genes found to be significantly and selectively upregulated in SemAFs were: Islr, Pdgrfa, Mmp2, Cygb, Hspa1a, Hspa1b, Cdh11, Thbs, Apoe, Bgn, Eng, Plxna4. In this sub-class, the main gene signature included Islr, Pdgfra Mmp2, shown to be fibroblast markers of tumor restraining (anti-tumor) CAFs (232–234), also correlated with the quiescent characteristics of Pancreatic Stellate Cells (PSCs, the major source of CAFs in PDAC). Moreover, this signature was characterized by Cygb and its downstream effectors Hspa1a and Hspa1b. These genes were instead responsible for decreasing pancreatic cancer progression via their ability of increasing antioxidant genes expression and through their ROS scavenging function. The other genes identified in the SemAFs signature were Eng, Cdh11, Thbs2, Apoe, Bgn, genes shown to have controversial roles across different cancers and experiment types, and not a typical gene signature of cancer-restraining phenotype.

To extensively support the anti-tumoral features of SemAFs, we implemented their differential expressed genes in Enrichr and confirmed that most of them were characteristically enriched in markers concerning the quiescence status of PSCs (Mmp2, Fap, Lrrc32, Pdgfra, Dcn, Prrx1, Tmem100, Bgn, Islr, Cygb, Cdh11, Cpxm1, Ebf1, Olfml3, Ednra). Furthermore, gene ontology enrichment analysis highlighted the involvement of those genes in epithelial to mesenchymal transition, ECM organization, apoptosis regulation.

Interestingly, genes such as IL-6 and Timp-1, associated to an inflammatory-like and immune suppressive CAF phenotype, shown to promote cancer invasiveness and metastasis (227), were down-modulated in SemAFs compared to controls.

Notably, among the SemAF gene signature, Islr coding for a protein called Meflin, showed to confer CAFs anti-tumor properties in PDAC. In fact, when over-expressed in CAFs by genetic and pharmacological approaches, significantly restrained PDAC progression (232,235) and improved the chemo sensitivity of mouse models of PDAC (236).

Taken together, our data indicate that the SemAF population displays an unconventional CAF phenotype, conferring a potential tumor-restraining-fibroblast role in PDAC.

2.6. SemAFs are present in PDAC tumors

To further verify and confirm the expression of the SemAF gene signature in PDAC, we performed RNA In Situ Hybridization (using RNAscope® Opal™ probes) on tumor tissue slides derived from mut-Sema3A-treated and untreated PDAC. Notably, we observed increased expression of meflin/Islr in the mut-Sema3A treated tumors. Interestingly, meflin was specifically localized in Dcn^+ fibroblasts (Dcn is a pan-CAF marker) across the tumor. (**Fig. 28**). We did not observe significant changes in α-SMA and Cygb expression between controls and Sema3A-treated tumors.

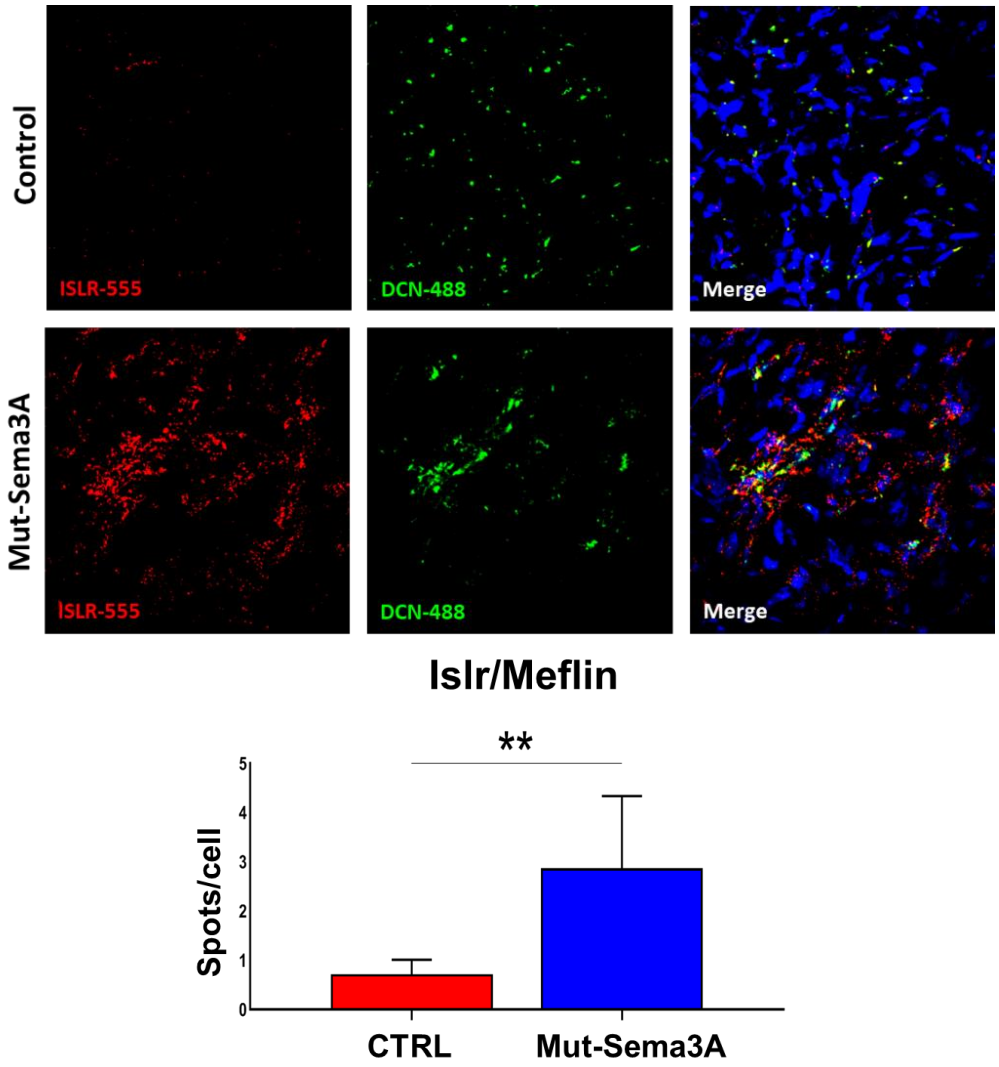

***Figure 28**. RNA In Situ Hybridization of Islr (Meflin) and Dcn (Decorin) on PDAC tissues display an increased expression of Islr following mut-Sema3A treatment in Dcn$^+$ CAFs. RNAscope® Opal™ probes hybridizing to Islr and Dcn mRNAs were used to define the number of Dcn$^+$ CAFs and to assess their expression for Islr. mRNAs for Islr increase significantly per cell following mut-Sema3A administration. Dots were quantified manually on ImageJ and dot co-localization was assessed with the Coste's method via the "Coloc2" tool of NIH ImageJ. Graph was plotted with GraphPad Prism 8 representing mean and SD. P-value (0.0032) was calculated using Student t-test.*

2.7. Visium Spatial Gene Expression coupled with sc-RNA-seq define and localize SemAF in murine PDAC

To further investigate the mut-Sema3A-induced CAF gene reprogramming in PDAC, we performed Spatial Transcriptomics (*10x Genomics* Visium Spatial gene expression) on frozen samples derived from mut-Sema3A-treated and control tumors (**Fig. 10 A**). This technique allowed us to visualize thousands of transcripts directly on the tumor slice (**Fig. 29**). Every tissue slide was divided into thousands of spots and, following RNA-sequencing, transcripts expression was reported as average per spot. Due to this limitation, we assumed that every spot was not a single cell but a group of up to 10 cells on average. Subsequently to the RNA-sequencing, spots have been clustered using Louvain modularity method implemented in Seurat, embedded in rCASC package.

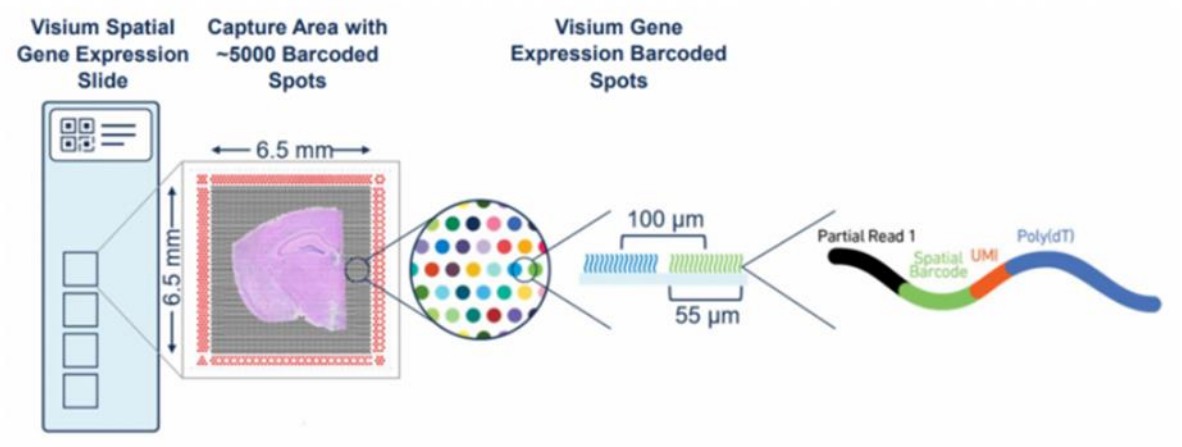

Figure 29*. Workflow of the 10x Genomics Visium Spatial gene expression analysis. Tissue slices are placed on specifically designed slides which contain chips bearing oligo-dT barcoded spots. Transcripts belonging to cells of the tissue slice hybridize to these oligo-dT that are subsequently sequenced through Illumina sequencers and their location of the slice is back-tracked thanks to the barcodes.*

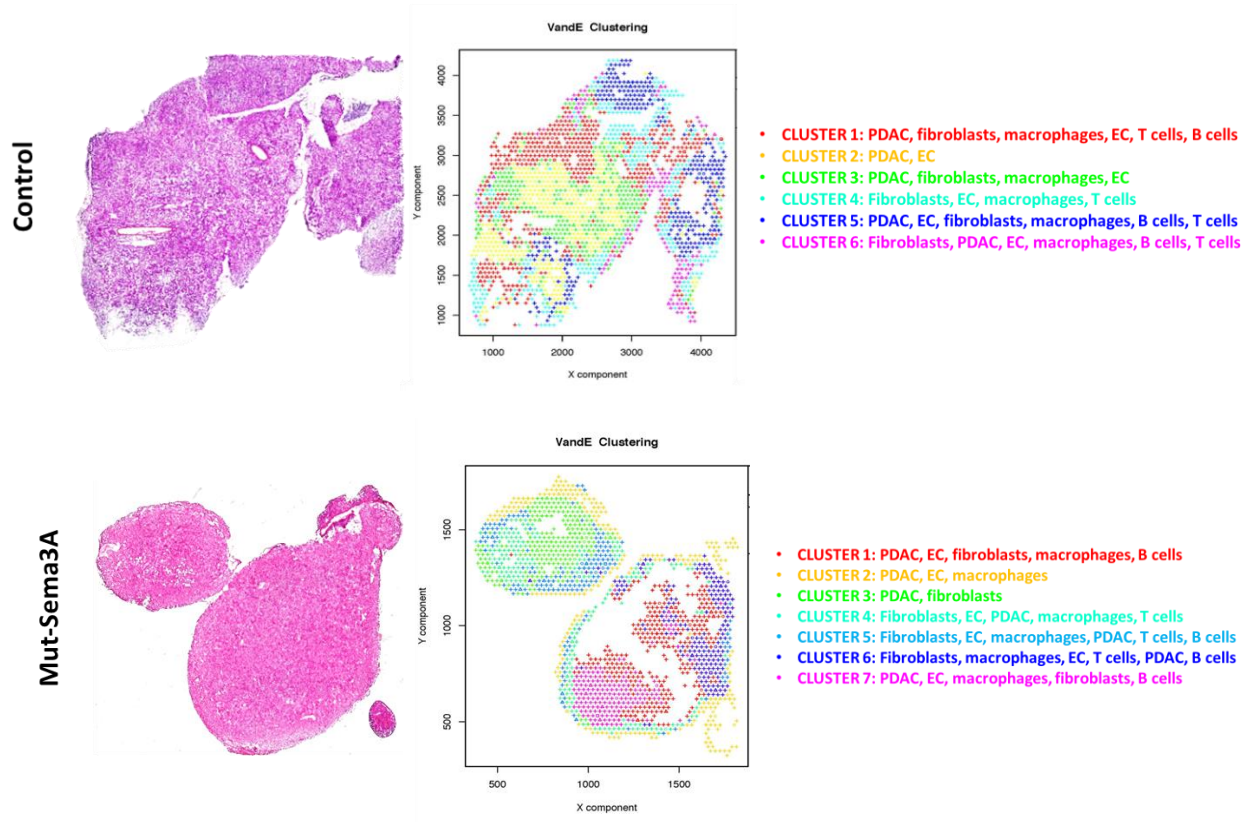

Figure 30. *Pictures showing the Hematoxylin and Eosin staining of PDAC control and mut-Sema3A treated tumors. The tissues underwent processing for Visium Spatial Gene Expression in which mRNAs found in cells at a tissue level were sequenced and subsequently clustered. The multi-color visualization represents cell-containing spots that have been clustered together based on their expression similarity. Color legends showing the most represented cell type for every Visium cluster.*

The number of clusters was defined based on the level of cluster stability, determined by the Cell Stability Score (CSS), implemented in rCASC. Since this was not a sc-RNA-sequencing, every

cluster contained different cell populations, that could be ranked according to the preponderance of marker genes characterizing the cluster. Regarding fibroblasts, there were some clusters containing more abundantly this population: in the control CAFs were better represented by cluster 4 and 6, while in the Mut-Sema3A treated sample they were more abundant in cluster 4, 5 and 6 (**Fig. 30, see legend**).

In parallel, in a complementary manner, we used the gene signature previously identified through sc-RNA-seq and implemented it in the data deriving from the Visium Spatial Gene Expression. More specifically we plotted the genes corresponding to the different CAF subpopulations on the Visium slides to visualize the localization of the cells throughout the tissue slice (**Fig. 30**). Interestingly, while in the control tissue the genes of myCAFs, iCAFs and apCAFs signatures were expressed and broadly distributed, these CAF sub-populations were almost completely absent in mut-Sema3A-treated tumor tissues. Intriguingly, the myCAF population was very scarce while the iCAF population was very abundant in the control sample, strengthening the already published data according to which iCAFs are pro-tumoral and immunosuppressive while myCAFs represent the tumor-encompassing fibroblast compartment (38,40,71,73,237).

Since a percentage of iCAFs were still present in the mut-Sema3A tissue, we hypothesized their belonging to the cluster 4 mut-Sema3A, that, contrarily to the cluster 3 still comprised a portion of iCAFs (**Fig. 27 B**). Conversely SemAF genes were expressed mostly in mut-Sema3A-treated tumors and were barely detectable in control tissues. Surprisingly, differently from the genes of the myCAFs, iCAFs and apCAFs signature, most of the SemAF genes were localized in the border of the tumor, completely overlapping the localization of fibroblasts defined by the clustering of the Visium-sequenced transcripts (**Fig. 30 see legend, 31**).

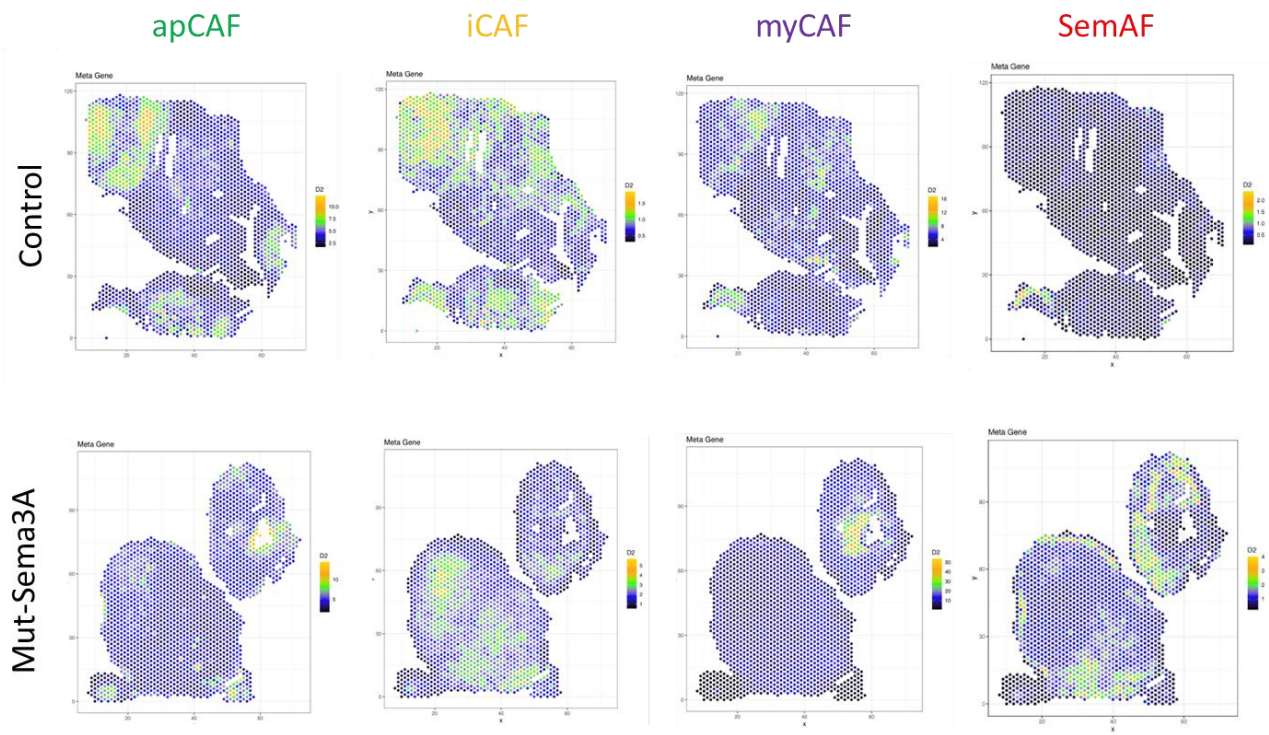

Figure 31*. Visium Spatial Gene Expression representation of the control and mut-Sema3A treated tumors. The gene signatures typical of myCAFs, iCAFs, apCAFs and SemAFs, identified through sc-RNA-sequencing, were plotted on the data deriving from the Visium transcriptomics. MyCAFs, iCAFs and apCAFs are clearly less present in the treated tumor, while SemAF are almost exclusive of the treated tumor, and are located on the tumor border.*

2.8. *In-vitro* mut-Sema3A treatment induces transcriptional changes in CAFs and impairs CAFs invasion potential

Based on the effect of mut-Sema3A on CAFs *in-vivo*, we sought to assess whether this gene-reprogramming observed in PDAC was due to a direct effect on fibroblasts. To this aim, we set up an *in-vitro* model using Pancreatic Stellate Cells (PSCs) extracted from healthy pancreata and activated as myCAFs using a system of 2D culturing on plastic culture dishes. Elyada and colleagues (70,71,73) demonstrated that the 2D culturing of PSCs on plastic devices automatically activates them as myCAFs, boosting their ability to express and secrete proteins of the extracellular matrix, collagens and α-SMA. We treated the cells with mut-Sema3A and assessed the variations of the expression levels of the genes of the SemAF signature. Interestingly, the treatment with mut-Sema3A in activated fibroblasts upregulated genes of the "*in-vivo*" signature such as Islr, Cxcl12, Cdh11, Thbs2, Cygb, Col1a1 (**Fig. 32 A**). Remarkably, the treatment with mut-Sema3A significantly up-regulated its own receptor, PlxnA4 (**Fig. 32 A**), further confirming our hypothesis that mut-mut-Sema3A3A was able of exerting a direct effect on PDAC CAFs.

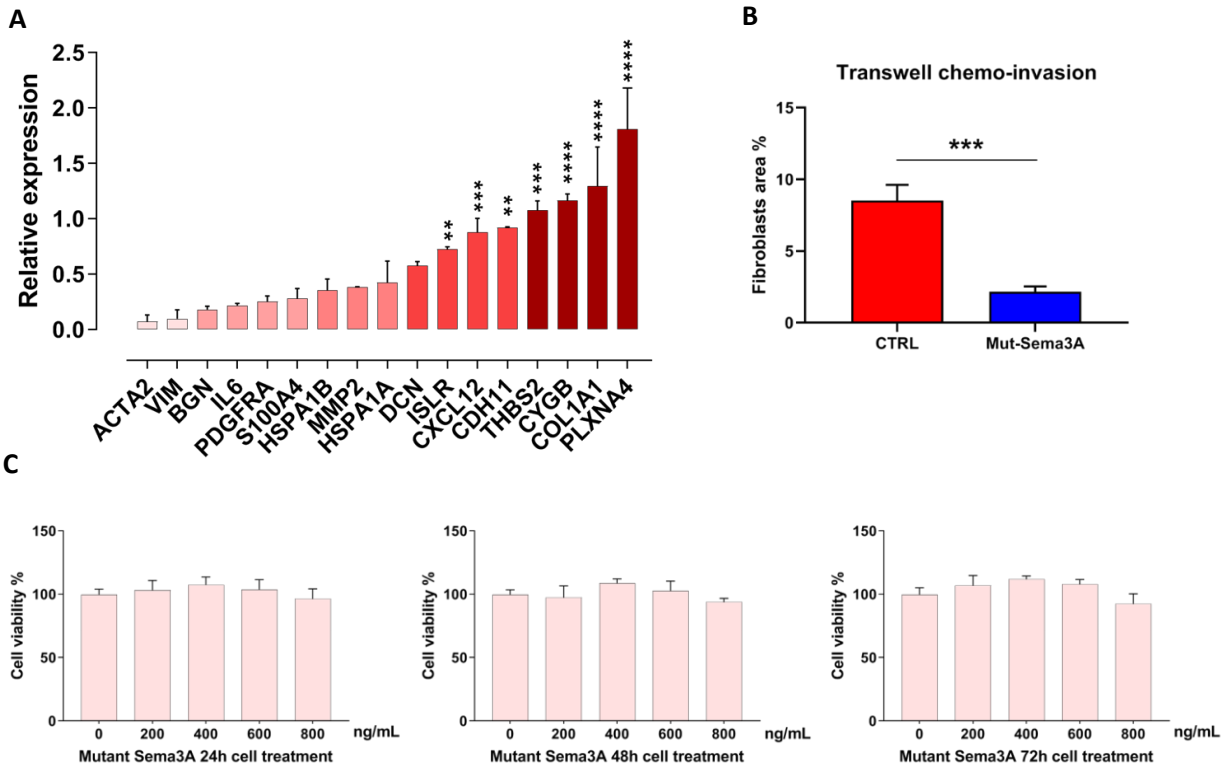

Figure 32**. **A)** Quantitative Real Time-PCR of the genes identified as SemAF-specific following sc-RNA-seq analysis. Among the 17 tested genes 7 of them were significantly upregulated in the mut-Sema3A treated sample: Islr, Cxcl12, Cdh11, Thbs2, Cygb, Col1a1 and Plxna4. Student t-test was performed on GraphPad Prism and the computed p-values are: * < 0.05; ** < 0.01; *** < 0.001; * < 0.0001. **B)** Transwell chemo-invasion assay displayed impairment of the CAFs potential to invade the Matrigel Matrix following a chemotactic gradient when treated with mut-Sema3A. The graph was plotted with GraphPad Prism 8 and mean and SD were plotted. Statistical significance was calculated through student t-test and the p-value > 0.001. **C)** Bar plots representing cell viability of activated CAFs following mut-Sema3A administration at 200, 400, 600, 800 ng/mL for 24, 48 and 72h. No effects were observed altering cell viability. Graphs were plotted with GraphPad Prism 8 and mean and SD were represented. Statistical significance was assessed through one-way ANOVA.*

To further assess whether mut-Sema3A was able to exert direct biological changes in activated fibroblasts, we evaluated the effects on cell viability. Therefore, we set up viability experiments using different treatment time points and testing several mut-Sema3A doses. Mut-Sema3A did not exert any effect on CAFs viability, independently on the administered dose or timing of treatment (**Fig. 32 C**).
Next, we evaluated the effect of the mut-Sema3A on the ability of activated fibroblasts to migrate and invade the Matrigel matrix®. We performed CAF invasion assays using transwell plates coated with Matrigel®. Notably, we observed that treatment with 800 ng/mL mut-Sema3A was able to strongly inhibit CAFs invasion across the Matrigel matrix® (**Fig. 32 B**).

2.9. *In-vitro* mut-Sema3A treatment induces PLXNA4 upregulation in CAFs

We observed a significant and unexpected increase of the Sema3A receptor PlexinA4 in CAFs that underwent *in-vitro* mut-Sema3A treatment (**Fig. 32 A**). This finding led us to further investigate whether PLXNA4 was upregulated also in mut-Sema3A treated PDAC tumors. To this aim, we performed *In Situ* Hybridization with a PLXNA4 probe on control and mut-Sema3A treated PDAC tissues. Notably, we observed increased expression of PLXNA4 in DCN^{+} expressing CAFs (**Fig. 33**). This finding may suggest a feedforward mechanism in which the mut-Sema3A acts directly on fibroblasts of the TME and stimulates the further production of its own receptor. Further investigations will be needed to better explore and understand the underlying mechanisms of the effect of mut-Sema3A on PlxnA4 in CAFs.

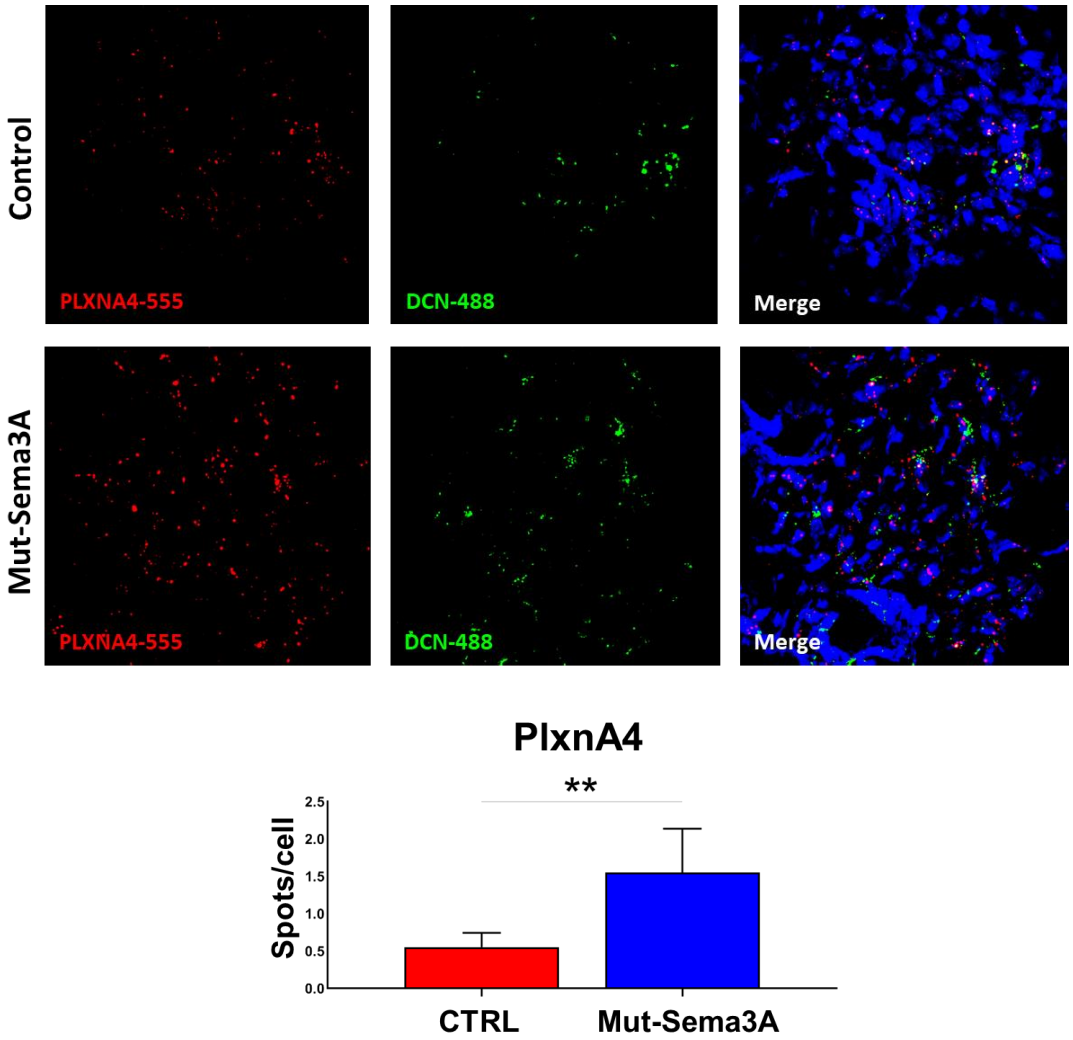

***Figure 33**. RNA In Situ Hybridization of Plxna4 (Plexin A4) and Dcn (Decorin) on PDAC tissues display an increased expression of Plxna4 following mut-Sema3A treatment in Dcn$^+$ CAFs. RNAscope® Opal™ probes hybridizing to Plxna4 and Dcn mRNAs were used to define the number of Dcn$^+$ CAFs and to assess their expression for Plxna4. mRNAs for Plxna4 increase significantly per cell following mut-Sema3A administration. Dots were quantified manually on ImageJ and dot co-localization was assessed with the Coste's method via the "Coloc2" tool of NIH ImageJ. Graph was plotted with GraphPad Prism 8 representing mean and SD. P-value (0.0017) was calculated using Student t-test.*

3. Mut-Sema3A induces VCAM-1 expression in endothelial cells

One of the effects of the mut-Sema3A in PDAC, demonstrated so far, is on endothelial cells and pericytes, by inducing the tumor vessel normalization in the tumor tissue (185). Based on the main aim of this project, focused on better understanding the crosstalk between the different cell populations of the TME, we started to further investigate the molecular changes induced by mut-Sema3A in endothelial cells, and how mut-Sema3A enables them to interact with the other cell types of the tumor ecosystem. Interestingly, our single cell RNA-sequencing data showed that pericytes are induced and increased following mut-Sema3A administration (**Fig. 24, 25**), further demonstrating the "normalizing" effect of Sema3A on tumor vessels in PDAC. We have previously (185) demonstrated that mut-Sema3A acts on endothelial cells (ECs) inhibiting the activation of Rap1 (**Fig. 34 A**), a small GTPase predominantly involved in cell adhesion and cell

junction formation. Recent studies have demonstrated that Rap1 inhibition in endothelial cells allows the activation of the pro-inflammatory signals deriving from TNF-α stimulation, leading to the upregulation of VCAM-1 expression, a very well-known transmembrane adhesion molecule fundamental for lymphocytes and leukocytes extravasation process (**Fig. 34 B**) (238). Based on these findings, we assessed the expression of VCAM-1 in our PDAC tissues prior and following mut-Sema3A administration, and we observed an increased co-expression of the adhesion molecule VCAM-1 with CD31, a known endothelial marker (**Fig. 34 C**). Notably, while VCAM-1 was not expressed by tumor vessels in control tumors, most of this protein was co-expressed in the vasculature of mut-Sema3A-treated tumors (**Fig. 34 C**). To further characterize these effects, we performed *in-vitro* experiments using human endothelial cells (ECs). We treated HUVECs with mut-Sema3A and evaluated the expression of VCAM-1.

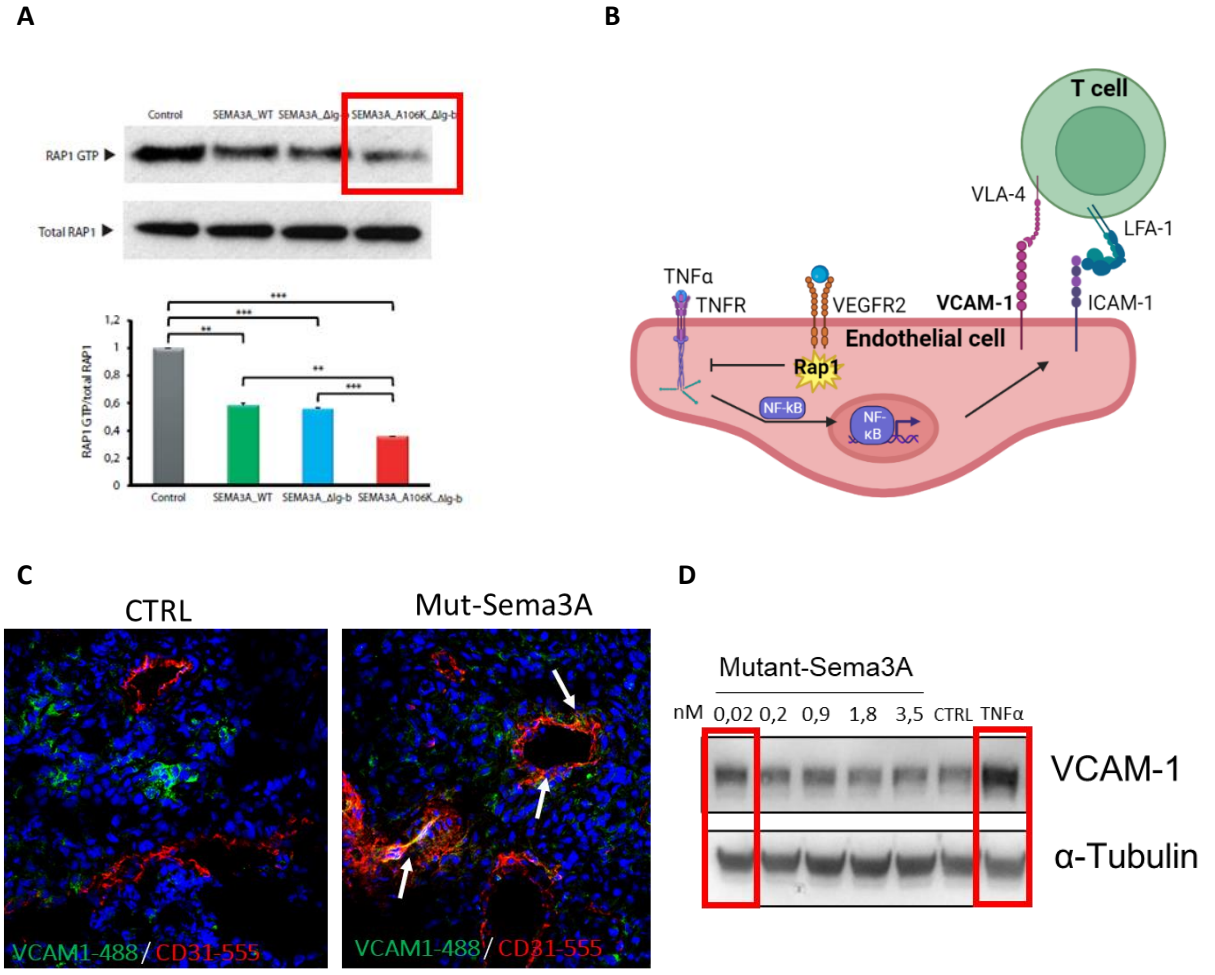

***Figure 34**. **A)** Active Rap1-GTP bound is decreased following HUVEC treatment with the mutated form of Semaphorin 3A, from Gioelli et al. (185). **B)** Schematic representation of Rap1 and TNF-α intertwined signaling pathways that affect VCAM-1 expression and exposition on endothelial cell plasma membrane. Exposition of VCAM-1 on the cell surface facilitates T lymphocytes extravasation from blood vessels. Cartoon realized with BioRender remaking a scheme from Sharma et al. (239). **C)** Immunofluorescence staining for CD31 in red and VCAM-1 in green. Co-staining of VCAM-1 inside of endothelial cells is absent in control PDAC mice and clearly observable in mut-Sema3A-treated mice (arrows). **D)** Western Blot assessing the presence of VCAM-1 inside HUVECs following mut-Sema3A or TNF-α treatment. Mut-Sema3A induces the expression of VCAM-1 similarly to TNF-α treatment.*

Mut-Sema3A, administered at very low doses, was capable of increasing the level of VCAM-1 on endothelial cells similarly to TNF-α stimulation (**Fig. 34 D**).
Taken together, these data suggest that mut-Sema3A is able of inducing VCAM-1 expression on endothelial cells both *in-vivo* and *in-vitro* models and indicate that it may regulate the extravasation and recruitment of leukocytes via the tumor vasculature in PDAC, through this mechanism. We will further assess this aspect in the following chapter 4.

4. Mut-Sema3A induces T CD8$^+$ lymphocytes recruitment to the tumor

Based on the enhanced VCAM-1 expression observed on PDAC tumor vessels upon mut-Sema3A administration, we sought to investigate the effect on the immune landscape in PDAC. Starting from the data deriving from our sc-RNA-seq analysis, that highlighted changes in some immune cell subpopulations in mut-Sema3A-treated tumors, we focused on better characterizing these variations at a tumor tissue level. Our immunophenotyping analysis concerned the following populations that have been relevantly perturbed by mut-Sema3A treatment: M1-like anti-tumor macrophages, M2-like pro-tumor macrophages, T-regulatory lymphocytes and cytotoxic CD8$^+$ T-lymphocytes.
Analyzing the effects on the myeloid cell populations, no significant changes were observed in the amount of M1-like macrophages and M2-like macrophages (**Fig. 35 A, B**). In addition, when we focused on investigating the effects of mut-Sema3A on T-cells, we did not notice any changes in the amount of T-regulatory lymphocytes (**Fig. 35 C**)**.**
Notably, a dramatic increase of recruited T-cells was found in the treated samples when we examinated the amount of CD8$^+$ T-lymphocytes (**Fig. 36 A**), and of the level of the marker granzyme B (**Fig. 36 B)** an indicator of the effector action of cytotoxic T lymphocytes.
These findings are of great importance, since, as previously demonstrated (239), untreated mPDAC mice have very low levels of infiltrated CD8$^+$-T cells. Mut-Sema3A is able therefore to switch a “cold” in “hot” PDAC tumor by enhancing the infiltration of CD8$^+$ T-lymphocytes at the tumor site.
Based on our experiments demonstrating that mut-Sema3A was able to up-regulate VCAM-1 in tumor vessels, it is conceivable to hypothesize that mut-Sema3A may recruit T lymphocytes by normalizing tumor vessels and increasing the expression of adhesion molecules such as VCAM-1, therefore promoting lymphocytes extravation towards the tumoral tissue. Future investigations are planned to better demonstrate this meachinism by *in-vivo* and *ex-vivo* experiments. For instance a series of experiments are planned to modulate VCAM-1 expression by acting on Rap-1 activation in mPDAC to formally demonstrate this specific effect of mut-Sema3A on tumor vessels and CD8$^+$ T-cells recruitment.

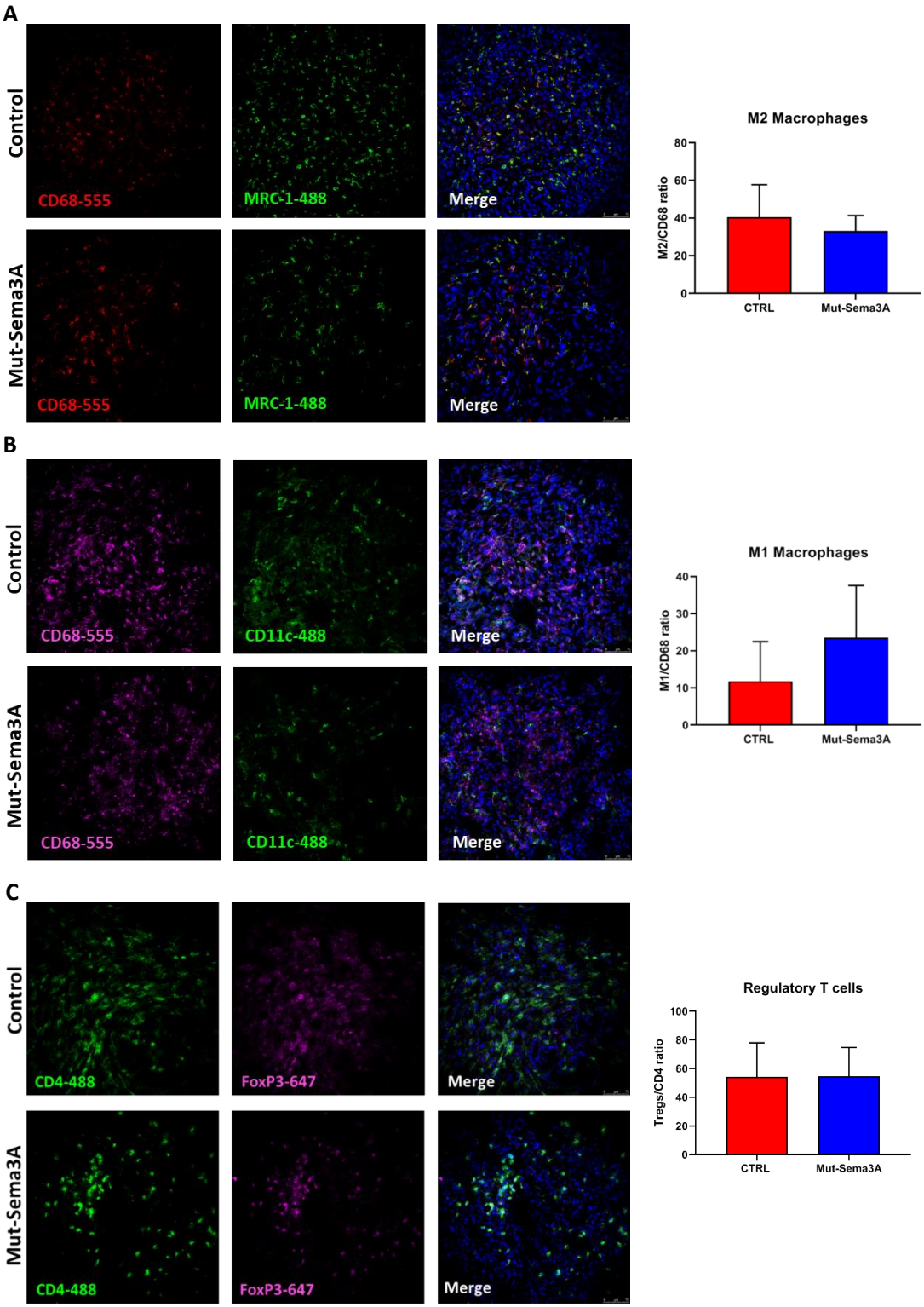

***Figure 35**. Immunophenotyping of frozen PDAC tissues for the identification and quantification of M1, M2 macrophages and Regulatory T cells. **A)** M2 pro-tumoral macrophages were identified using MRC1 and CD68 antibodies. Cells that were presenting co-staining were considered M2 macrophages. **B)** M1 anti-tumoral macrophages were identified using CD11c and CD68. **C)** Regulatory T cells were identified using FoxP3 and CD4 markers. No significant differences were detected following mut-Sema3A treatment of PDAC in these three populations. Graphs were plotted with GraphPad Prism 8 and the plotted values represent the ratio between the area fraction of colocalization divided by the total CD68 or CD4 area. Mean and SD were plotted. $N \geq 4$.*

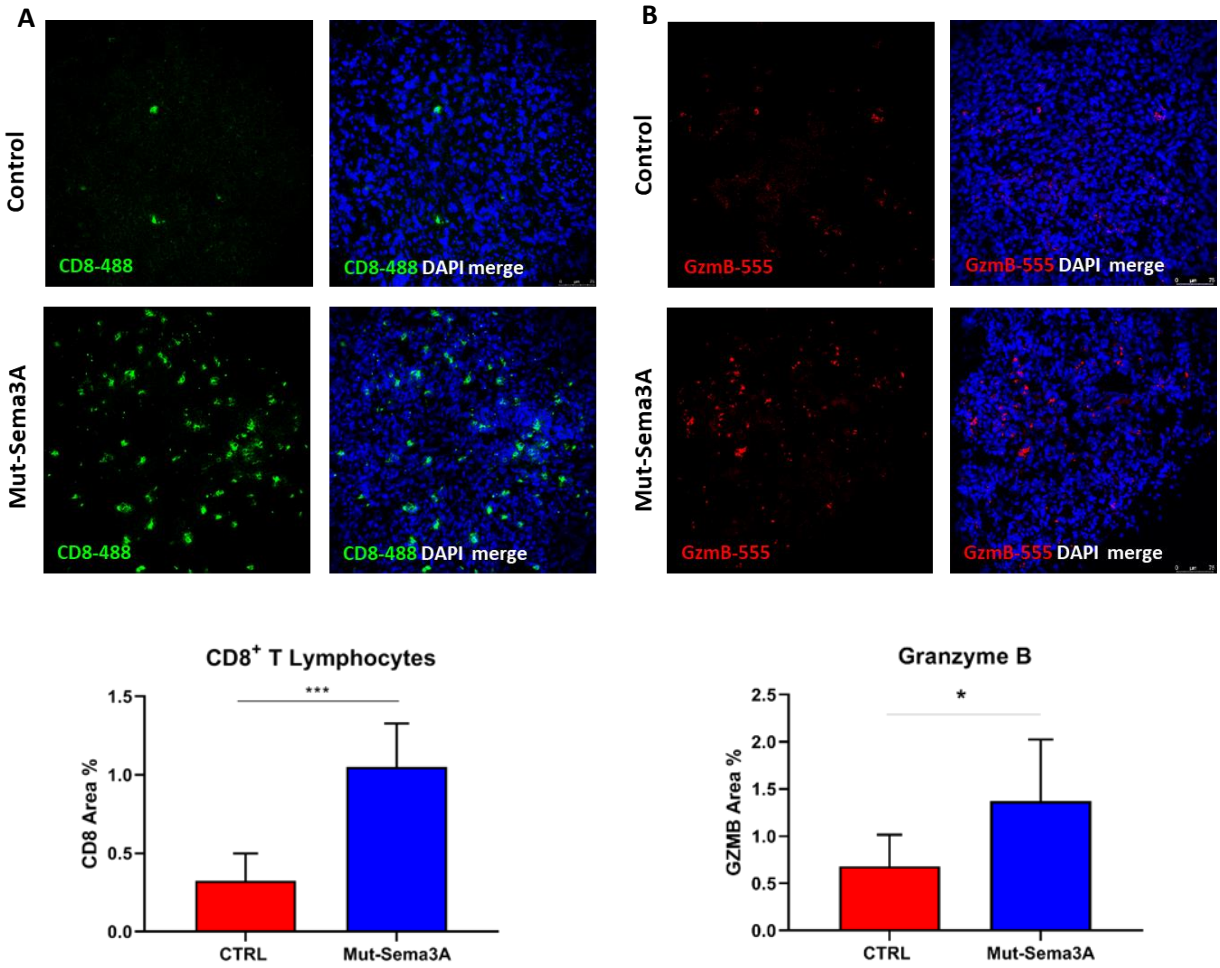

Figure 36. *Immunofluorescence of frozen PDAC tissues aimed at identifying and quantifying cytotoxic CD8$^+$ T lymphocytes and the presence of Granzyme B (GZMB).* ***A)*** *Cytotoxic CD8$^+$ T lymphocytes resulted to be significantly augmented inside the PDAC tissue following mut-Sema3A administration, suggesting an improved recruitment and extravasation.* ***B)*** *The amount of intra-tumoral GZMB$^+$ cells increase notably following mut-Sema3A administration in vivo. Graphs were plotted with GraphPad Prism 8 and the plotted values represent the area fraction of CD8 or GZMB. Mean and SD were plotted. N ≥ 5.*

5. Mut-Sema3A enhances the effect of immunotherapy

5.1. Mut-Sema3A coupled with diverse immunotherapeutic agents has a synergic effect in hampering tumor growth

Based on the strong increase of CD8$^+$-T cell recruitment and activation in PDAC induced by mut-Sema3A, we sought to assess whether the combination of mut-Sema3a with immune-checkpoint inhibitors was able to enhance the anti-tumor effect, previously demonstrated. It is widely shown that, up to date, immune checkpoint inhibitors had not reached the foreseen effects and very poor efficacy has been shown in clinical trials in PDAC patients (240). We started to investigate the combination of mut-Sema3A with α-PD1 and α-CTLA4 blocking antibody in inhibiting tumor growth in mPDAC mice. The choice of using these immune checkpoint inhibitors was based on the fact that both PD1 and CTLA4 have an important role in downmodulating the T-cells activation while enhancing T regulatory cell functions (241). These therapeutic agents could exert additional

anti-tumor effect since our PDAC model displayed increased $CD8^+$-T cells recruitment, a large proportion of $FoxP3^+$ cells among the $CD4^+$ T lymphocytes (**Fig. 35 C**, (239)) and mut-Sema3A did not target or modulate the T-reg subset when administered individually (**Fig. 35 C**). As expected from clinical data, the monotherapy of α-PD1 did not exert any significant anti-tumor effect **(Fig. 37 B)**. As expected from the abundance and immune-suppressive effects of T-regs in our mPDAC model, the α-CTLA4 treatment, as single agent, induced a reduction of tumor volume, comparable to the effect exerted by mut-Sema3A (**Fig. 37 C**). Unfortunately, we did not detect any enhancement of tumor inhibition when mut-Sema3A was combined with α-CTLA4 (**Fig. 37 C**). Similarly, we did not observe any synergistic effect combining α-PD1 and α-CTLA4 blocking antibodies or combining mut-Sema3A with α-PD1 + α-CTLA4 blocking antibodies in decreasing tumor volume compared to mut-Sema3A used as single agent (**Fig. 37 D**).

Despite the positive effects of mut-Sema3A on normalizing the tumor vasculature and recruiting $CD8^+$ T cells, we were not able to enhance the anti-tumor effect with α-PD1 or α-CTLA4 combinations. Therefore, we proceeded to test new combinatorial treatments. We focused on another immune-modulatory agent, the α-CD40 antibody, an agonist that has a stimulatory action on CD40, exposed on the surface of several Antigen Presenting Cells (APCs) such as Dendritic Cells (DCs), B lymphocytes, $CD4^+$ T cells and platelets. Indeed, the effect of α-CD40 is to induce maturation of dendritic cells into professional anti-tumor APC, T cells activation and secretion of inflammatory cytokines involved in the immune response in PDAC. Indeed, by improving anti-tumoral immunity activation it facilitates the polarization of TAMs into M1-like anti-tumoral macrophages in spite of M2-like pro-tumoral macrophages (242,243). Therefore, we treated mPDAC with α-CD40 alone or in combination with mut-Sema3A. While α-CD40 exerted, to some extents, an anti-tumor activity, even if less potent than mut-Sema3A alone, the combination of mut-Sema3A with α-CD40 failed to induce synergistic effects (**Fig 37 E**).

Treatment of mPDAC mice with the drug administration schedule in **Fig. 37 A** allowed us to conclude that α-CD40 and α-CTLA4 individual therapies exert an effect on PDAC growth similar or lower to the one observed in mut-Sema3A-treated mice (**Fig. 37 D, E**), and that the combination of one of the two agents with mut-Sema3A was not sufficient to improve the outstanding effect of the mut-Sema3A (**Fig. 37 C-E**). Finally, we decided to treat mPDAC mice with a triple combination of α-CD40 + α-CTLA4 with mut-Sema3A. Interestingly, while α-CD40 and α-CTLA4 combined together did not exert additional an anti-tumor effect compared to mut-Sema3A, when the three agents were co-administered, we observed a remarkable impairment of PDAC growth (**Fig. 37 F**).

These data demonstrate that mut-Sema3A re-programs the immune cells improving the anti-tumor efficacy of the immunotherapy in PDAC. We can hypothesize that the observed synergistic effect may be due to the modulation of different immune cell populations: i) α-CTLA4 targeted mainly T-regs; ii) α-CD40 promoted the activation of anti-tumoral myeloid cells; iii) mut-Sema3A activated $CD8^+$-T cells.

We started to provide more compelling experimental evidence to confirm this hypothesis, as described in the following chapter 5.2.

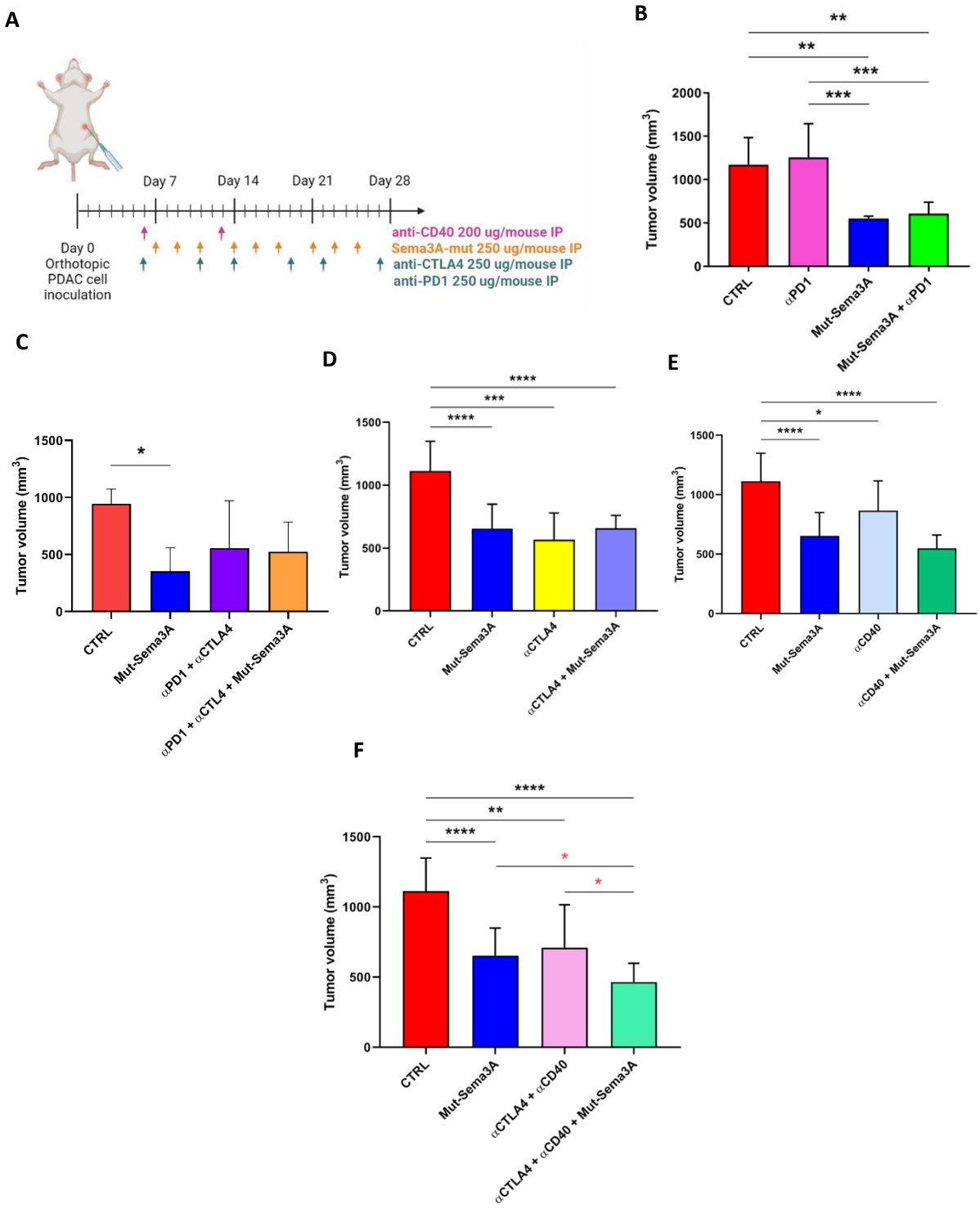

Figure 37. A) *Treatment schedule of the PDAC mouse model with combination therapy. The therapeutic regimen started one week following tumor cell inoculation and lasted for 3 weeks. Mut-Sema3A was administered at 250 µg/mouse via intraperitoneal injection three times a week; αCTLA4 and αPD1 were administered at 250 µg/mouse via intraperitoneal injection two times a week; αCD40 was administered at day 6 and day 13 following tumor cell inoculation at 200 µg/mouse via intraperitoneal injection.* ***B)*** *Combination therapy of mut-Sema3A with αPD1 blocking antibody. αPD1 alone does not exert any effect on PDAC tumor volume. Similarly, the combination of αPD1 with mut-Sema3A does not have a synergic effect on impairing tumor growth.* ***C)*** *Combination therapy with mut-Sema3A, αPD1, and αCTLA4 blocking antibodies. αPD1 and αCTLA4 do not improve the anti-tumoral effect of mut-Sema3A*

Figure 37. D) *Combination therapy of mut-Sema3A coupled with αCTLA4 blocking antibody. Contrarily to αPD1 treatment alone αCTLA4 alone is able of reducing PDAC tumor volume, but its combination with mut-Sema3A does not induce an additional effect.* ***E)*** *Combination therapy of mut-Sema3A with αCD40 agonist. αCD40 is able of inducing a slight reduction of PDAC tumor volume, but it is not able of improving mut-Sema3A effect when co-administered.* ***F)*** *Triple combination therapy including mut-Sema3A, αCD40 and αCTLA4. The immunotherapy co-administration of αCD40 and αCTLA4 is able of reducing tumor volume similarly to mut-Sema3A, but when all the three molecules are injected together, they exert a synergic effect on PDAC growth that is significantly higher to mut-Sema3A effect or αCD40 and αCTLA4 effect alone (red *).*

*All trials have been performed observing the animal facility regulations and graphs were plotted with GraphPAD Prism 8. Mean and SD were plotted for n ≥ 5. Statistical significance was analyzed with ANOVA tests and the p-values are: * < 0.05; ** < 0.01; *** < 0.001; **** < 0.0001.*

5.2. The three-agent combinatorial approach drives macrophages polarization towards the M1-like phenotype

Considering the great outcome of the triple therapy on decreasing the tumor volume, we sought to investigate the changes in the immune compartment in the PDAC tissues derived from the different treatment groups. Based on our previous results demonstrating enhanced recruitment, infiltration and activation of $CD8^+$ T lymphocytes induced by mut-Sema3A as single agent, we assessed their distribution in PDAC tissues, derived from α-CD40 and α-CTLA4 and the triple combination of α-CD40, α-CTLA4 and mut-Sema3A, compared to controls. We observed increased levels of $CD8^+$ T lymphocytes in all the conditions, compared to controls (**Fig. 38 A, D**). Therefore, by checking the effects on macrophages, interestingly we observed that there was a synergic effect between mut-Sema3A and the immunotherapeutic agents, by increasing the number of M1-like anti-tumoral macrophages, significantly enriched respect to the control (**Fig. 38 B, E**). Prompted by these observations, we also examined the proportion of M2-like pro-tumoral macrophages in the different treatment groups, but we did not detect significant differences among the groups (**Fig. 38 C, F**).

Taken together, these data suggest that the effect on $CD8^+$ T lymphocyte recruitment and activation is mainly attributable to the action of mut-Sema3A, while the polarization of macrophages towards a M1-like anti-tumoral phenotype is imputable mainly to α-CD40 or to the synergic effect exerted by the multiple administration of mut-Sema3A, α-CD40 and α-CTLA4.

Further investigation is needed to better study the changes in the immune landscape in mPDAC mice in the triple immune-therapy combination. We are currently investigating the functional contribution of other immune cell types. For instance, our sc-RNA-seq analysis showed a significant reduction of neutrophils in mut-Sema3A-treated PDAC compared to controls. Recent studies demonstrate how this subpopulation of myeloid cells can contribute to the immune suppression and tumor progression in different tumor types, including PDAC (126,135).

We expect that tumor associated neutrophils (TAN-2) could contribute to tumor progression in mPDAC and that mut-Sema3A could exert an effect on this immune sub-population.

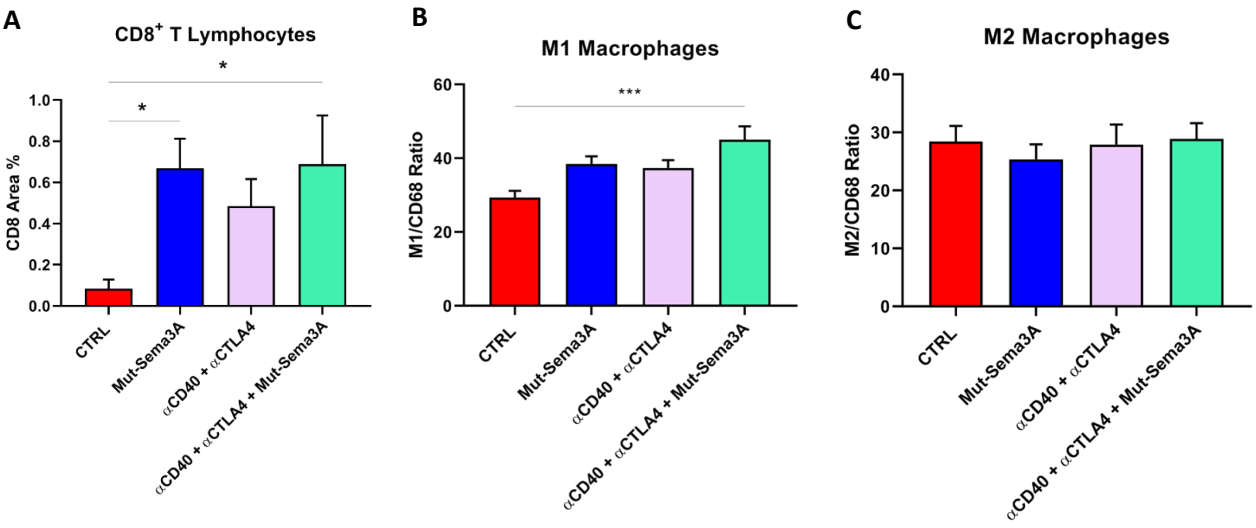
A
CD8+ T Lymphocytes
CD8 Area %
1.0
0.8
0.6
0.4
0.2
0.0
*
*
CTRL
Mut-Sema3A
αCD40 + αCTLA4
αCD40 + αCTLA4 + Mut-Sema3A
B
M1 Macrophages
M1/CD68 Ratio
60
40
20
0
***
CTRL
Mut-Sema3A
αCD40 + αCTLA4
αCD40 + αCTLA4 + Mut-Sema3A
C
M2 Macrophages
M2/CD68 Ratio
40
30
20
10
0
CTRL
Mut-Sema3A
αCD40 + αCTLA4
αCD40 + αCTLA4 + Mut-Sema3A

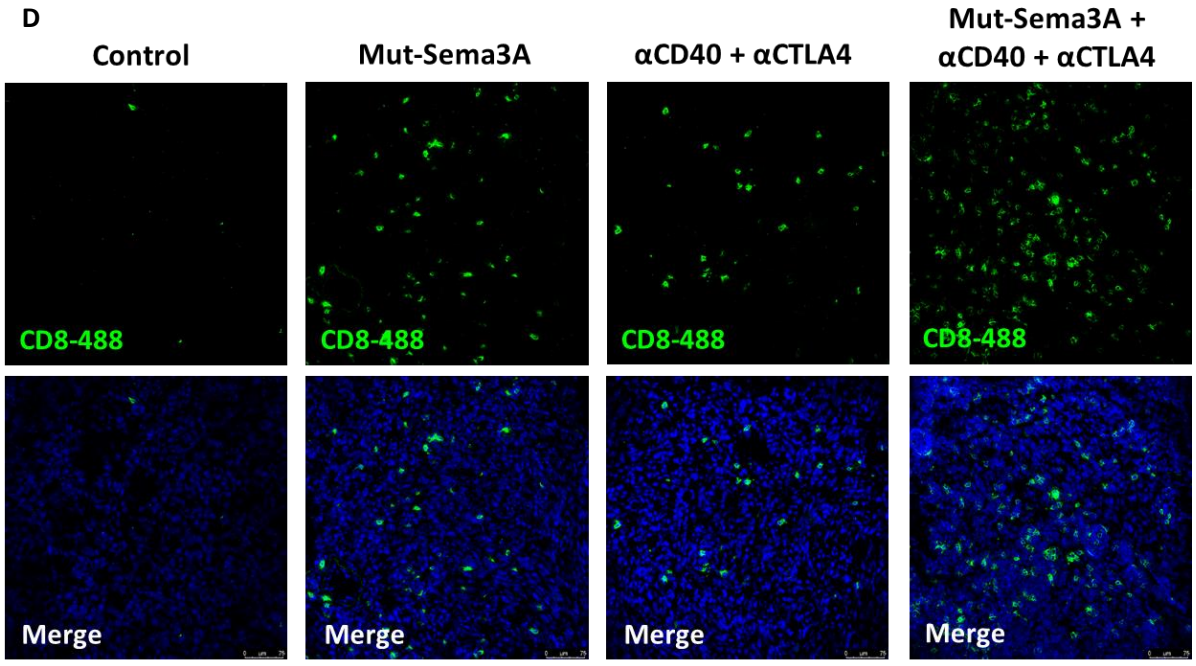
D
Control
Mut-Sema3A
αCD40 + αCTLA4
Mut-Sema3A +
αCD40 + αCTLA4
CD8-488
CD8-488
CD8-488
CD8-488
Merge
Merge
Merge
Merge

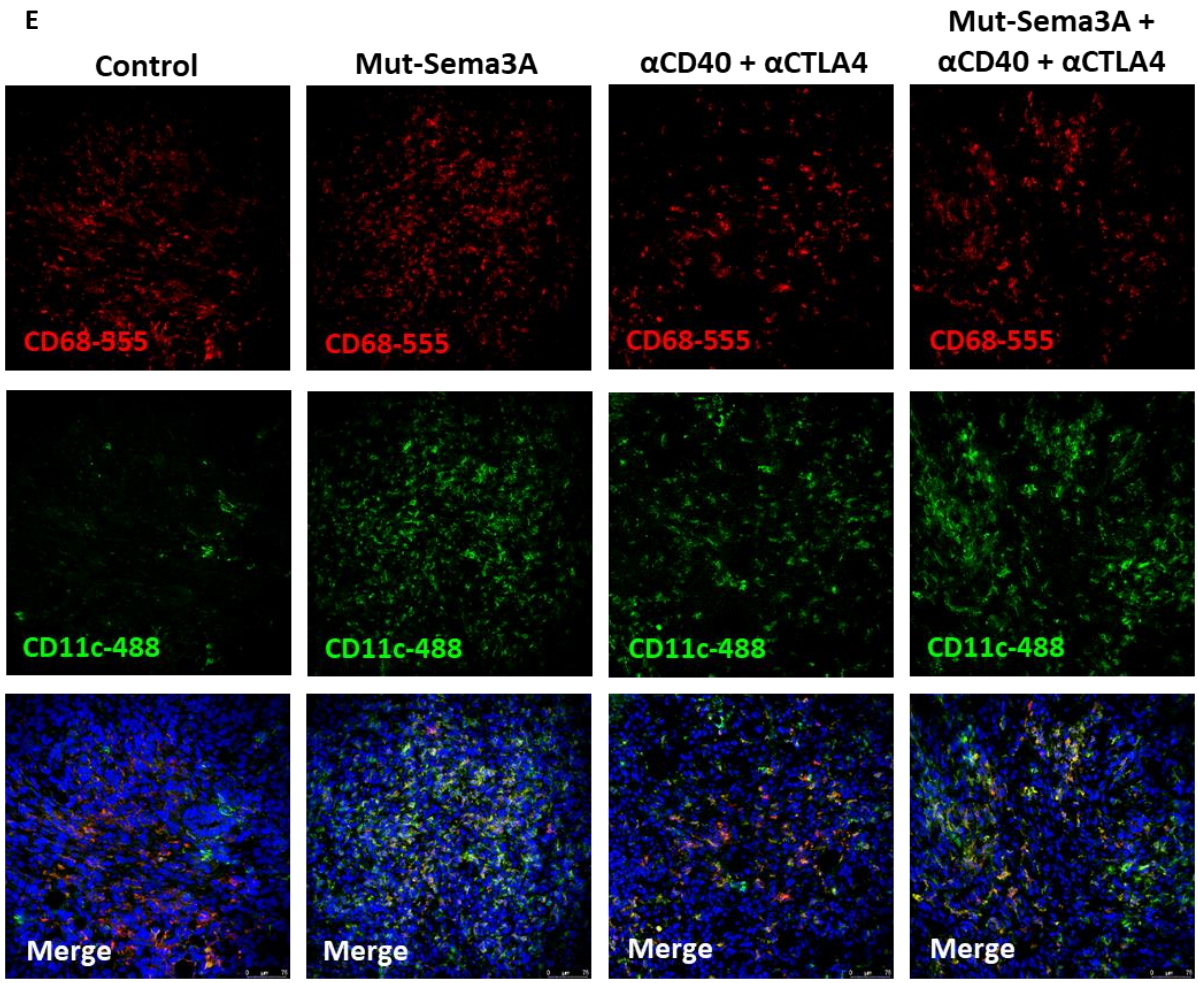
E
Control
Mut-Sema3A
αCD40 + αCTLA4
Mut-Sema3A +
αCD40 + αCTLA4
CD68-555
CD68-555
CD68-555
CD68-555
CD11c-488
CD11c-488
CD11c-488
CD11c-488
Merge
Merge
Merge
Merge

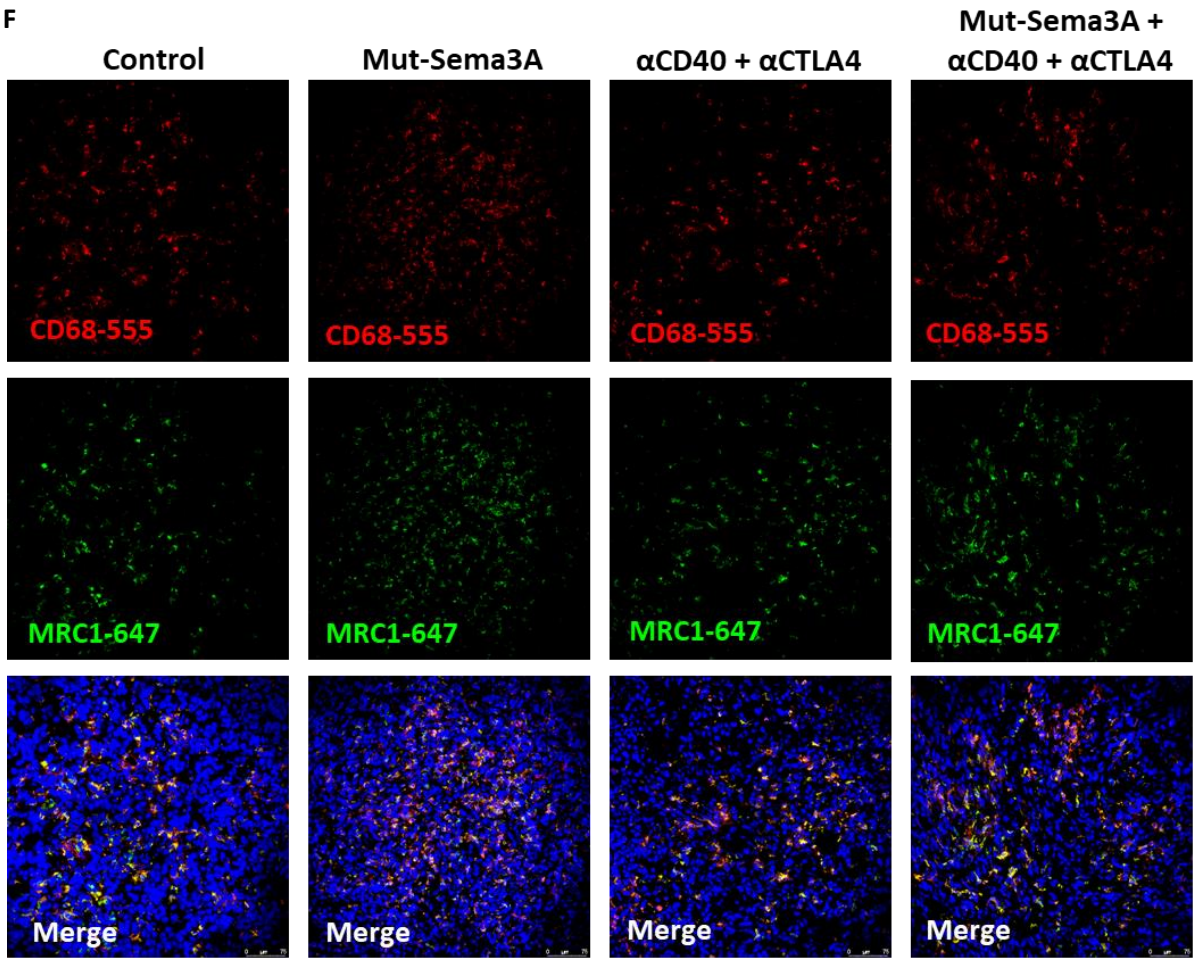

Figure 38*. Immunofluorescent stainings with markers identifying cytotoxic T lymphocytes, M1 and M2-like macrophages.* ***A)*** *Bar plots of the $CD8^+$ area percentage.* ***B)*** *Ratio of the colocalization of CD11c/CD68 on total $CD68^+$ macrophages.* ***C)*** *Ratio of the colocalization of MRC1/CD68 on total $CD68^+$ macrophages.* ***D)*** *Cytotoxic $CD8^+$ T lymphocytes resulted to be significantly increased following individual treatment with mut-Sema3A and combination treatment with mut-Sema3A, αCD40 and αCTLA4, nevertheless, the combinatorial approach did not exert a synergic effect and the percentage of $CD8^+$ T lymphocytes is comparable with the one observed in the mut-Sema3A condition.* ***E)*** *M1-like macrophages highlighted by the co-expression of CD68 and CD11c resulted to be significantly more abundant following administration of the triple therapy mut-Sema3A, αCD40 and αCTLA4.* ***F)*** *M2-like macrophages highlighted by the co-expression of CD68 and MRC-1 did not show any variation in number following the three different therapeutic conditions. Graphs were plotted with GraphPAD Prism 8. Mean and SD were plotted for $n \geq 8$. Statistical significance was assessed with one-way ANOVA and the p-values are: * < 0.05; ** < 0.01; *** < 0.001; **** < 0.0001.*

DISCUSSION

Pancreatic cancer represents a major public health concern since it is ranked in the top 10 leading types of cancer deaths in over 130 countries, moreover, its incidence and death rate have increased importantly since 2000, and it is predicted to become the fourth leading cause of cancer death by 2040 (1,2).

The bad prognosis is attributable to its late diagnosis, often due to lack of symptoms, and the standard treatment still consists of surgical resection (only practicable in the 20% of cases) and outmoded chemotherapeutic approaches such as Gemcitabine, Nab-Paclitaxel and FOLFIRINOX (7,10).

Besides the diagnosis at an already advanced tumor progression stage, pancreatic ductal adenocarcinoma is one of the most aggressive and hardly treatable cancers because of several peculiar characteristics. Among these features there are i) differentiation stage of tumor cells; ii) migratory and invasive potential of tumor cells; iii) resistance to chemotherapeutics; iv) prevalent suppressive immune microenvironment; v) highly desmoplastic stroma (15–17).

Desmoplasia is a condition that consists in the overactivation of CAFs, promoted by inflammatory stimuli and growth factors secreted by cancer cells, leading to the production of important amounts of extracellular matrix (ECM) with subsequent deregulation of the tumoral microenvironment (29). The considerable deposition of EC fibers causes impaired immune cell tumor infiltration and inefficient drug delivery, moreover, the immune cells that are allowed into the tumor, establish and enhance immunosuppression (36).

The vessel network is affected by the deregulated molecular signals and by desmoplasia as well and tumor vessels appear compressed, twisted and contemporarily stimulated by pro-angiogenic factors, indeed they are poorly covered by pericytes, they work inefficiently, perfusion is impaired and vessel leakage represents the outcome of all these conditions (33,34).

It has been demonstrated that establishing a balance between pro- and anti-angiogenic factors at a tumoral level leads to vessel normalization. This condition indicates an improvement in vessel architecture and functioning with subsequent drug delivery amelioration and immune cell extravasation facilitation. Furthermore, vessel normalization is coupled with stromal normalization, that represents repopulation of the tumoral stroma with anti-tumoral immune cells and tumor restraining fibroblasts. Indeed, several studies have shown that there is a complex network between endothelial cells, pericytes and immune cells, ruled by the secretion of cytokine and chemokines and by the expression of adhesion molecules and receptors involved in immune activation. This complex interaction has several benefic effects such as increased immune infiltration and activation, decreased tumor hypoxia and metastasis, improved perfusion efficiency and ameliorated vessel leakage (185,186,188).

Some proteins of the Semaphorin family have been correlated with a potent capability of inducing vessel normalization. Semaphorin3A that has been shown to hamper tumor growth and metastatic spreading. To date, little is known of its effect on immune cells or other cell types of the TME in PDAC.

Sema3A exerts its downstream signaling by acting on Neuropilin-1 and successively transducing the signal through Plexin A4. Since its interaction with Neuropilin-1 has also shown to induce the recruitment of M2 pro-tumoral macrophages at the tumor site, we sought to create a more powerful form of Sema3A: the mutant-Sema3A. Mutant-Sema3A has been previously patented by our lab and it was carefully designed in order to i) not being cleavable by the furin protease that regulates

Sema3A activity level; ii) act in a Neuropilin-1-independent manner; iii) bind with high affinity Plexin A4 (185,190,191,202).

Our laboratory previously demonstrated that mut-Sema3A was potent at inducing vessel normalization, increasing pericyte coverage, improving the oxygenation level intratumorally, increasing vessel permeability to chemotherapeutic agents, decreasing metastatic dissemination and primary tumor volume, and improving gemcitabine efficacy against PDAC growth (185).

Considering these promising effects of mut-Sema3A we sought to further investigate its actions on the TME landscape in order to assess its outcome in the tumor ecosystem. Therefore, we decided to perform a comprehensive analysis of control and mut-Sema3A treated PDAC tissues by single cell RNA-sequencing and Visium Spatial Gene Expression.

To set up a suitable and functional protocol of sc-RNA-sequencing we adapted several protocols from the literature to our experimental needs in the mPDAC model (71,224,225), and through complex procedures we succeeded in obtaining a tumor derived cell suspension depleted of $EpCAM^+$ epithelial tumoral cells, to enrich our samples of TME cells. We therefore proceeded with sequencing almost exclusively stromal cells from our samples, and subsequently clustered the single cell derived data and annotated the identified clusters. 11 clusters were pointed out in the PDAC control condition, and they were constituted by macrophages, neutrophils, fibroblasts, dendritic cells, B and T lymphocytes. 8 clusters were annotated in the mut-Sema3A-treated condition, and they were composed by macrophages, neutrophils, fibroblasts, T cells and pericytes. When assessing the cell percentage for every cluster, it emerged that the cellular compositions were variable between control and mut-Sema3A tumors, indeed macrophages and neutrophils were decreased following treatment, while T lymphocytes and fibroblasts resulted to be increased in number. The reduction in the myeloid compartment is consistent with the impaired tumor growth following mut-Sema3A administration, because it is well known that macrophages and neutrophils inside the PDAC stroma are prevalently pro-tumoral and immunosuppressive (120,133–135).

The most surprising finding following cluster annotation was a significant increase in the population of cancer associated fibroblasts (CAFs). While we were more focused on investigating the effect on immune cells, this specific outcome on CAFs was completely unexpected. To date, very few observations demonstrated how axon guidance cues can regulate CAF function (202). Therefore, we started to better analyze the transcriptomic profile of CAFs in mut-Sema3A-treated tumors. Firstly, the unique fibroblast cluster of the control samples resulted to be split in two different clusters in the treated samples. Secondly, the total number of fibroblasts was represented by 9.06% of cells in the control and by 20.71% of cells in the mut-Sema3A-treated, indicating that mut-Sema3A doubled the number of total fibroblasts following the treatment. Therefore, we started to study and compare the CAF gene signatures starting from published data that described well defined CAF sub-populations clustering them in three main classes: myofibroblastic (myCAFs), inflammatory (iCAFs) and antigen presenting (apCAFs) (71).

By crossing our data with the identified gene signatures, we were able to reproduce these CAFs sub-populations in our control PDAC. The control fibroblasts were therefore clearly separated into myCAFs, iCAFs and apCAFs, while, in contrast, mut-Sema3A-treated CAFs displayed a different gene signature. Cluster 4 mut-Sema3A fibroblasts signature was resembling control fibroblasts, even though it was not fitting entirely with the control signature. Remarkably, cluster 3 fibroblasts of mut-Sema3A-treated tumors displayed a totally new signature. 5% of the cluster 3 fibroblasts were iCAFs, 13% were apCAFs, and the remaining (82%) of them, that we named Semaphorin-Associated-Fibroblasts (SemAFs), showed a specific and completely different transcriptomic

profile. Therefore, using the EnrichR platform we better studied the SemAF signature by inquiring its functions and cellular specificity. Furthermore, we intersected these genes with pre-existing literature in order to identify their involvement in cancer progression. Interestingly, at least 11 genes of this new signature were described as anti-tumor effectors or were defining a "CAF-restraining" phenotype. Among these, Islr (coding for the Meflin protein), a marker of mesenchymal stem cells, has been shown to be expressed by pancreatic stellate cells that represent the main precursor giving rise to cancer associated fibroblasts in PDAC. Notably, Meflin has been indicated as a novel CAF marker in PDAC, and the Meflin^{+} CAF infiltration has been correlated with favorable patient outcome. Moreover, Meflin ablation enhanced tumor progression, while Meflin overexpression in CAFs resulted in PDAC growth suppression in xenograft mouse models (232). Finally, Meflin overexpression was also correlated with abundant Pdgfra and poor Acta2 expression (232). Based on these recent findings, Meflin has been described as one of the most important cancer-restraining CAF markers (232,235,236).

Among the other genes enclosed in the SemAF signature, Cygb, encoding for Cytoglobin is a hemeprotein involved in liver fibrosis and cancer progression and it has recently been negatively correlated with tumor size in pancreatic cancer (233). Cytoglobin is expressed by pancreatic stellate cells and findings demonstrated that it was able to impair CAF activation and to counteract oxidative damage by acting on downstream heat shock proteins. Other genes, such as Bgn, Cdh11, Mmp2, specifically expressed by SemAFs, have been shown to be strictly correlated with the quiescent status of pancreatic stellate cells (228,234,244). Therefore, we can hypothesize that the mut-Sema3A treatment re-programs activated CAFs towards a more quiescent and anti-tumor phenotype in PDAC. We further confirmed the above-mentioned gene signature following mut-Sema3A administration in PDAC tumors, by analyzing control and treated tumor tissues by means of *in situ* hybridization and spatial gene expression, and, in both cases, we could state that indeed fibroblasts expressing the SemAF signature were increased following the treatment, strengthening the finding that mut-Sema3A could act through tumor fibroblasts in order to exert its anti-tumor effects. These findings encouraged us to better assess whether mut-Sema3A was acting directly on the fibroblastic compartment. To this aim, we treated with mut-Sema3A ex-vivo activated mouse pancreatic fibroblasts and we evaluated the changes in the expression of several genes of the SemAF signature. Remarkably, we successfully identified a significant upregulation level of Islr, Cygb, Cdh11, Cxcl12, Thbs2, Col1a1, confirming what observed in vivo. Intriguingly, we observed, both by RT-PCR and *in situ* Hybridization, that one of the most up-regulated genes in mut-Sema3A fibroblasts was its selective receptor PlxnA4. These data suggest a possible feed-forward mechanism wherein the ligand enhances the expression of its own receptor, via an autocrine loop in CAFs. The presence of Sema3A autocrine loops have already been demonstrated in vessels in pathological conditions. For instance, it has been described that Sema3A autocrine loops in bone marrow endothelial cells were lost in patients with multiple myeloma (245), but this putative auto-stimulatory mechanism remains still poorly characterized when considering Sema3A-PlxnA4 interaction in ECs or other TME cell types in PDAC. We are planning to further investigate this interesting new biological mechanism both in CAFs and ECs (245).

One of the first observations regarding the mechanism of action of mut-Sema3A treatment in PDAC, was demonstrating its profound effect on tumor vessels and its ability to induce vessel normalization (185), therefore we sought to better understand which were the molecular processes underlying this outcome. We showed that mut-Sema3A was able to inhibit the active form of the small GTPase Rap1 in ECs, therefore affecting cellular adhesion and cell junction formation (185). Interestingly, other studies demonstrated that Rap1 inhibition allows the activation of the pro-inflammatory route that leads to the overexpression of adhesion molecules on the surface of

endothelial cells that enhance leukocytes transmigration from the blood stream towards the tumor tissue (238,246,247).

Based on these findings, we investigated the presence of such adhesion molecules on the intra-tumoral blood vessels. We focused on one of the most important adhesion molecules in vasculature, VCAM-1, and verified its expression level both in tumor tissue and *in-vitro* in Human Umbilical Vein Endothelial Cells (HUVEC)s. Remarkably we detected an increased expression of VCAM-1 following mut-Sema3A treatment in both tumor tissues and HUVECs. We can therefore hypothesize that mut-Sema3A is able to induce vessel remodeling and to regulate and enhance immune cell extravasation in PDAC tumors, by inhibiting Rap1 in tumor vessels and, consequently, by enhancing the downstream expression of adhesion molecules such as VCAM-1. Based on these mechanisms it is conceivable that the enhanced recruitment of $CD8^+$ T-cells observed in the PDAC tumors, could be due, at least in part, to the ability of mut-Sema3A to increase VCAM-1 expression on vessels, allowing leukocyte entrance throughout the tumor tissue (248). To further prove this hypothesis, we still have to functionally demonstrate the role of mut-Sema3A in regulating Rap1/VCAM-1 signaling axis in tumor vessels. It would be interesting, for instance, to re-activate the Rap1 signaling in *ex-vivo* settings and in PDAC mice treated or not with mut-Sema3A, by using specific Rap1 activators commercially available, to observe any potential abrogation of mut-Sema3A-induced T-cell recruitment in tumors.

To further and better analyze the effect of mut-Sema3A on the immune landscape, we subsequently performed immunofluorescent stainings to investigate the composition of the immune compartment at a tissue level, following mut-Sema3A treatment. We did not detect any significant changes of the amounts of M2-like macrophages and regulatory T cells in mut-Sema3A-treated tumors. In addition, we noticed a slight but not statistically significant increase in the percentage of M1 anti-tumoral macrophages. The most relevant and straight forward result achieved with mut-Sema3A on the immune population is the strong increase of $CD8^+$ cytotoxic T lymphocytes recruitment and activation, measured through granzyme B production. Even though it is conceivable to hypothesize that this dramatic increase of $CD8^+$ cytotoxic T lymphocytes in PDAC induced by mut-Sema3A may be due in part to its "pro-normalizing" effect and up-regulation of VCAM-1 in the tumor vasculature, we cannot exclude that other direct or indirect mechanisms contribute to this effect. For instance it has been shown that PlxnA4 is expressed not only by tumor vessels, but also by T-cells, and that it negatively regulates their function in autoimmune encephalomyelitis (249). Other findings demonstrated that Nrp-1/Sema3A/PlxnA4 formed a complex with B7-H4 enhancing regulatory $CD4^+$ T cell function in auto-immune diseases (250). More recently, it has been shown that PlxnA4 and Nrp-1 are expressed in circulating T-cells and that they regulate the activation and the homing to lymph nodes in a mouse model of melanoma in Sema3A independent manner (251). These findings suggest that PlxnA4 could also be expressed on $CD8^+$ T-cells in PDAC and that it could directly regulate their function, motility and recruitment. We started to evaluate PlxnA4 expression in T cells purified from our mPDAC model and, by means of RT-PCR, we observed a basal expression of PlxnA4. However, to date, we cannot fully confirm these observations since more experiments and repetitions need to be done. One of the technical problems we had was the low gain of $CD8^+$ T cells obtained from PDAC tumors and the lack of selective PlxnA4 antibodies able to confirm protein expression. If PlxnA4 is significantly expressed in T cells in mPDAC, we can expect that it may contribute to Sema3A-induced T cell recruitment and activation, in a Nrp-1 independent manner, with different mechanisms of action compared to the ones observed in the melanoma model (251).

Taking advantage of the fact the mut-Sema3A has a remarkable ability to recruit and activate cytotoxic T lymphocytes inside the tumor tissue, we wanted to investigate whether its effect could be potentiated by the combination with immunotherapeutic agents. Since our data suggest that mut-Sema3A acts by enhancing the anti-tumor immunity of $CD8^+$ T-cells, we sought to design a therapeutic combination simultaneously targeting diverse immune cells (163). We started by combining mut-Sema3A treatment with the monoclonal antibody antagonizing PD-1, an immune checkpoint receptor expressed on several T cell subsets that induces exhaustion and cell death when bound by its ligands, already used in clinical trials in PDAC patients (252). Disappointingly, no synergic effect was observable following the administration of these two molecules respect to the mut-Sema3A alone. Interestingly, as demonstrated in the PDAC patients, α-PD1 was not able to inhibit tumor growth in our mPDAC model, suggesting that in this combination mut-Sema3A is the only drug able to inhibit tumor growth and to activate $CD8^+$ T-cells.

We decided to use another immune checkpoint inhibitor, CTLA4 used alone or in combination with α-PD1 in PDAC (253) targeting the immune suppressive T-regs. We used therefore the α-CTLA4 monoclonal antibody to block CTLA4 which binding to CD80/CD86 competes with CD28, a co-stimulatory T cell co-receptor, hence transmitting a co-inhibitory signal (153,254).

Differently from α-PD1, α-CTLA4, as single agent, exerted an anti-tumor effect similarly to what we observed with mut-Sema3A. But the combination of both reagents did not produce a synergistic effect in reducing tumor growth. These data are interesting since suggest that in our mPDAC model T-regs are important for tumor progression, as previously shown (239) and that CTLA4 inhibition can partially hamper tumor growth. In addition, these findings indicate that mut-Sema3A and α-CTLA4 are both immune-modulators in our model, targeting distinct immune sub-populations, $CD8^+$ T-cells and T-regs, respectively. Since we did not observe any synergistic effects in their combination, we sought to further investigate whether other immune cell types were involved in PDAC progression and immunosuppression.

Myeloid cells and M2-like pro-tumoral macrophages have been described as important immune cells involved in the immune suppression and tumor progression in PDAC (109,121) and in our mPDAC model (239). We decided therefore to treat mPDAC mice with an agonist of the CD40 membrane receptor, expressed on the surface of antigen presenting cells (APCs) such as dendritic cells, B lymphocytes and macrophages, and which function is to lead APCs towards maturation in order to enhance cytotoxic responses and increase pro-inflammatory cytokine production (240,242,243,255,256). Notably, CD40 agonist exerted, even if with a lesser extent as compared to α-CTLA4 and mut-Sema3A, an anti-tumor effect as single agent, suggesting indeed that tumor associated macrophages may be a further target for mPDAC treatment. These data prompted us to try to combine the three drugs to see any improvement in tumor growth reduction observed with mut-Sema3A alone. Remarkably, we observed that only the triple combination of α-CD40, α-CTLA4 with mut-Sema3A was able to exert a significant synergistic effect in reducing tumor growth. In fact, we observed that α-CD40, α-CTLA4 and mut-Sema3A, reduced the tumor volume by 58% respect to the control, by 35% respect to the combination of α-CD40, α-CTLA4 and by 29% respect to the mut-Sema3A alone. These data together suggest that simultaneously targeting of multiple immune cell types (*i.e.* cytotoxic $CD8^+$ T-cells with mut-Sema3A, T-regs with α-CTLA4 and M1 macrophages polarization with α-CD40) in mPDAC may represent a more efficient therapeutic strategy to hamper PDAC growth.

We started to further investigate the changes in the immune cells landscape in PDAC tumors derived from the "triple" immune combination, through IF and confocal microscopy of tumor tissues. First, we did not observe any significant increase of $CD8^+$ T cells infiltration in the triple

treatment respect to mut-Sema3A alone, further confirming our hypothesis that the effect on T cell recruitment and activation is mainly due to the actions of mut-Sema3A and not strictly dependent on α-CD40 or α-CTLA4. Notably, while the amount of M2 pro-tumoral macrophages remained consistent between the different treatment conditions, the number of M1 anti-tumoral macrophages increased with synergic behavior in the triple combination. Indeed, while mut-Sema3A exerted a minor effect on M1, the synergistic combination with α-CD40 and α-CTLA4 was able to significantly enhance M1 amounts. These data indicate that, to efficiently impair tumor growth in the mPDAC model and to reduce the immune suppression, a simultaneous targeting is required, including T cell activation along with the modulation of macrophages towards an anti-tumor activity. Taking together, these data suggest that mut-Sema3A represents a suitable new candidate to be coupled with immunotherapy for clinical treatment of PDAC, since it has complementary effects on the recruitment of different immune populations.

Further analysis is needed to better understand the mechanism of action of mut-Sema3A on immune cells and in the combination therapies with immune-checkpoint inhibitors. For instance, we are planning to perform Flow Cytometry analysis of tumors derived from the "triple combination" compared to single treatment in mPDAC to assess, more precisely and in quantitative manner, the changes of sub classes of immune cells. We already set up a panel of antibodies to detect, by Flow Cytometry, T-cells, B-cells, NK and myeloid sub-types specifically designed for our instrument present at IRCC Cancer Institute. Our hope is to assess the functional contribution of other and specific subpopulations of immune cells. In addition, we will further analyze the changes in the immune ecosystem of mPDAC mice induced by mut-Sema3A and sequenced through sc-RNA-seq to uncover new immune sub-types modulated by the treatment. This analysis already suggested us that mut-Sema3A increased T cell amounts and induced M1 macrophages in PDAC tumors. Interestingly, we noticed that mut-Sema3A significantly reduced neutrophil levels as well. Neutrophils are a subtype of myeloid cells that are implicated, at different extents, to tumor progression with pro- and anti-tumor effects, and that can influence the outcome of immunotherapy (126,134,135). We are therefore planning to analyze neutrophil levels in the tumors derived from the triple combination compared to the single treatments, by microscope analysis and Flow Cytometry, through use of multiple and selective markers.

In conclusion, herein we show that mut-Sema3A is a potent molecule hampering PDAC progression and able of reprogramming the tumor microenvironment acting on several stromal populations. We unveiled for the first time that mut-Sema3A increases the number of fibroblasts and reprograms CAFs by switching their gene signature towards a cancer-restraining phenotype, defining a new subpopulation, the SemAFs. In fact, mut-Sema3A was able to upregulate genes typically expressed in the pancreatic stellate cells at their inactivation status and genes correlated with good PDAC prognosis. Moreover, mut-Sema3A is able of acting on CAFs directly, impairing their invasion potential, by acting and up-regulating its own receptor Plexin A4. Furtherly investigating the effect of mut-Sema3A on tumor vasculature and the better characterization of the "normalizing" effect on intra-tumoral blood vessels and its inhibition of Rap1 signaling in endothelial cells, we discovered that a potential mechanism of action could be the consequent upregulation of adhesion molecules such as VCAM-1 on normalized tumor vessels. These data allowed us to hypothesize that this mut-Sema3A-dependent VCAM-1 up-regulation could be in part responsible for the enhanced recruitment and trans-migration of T cells into the PDAC tumor tissues. Finally, mut-Sema3A reprogrammed the immune compartment of the tumor stroma inducing the recruitment and activation of $CD8^+$ cytotoxic T lymphocytes, and, together with α-CD40 and α-CTLA4 increased the number of anti-tumoral M1 macrophages, inducing a greater

anti-tumor activity in hampering PDAC growth. The molecular mechanisms leading to the anti-tumor synergistic effects, the immune and CAFs reprogramming and, above all, the molecular mechanisms and cellular signaling that regulates the cross-talk among the TME cells and that mediate the action of mut-Sema3A, are still to be investigated and are object of ongoing projects. The current data allows us to suggest that mut-Sema3A is a powerful and novel re-programmer of the tumor ecosystem that can be tested in pre-clinical and clinical combinatorial treatments as a TME modulator in PDAC.

REFERENCES

1. Siegel RL, Miller KD, Jemal A. Cancer statistics, 2020. CA Cancer J Clin. United States; 2020;70:7–30.

2. Jiang Y, Sohal DPS. Pancreatic Adenocarcinoma Management. JCO Oncol Pract. United States; 2022;OP2200328.

3. Cabasag CJ, Ferlay J, Laversanne M, Vignat J, Weber A, Soerjomataram I, et al. Pancreatic cancer: an increasing global public health concern. Gut. England; 2022;71:1686–7.

4. McGuire S. World Cancer Report 2014. Geneva, Switzerland: World Health Organization, International Agency for Research on Cancer, WHO Press, 2015. Adv Nutr. United States; 2016;7:418–9.

5. Schawkat K, Manning MA, Glickman JN, Mortele KJ. Pancreatic Ductal Adenocarcinoma and Its Variants: Pearls and Perils. Radiographics. United States; 2020;40:1219–39.

6. Khorana AA, Mangu PB, Berlin J, Engebretson A, Hong TS, Maitra A, et al. Potentially Curable Pancreatic Cancer: American Society of Clinical Oncology Clinical Practice Guideline. J Clin Oncol. United States; 2016;34:2541–56.

7. Noda Y, Tomita H, Ishihara T, Tsuboi Y, Kawai N, Kawaguchi M, et al. Prediction of overall survival in patients with pancreatic ductal adenocarcinoma: histogram analysis of ADC value and correlation with pathological intratumoral necrosis. BMC Med Imaging. England; 2022;22:23.

8. Sultana A, Smith CT, Cunningham D, Starling N, Neoptolemos JP, Ghaneh P. Meta-analyses of chemotherapy for locally advanced and metastatic pancreatic cancer. J Clin Oncol. United States; 2007;25:2607–15.

9. Principe DR, Underwood PW, Korc M, Trevino JG, Munshi HG, Rana A. The Current Treatment Paradigm for Pancreatic Ductal Adenocarcinoma and Barriers to Therapeutic Efficacy. Front Oncol. Switzerland; 2021;11:688377.

10. Von Hoff DD, Ervin T, Arena FP, Chiorean EG, Infante J, Moore M, et al. Increased survival in pancreatic cancer with nab-paclitaxel plus gemcitabine. N Engl J Med. United States; 2013;369:1691–703.

11. Conroy T, Hammel P, Hebbar M, Ben Abdelghani M, Wei AC, Raoul J-L, et al. FOLFIRINOX or Gemcitabine as Adjuvant Therapy for Pancreatic Cancer. N Engl J Med. United States; 2018;379:2395–406.

12. Fumarola C, Bonelli MA, Petronini PG, Alfieri RR. Targeting PI3K/AKT/mTOR pathway in non small cell lung cancer. Biochem Pharmacol. England; 2014;90:197–207.

13. Wolchok JD, Hoos A, O'Day S, Weber JS, Hamid O, Lebbé C, et al. Guidelines for the evaluation of immune therapy activity in solid tumors: immune-related response criteria. Clin Cancer Res. United States; 2009;15:7412–20.

14. Sarantis P, Koustas E, Papadimitropoulou A, Papavassiliou AG, Karamouzis MV. Pancreatic ductal adenocarcinoma: Treatment hurdles, tumor microenvironment and immunotherapy. World J Gastrointest Oncol. China; 2020;12:173–81.

15. Grant TJ, Hua K, Singh A. Molecular Pathogenesis of Pancreatic Cancer. Prog Mol Biol Transl Sci. Netherlands; 2016;144:241–75.

16. Samuel N, Hudson TJ. The molecular and cellular heterogeneity of pancreatic ductal adenocarcinoma. Nat Rev Gastroenterol Hepatol. England; 2011;9:77–87.

17. Jiang B, Zhou L, Lu J, Wang Y, Liu C, You L, et al. Stroma-Targeting Therapy in Pancreatic Cancer: One Coin With Two Sides? Front Oncol. Switzerland; 2020;10:576399.

18. Yang F, Jin C, Subedi S, Lee CL, Wang Q, Jiang Y, et al. Emerging inorganic nanomaterials for pancreatic cancer diagnosis and treatment. Cancer Treat Rev. Netherlands; 2012;38:566–79.

19. Neesse A, Michl P, Frese KK, Feig C, Cook N, Jacobetz MA, et al. Stromal biology and therapy in pancreatic cancer. Gut. England; 2011;60:861–8.

20. McCleary-Wheeler AL, McWilliams R, Fernandez-Zapico ME. Aberrant signaling pathways in pancreatic cancer: a two compartment view. Mol Carcinog. United States; 2012;51:25–39.

21. Li B, Wang Y, Jiang H, Li B, Shi X, Gao S, et al. Pros and Cons: High Proportion of Stromal Component Indicates Better Prognosis in Patients With Pancreatic Ductal Adenocarcinoma-A Research Based on the Evaluation of Whole-Mount Histological Slides. Front Oncol. Switzerland; 2020;10:1472.

22. Melzer MK, Arnold F, Stifter K, Zengerling F, Azoitei N, Seufferlein T, et al. An Immunological Glance on Pancreatic Ductal Adenocarcinoma. Int J Mol Sci. Switzerland; 2020;21.

23. Perez VM, Kearney JF, Yeh JJ. The PDAC Extracellular Matrix: A Review of the ECM Protein Composition, Tumor Cell Interaction, and Therapeutic Strategies. Front Oncol. Switzerland; 2021;11:751311.

24. Wu XZ, Chen D, Xie GR. Extracellular matrix remodeling in hepatocellular carcinoma: effects of soil on seed? Med Hypotheses. United States; 2006;66:1115–20.

25. Parker AL, Cox TR. The Role of the ECM in Lung Cancer Dormancy and Outgrowth. Front Oncol. Switzerland; 2020;10:1766.

26. Cukierman E, Bassi DE. Physico-mechanical aspects of extracellular matrix influences on tumorigenic behaviors. Semin Cancer Biol. England; 2010;20:139–45.

27. Tian C, Clauser KR, Öhlund D, Rickelt S, Huang Y, Gupta M, et al. Proteomic analyses of ECM during pancreatic ductal adenocarcinoma progression reveal different contributions by tumor and stromal cells. Proc Natl Acad Sci U S A. United States; 2019;116:19609–18.

28. Weniger M, Honselmann KC, Liss AS. The Extracellular Matrix and Pancreatic Cancer: A Complex Relationship. Cancers (Basel). Switzerland; 2018;10.

29. Xu Z, Pothula SP, Wilson JS, Apte MV. Pancreatic cancer and its stroma: a conspiracy theory. World J Gastroenterol. United States; 2014;20:11216–29.

30. von Ahrens D, Bhagat TD, Nagrath D, Maitra A, Verma A. The role of stromal cancer-associated fibroblasts in pancreatic cancer. J Hematol Oncol. England; 2017;10:76.

31. Adiseshaiah PP, Crist RM, Hook SS, McNeil SE. Nanomedicine strategies to overcome the pathophysiological barriers of pancreatic cancer. Nat Rev Clin Oncol. England; 2016;13:750–65.

32. Meng H, Nel AE. Use of nano engineered approaches to overcome the stromal barrier in pancreatic cancer. Adv Drug Deliv Rev. Netherlands; 2018;130:50–7.

33. Natarajan V, Ha S, Delgado A, Jacobson R, Alhalhooly L, Choi Y, et al. Acquired αSMA Expression in Pericytes Coincides with Aberrant Vascular Structure and Function in Pancreatic Ductal Adenocarcinoma. Cancers (Basel). Switzerland; 2022;14.

34. Erkan M, Michalski CW, Rieder S, Reiser-Erkan C, Abiatari I, Kolb A, et al. The activated stroma index is a novel and independent prognostic marker in pancreatic ductal adenocarcinoma. Clin Gastroenterol Hepatol. United States; 2008;6:1155–61.

35. Thind K, Padrnos LJ, Ramanathan RK, Borad MJ. Immunotherapy in pancreatic cancer treatment: a new frontier. Therap Adv Gastroenterol. England; 2017;10:168–94.

36. Ferrara B, Pignatelli C, Cossutta M, Citro A, Courty J, Piemonti L. The Extracellular Matrix in Pancreatic Cancer: Description of a Complex Network and Promising Therapeutic Options. Cancers (Basel). Switzerland; 2021;13.

37. Lee JJ, Perera RM, Wang H, Wu D-C, Liu XS, Han S, et al. Stromal response to Hedgehog signaling restrains pancreatic cancer progression. Proc Natl Acad Sci U S A. United States; 2014;111:E3091-3100.

38. Özdemir BC, Pentcheva-Hoang T, Carstens JL, Zheng X, Wu C-C, Simpson TR, et al. Depletion of Carcinoma-Associated Fibroblasts and Fibrosis Induces Immunosuppression and Accelerates Pancreas Cancer with Reduced Survival. Cancer Cell. United States; 2015;28:831–3.

39. Kim EJ, Sahai V, Abel EV, Griffith KA, Greenson JK, Takebe N, et al. Pilot clinical trial of hedgehog pathway inhibitor GDC-0449 (vismodegib) in combination with gemcitabine in patients with metastatic pancreatic adenocarcinoma. Clin Cancer Res. United States; 2014;20:5937–45.

40. Rhim AD, Oberstein PE, Thomas DH, Mirek ET, Palermo CF, Sastra SA, et al. Stromal elements act to restrain, rather than support, pancreatic ductal adenocarcinoma. Cancer Cell. United States; 2014;25:735–47.

41. Jiang H, Torphy RJ, Steiger K, Hongo H, Ritchie AJ, Kriegsmann M, et al. Pancreatic ductal adenocarcinoma progression is restrained by stromal matrix. J Clin Invest. United States; 2020;130:4704–9.

42. Torphy RJ, Wang Z, True-Yasaki A, Volmar KE, Rashid N, Yeh B, et al. Stromal Content Is Correlated With Tissue Site, Contrast Retention, and Survival in Pancreatic Adenocarcinoma. JCO Precis Oncol. United States; 2018;2018.

43. Roberts KJ, Kershner AM, Beachy PA. The Stromal Niche for Epithelial Stem Cells: A Template for Regeneration and a Brake on Malignancy. Cancer Cell. United States; 2017;32:404–10.

44. Öhlund D, Elyada E, Tuveson D. Fibroblast heterogeneity in the cancer wound. J Exp Med. United States; 2014;211:1503–23.

45. Arina A, Idel C, Hyjek EM, Alegre M-L, Wang Y, Bindokas VP, et al. Tumor-associated fibroblasts predominantly come from local and not circulating precursors. Proc Natl Acad Sci U S A. United States; 2016;113:7551–6.

46. Neuzillet C, Tijeras-Raballand A, Ragulan C, Cros J, Patil Y, Martinet M, et al. Inter- and intra-tumoural heterogeneity in cancer-associated fibroblasts of human pancreatic ductal adenocarcinoma. J Pathol. England; 2019;248:51–65.

47. Moir JAG, Mann J, White SA. The role of pancreatic stellate cells in pancreatic cancer. Surg Oncol. Netherlands; 2015;24:232–8.

48. Apte MV, Xu Z, Pothula S, Goldstein D, Pirola RC, Wilson JS. Pancreatic cancer: The microenvironment needs attention too! Pancreatology. Switzerland; 2015;15:S32-38.

49. Sun Q, Zhang B, Hu Q, Qin Y, Xu W, Liu W, et al. The impact of cancer-associated fibroblasts on major hallmarks of pancreatic cancer. Theranostics. Australia; 2018;8:5072–87.

50. Liu T, Han C, Wang S, Fang P, Ma Z, Xu L, et al. Cancer-associated fibroblasts: an emerging target of anti-cancer immunotherapy. J Hematol Oncol. England; 2019;12:86.

51. Liot S, Balas J, Aubert A, Prigent L, Mercier-Gouy P, Verrier B, et al. Stroma Involvement in Pancreatic Ductal Adenocarcinoma: An Overview Focusing on Extracellular Matrix Proteins. Front Immunol. Switzerland; 2021;12:612271.

52. Mao X, Xu J, Wang W, Liang C, Hua J, Liu J, et al. Crosstalk between cancer-associated fibroblasts and immune cells in the tumor microenvironment: new findings and future perspectives. Mol Cancer. England; 2021;20:131.

53. Nielsen MFB, Mortensen MB, Detlefsen S. Identification of markers for quiescent pancreatic stellate cells in the normal human pancreas. Histochem Cell Biol. Germany; 2017;148:359–80.

54. Haber PS, Keogh GW, Apte MV, Moran CS, Stewart NL, Crawford DH, et al. Activation of pancreatic stellate cells in human and experimental pancreatic fibrosis. Am J Pathol. United States; 1999;155:1087–95.

55. Ota S, Nishimura M, Murakami Y, Birukawa NK, Yoneda A, Nishita H, et al. Involvement of Pancreatic Stellate Cells in Regeneration of Remnant Pancreas after Partial Pancreatectomy. PLoS One. United States; 2016;11:e0165747.

56. Boyd CA, Benarroch-Gampel J, Sheffield KM, Cooksley CD, Riall TS. 415 patients with adenosquamous carcinoma of the pancreas: a population-based analysis of prognosis and survival. J Surg Res. United States; 2012;174:12–9.

57. McGranahan N, Swanton C. Clonal Heterogeneity and Tumor Evolution: Past, Present, and the Future. Cell. United States; 2017;168:613–28.

58. Waddell N, Pajic M, Patch A-M, Chang DK, Kassahn KS, Bailey P, et al. Whole genomes redefine the mutational landscape of pancreatic cancer. Nature. England; 2015;518:495–501.

59. Truong L-H, Pauklin S. Pancreatic Cancer Microenvironment and Cellular Composition: Current Understandings and Therapeutic Approaches. Cancers (Basel). Switzerland; 2021;13.

60. Lafaro KJ, Melstrom LG. The Paradoxical Web of Pancreatic Cancer Tumor Microenvironment. Am J Pathol. United States; 2019;189:44–57.

61. Whatcott CJ, Diep CH, Jiang P, Watanabe A, LoBello J, Sima C, et al. Desmoplasia in Primary Tumors and Metastatic Lesions of Pancreatic Cancer. Clin Cancer Res. United States; 2015;21:3561–8.

62. Mace TA, Bloomston M, Lesinski GB. Pancreatic cancer-associated stellate cells: A viable target for reducing immunosuppression in the tumor microenvironment. Oncoimmunology. United States; 2013;2:e24891.

63. Ene-Obong A, Clear AJ, Watt J, Wang J, Fatah R, Riches JC, et al. Activated pancreatic stellate cells sequester CD8+ T cells to reduce their infiltration of the juxtatumoral compartment of pancreatic ductal adenocarcinoma. Gastroenterology. United States; 2013;145:1121–32.

64. Orhan A, Vogelsang RP, Andersen MB, Madsen MT, Hölmich ER, Raskov H, et al. The prognostic value of tumour-infiltrating lymphocytes in pancreatic cancer: a systematic review and meta-analysis. Eur J Cancer. England; 2020;132:71–84.

65. Feig C, Jones JO, Kraman M, Wells RJB, Deonarine A, Chan DS, et al. Targeting CXCL12 from FAP-expressing carcinoma-associated fibroblasts synergizes with anti-PD-L1 immunotherapy in pancreatic cancer. Proc Natl Acad Sci U S A. United States; 2013;110:20212–7.

66. Bockorny B, Semenisty V, Macarulla T, Borazanci E, Wolpin BM, Stemmer SM, et al. BL-8040, a CXCR4 antagonist, in combination with pembrolizumab and chemotherapy for pancreatic cancer: the COMBAT trial. Nat Med. United States; 2020;26:878–85.

67. Krishnamoorthy M, Lenehan JG, Burton JP, Maleki Vareki S. Immunomodulation in Pancreatic Cancer. Cancers (Basel). Switzerland; 2020;12.

68. Norton J, Foster D, Chinta M, Titan A, Longaker M. Pancreatic Cancer Associated Fibroblasts (CAF): Under-Explored Target for Pancreatic Cancer Treatment. Cancers (Basel). Switzerland; 2020;12.

69. Huang T-X, Guan X-Y, Fu L. Therapeutic targeting of the crosstalk between cancer-associated fibroblasts and cancer stem cells. Am J Cancer Res. United States; 2019;9:1889–904.

70. Öhlund D, Handly-Santana A, Biffi G, Elyada E, Almeida AS, Ponz-Sarvise M, et al. Distinct populations of inflammatory fibroblasts and myofibroblasts in pancreatic cancer. J Exp Med. United States; 2017;214:579–96.

71. Elyada E, Bolisetty M, Laise P, Flynn WF, Courtois ET, Burkhart RA, et al. Cross-Species Single-Cell Analysis of Pancreatic Ductal Adenocarcinoma Reveals Antigen-Presenting Cancer-Associated Fibroblasts. Cancer Discov. United States; 2019;9:1102–23.

72. Kraman M, Bambrough PJ, Arnold JN, Roberts EW, Magiera L, Jones JO, et al. Suppression of antitumor immunity by stromal cells expressing fibroblast activation protein-alpha. Science. United States; 2010;330:827–30.

73. Biffi G, Oni TE, Spielman B, Hao Y, Elyada E, Park Y, et al. IL1-Induced JAK/STAT Signaling Is Antagonized by TGFβ to Shape CAF Heterogeneity in Pancreatic Ductal Adenocarcinoma. Cancer Discov. United States; 2019;9:282–301.

74. Axelrod ML, Cook RS, Johnson DB, Balko JM. Biological Consequences of MHC-II Expression by Tumor Cells in Cancer. Clin Cancer Res. United States; 2019;25:2392–402.

75. DeSelm CJ, Tano ZE, Varghese AM, Adusumilli PS. CAR T-cell therapy for pancreatic cancer. J Surg Oncol. United States; 2017;116:63–74.

76. Fang Z, Meng Q, Xu J, Wang W, Zhang B, Liu J, et al. Signaling pathways in cancer-associated fibroblasts: recent advances and future perspectives. Cancer Commun (Lond). United States; 2023;43:3–41.

77. Martinez-Bosch N, Vinaixa J, Navarro P. Immune Evasion in Pancreatic Cancer: From Mechanisms to Therapy. Cancers (Basel). Switzerland; 2018;10.

78. Woo S-R, Corrales L, Gajewski TF. Innate immune recognition of cancer. Annu Rev Immunol. United States; 2015;33:445–74.

79. Stone ML, Beatty GL. Cellular determinants and therapeutic implications of inflammation in pancreatic cancer. Pharmacol Ther. England; 2019;201:202–13.

80. de Visser KE, Eichten A, Coussens LM. Paradoxical roles of the immune system during cancer development. Nat Rev Cancer. England; 2006;6:24–37.

81. Hinshaw DC, Shevde LA. The Tumor Microenvironment Innately Modulates Cancer Progression. Cancer Res. United States; 2019;79:4557–66.

82. Bailey P, Chang DK, Nones K, Johns AL, Patch A-M, Gingras M-C, et al. Genomic analyses identify molecular subtypes of pancreatic cancer. Nature. England; 2016;531:47–52.

83. Leung L, Radulovich N, Zhu C-Q, Organ S, Bandarchi B, Pintilie M, et al. Lipocalin2 promotes invasion, tumorigenicity and gemcitabine resistance in pancreatic ductal adenocarcinoma. PLoS One. United States; 2012;7:e46677.

84. Carstens JL, Correa de Sampaio P, Yang D, Barua S, Wang H, Rao A, et al. Spatial computation of intratumoral T cells correlates with survival of patients with pancreatic cancer. Nat Commun. England; 2017;8:15095.

85. Balli D, Rech AJ, Stanger BZ, Vonderheide RH. Immune Cytolytic Activity Stratifies Molecular Subsets of Human Pancreatic Cancer. Clin Cancer Res. United States; 2017;23:3129–38.

86. Huber M, Brehm CU, Gress TM, Buchholz M, Alashkar Alhamwe B, von Strandmann EP, et al. The Immune Microenvironment in Pancreatic Cancer. Int J Mol Sci. Switzerland; 2020;21.

87. Liu X, Xu J, Zhang B, Liu J, Liang C, Meng Q, et al. The reciprocal regulation between host tissue and immune cells in pancreatic ductal adenocarcinoma: new insights and therapeutic implications. Mol Cancer. England; 2019;18:184.

88. Gabitass RF, Annels NE, Stocken DD, Pandha HA, Middleton GW. Elevated myeloid-derived suppressor cells in pancreatic, esophageal and gastric cancer are an independent prognostic factor and are associated with significant elevation of the Th2 cytokine interleukin-13. Cancer Immunol Immunother. Germany; 2011;60:1419–30.

89. Feig C, Gopinathan A, Neesse A, Chan DS, Cook N, Tuveson DA. The pancreas cancer microenvironment. Clin Cancer Res. United States; 2012;18:4266–76.

90. Mitchem JB, Brennan DJ, Knolhoff BL, Belt BA, Zhu Y, Sanford DE, et al. Targeting tumor-infiltrating macrophages decreases tumor-initiating cells, relieves immunosuppression, and improves chemotherapeutic responses. Cancer Res. United States; 2013;73:1128–41.

91. Pylayeva-Gupta Y, Lee KE, Hajdu CH, Miller G, Bar-Sagi D. Oncogenic Kras-induced GM-CSF production promotes the development of pancreatic neoplasia. Cancer Cell. United States; 2012;21:836–47.

92. Gabrilovich DI. Myeloid-Derived Suppressor Cells. Cancer Immunol Res. United States; 2017;5:3–8.

93. Clark CE, Hingorani SR, Mick R, Combs C, Tuveson DA, Vonderheide RH. Dynamics of the immune reaction to pancreatic cancer from inception to invasion. Cancer Res. United States; 2007;67:9518–27.

94. Pinton L, Solito S, Damuzzo V, Francescato S, Pozzuoli A, Berizzi A, et al. Activated T cells sustain myeloid-derived suppressor cell-mediated immune suppression. Oncotarget. United States; 2016;7:1168–84.

95. Huang B, Pan P-Y, Li Q, Sato AI, Levy DE, Bromberg J, et al. Gr-1+CD115+ immature myeloid suppressor cells mediate the development of tumor-induced T regulatory cells and T-cell anergy in tumor-bearing host. Cancer Res. United States; 2006;66:1123–31.

96. Siret C, Collignon A, Silvy F, Robert S, Cheyrol T, André P, et al. Deciphering the Crosstalk Between Myeloid-Derived Suppressor Cells and Regulatory T Cells in Pancreatic Ductal Adenocarcinoma. Front Immunol. Switzerland; 2019;10:3070.

97. Liu C, Yu S, Kappes J, Wang J, Grizzle WE, Zinn KR, et al. Expansion of spleen myeloid suppressor cells represses NK cell cytotoxicity in tumor-bearing host. Blood. United States; 2007;109:4336–42.

98. Ostrand-Rosenberg S, Sinha P, Beury DW, Clements VK. Cross-talk between myeloid-derived suppressor cells (MDSC), macrophages, and dendritic cells enhances tumor-induced immune suppression. Semin Cancer Biol. England; 2012;22:275–81.

99. Sinha P, Clements VK, Bunt SK, Albelda SM, Ostrand-Rosenberg S. Cross-talk between myeloid-derived suppressor cells and macrophages subverts tumor immunity toward a type 2 response. J Immunol. United States; 2007;179:977–83.

100. Stromnes IM, Brockenbrough JS, Izeradjene K, Carlson MA, Cuevas C, Simmons RM, et al. Targeted depletion of an MDSC subset unmasks pancreatic ductal adenocarcinoma to adaptive immunity. Gut. England; 2014;63:1769–81.

101. Zhang Y, Velez-Delgado A, Mathew E, Li D, Mendez FM, Flannagan K, et al. Myeloid cells are required for PD-1/PD-L1 checkpoint activation and the establishment of an immunosuppressive environment in pancreatic cancer. Gut. England; 2017;66:124–36.

102. Zhou J, Tang Z, Gao S, Li C, Feng Y, Zhou X. Tumor-Associated Macrophages: Recent Insights and Therapies. Front Oncol. Switzerland; 2020;10:188.

103. Gordon S, Taylor PR. Monocyte and macrophage heterogeneity. Nat Rev Immunol. England; 2005;5:953–64.

104. Santoni M, Bracarda S, Nabissi M, Massari F, Conti A, Bria E, et al. CXC and CC chemokines as angiogenic modulators in nonhaematological tumors. Biomed Res Int. United States; 2014;2014:768758.

105. Biswas SK, Mantovani A. Macrophage plasticity and interaction with lymphocyte subsets: cancer as a paradigm. Nat Immunol. United States; 2010;11:889–96.

106. Mosser DM, Edwards JP. Exploring the full spectrum of macrophage activation. Nat Rev Immunol. England; 2008;8:958–69.

107. Bolli E, Movahedi K, Laoui D, Van Ginderachter JA. Novel insights in the regulation and function of macrophages in the tumor microenvironment. Curr Opin Oncol. United States; 2017;29:55–61.

108. Sica A, Schioppa T, Mantovani A, Allavena P. Tumour-associated macrophages are a distinct M2 polarised population promoting tumour progression: potential targets of anti-cancer therapy. Eur J Cancer. England; 2006;42:717–27.

109. Bayne LJ, Beatty GL, Jhala N, Clark CE, Rhim AD, Stanger BZ, et al. Tumor-derived granulocyte-macrophage colony-stimulating factor regulates myeloid inflammation and T cell immunity in pancreatic cancer. Cancer Cell. United States; 2012;21:822–35.

110. Monti P, Leone BE, Marchesi F, Balzano G, Zerbi A, Scaltrini F, et al. The CC chemokine MCP-1/CCL2 in pancreatic cancer progression: regulation of expression and potential mechanisms of antimalignant activity. Cancer Res. United States; 2003;63:7451–61.

111. Allavena P, Sica A, Solinas G, Porta C, Mantovani A. The inflammatory micro-environment in tumor progression: the role of tumor-associated macrophages. Crit Rev Oncol Hematol. Netherlands; 2008;66:1–9.

112. Sica A, Allavena P, Mantovani A. Cancer related inflammation: the macrophage connection. Cancer Lett. Ireland; 2008;267:204–15.

113. Garcia Garcia CJ, Huang Y, Fuentes NR, Turner MC, Monberg ME, Lin D, et al. Stromal HIF2 Regulates Immune Suppression in the Pancreatic Cancer Microenvironment. Gastroenterology. United States; 2022;162:2018–31.

114. Osipov A, Saung MT, Zheng L, Murphy AG. Small molecule immunomodulation: the tumor microenvironment and overcoming immune escape. J Immunother Cancer. England; 2019;7:224.

115. Rubin SJS, Sojwal RS, Gubatan J, Rogalla S. The Tumor Immune Microenvironment in Pancreatic Ductal Adenocarcinoma: Neither Hot nor Cold. Cancers (Basel). Switzerland; 2022;14.

116. Mantovani A, Sica A. Macrophages, innate immunity and cancer: balance, tolerance, and diversity. Curr Opin Immunol. England; 2010;22:231–7.

117. Noy R, Pollard JW. Tumor-associated macrophages: from mechanisms to therapy. Immunity. United States; 2014;41:49–61.

118. Wan S, Zhao E, Kryczek I, Vatan L, Sadovskaya A, Ludema G, et al. Tumor-associated macrophages produce interleukin 6 and signal via STAT3 to promote expansion of human hepatocellular carcinoma stem cells. Gastroenterology. United States; 2014;147:1393–404.

119. Solinas G, Germano G, Mantovani A, Allavena P. Tumor-associated macrophages (TAM) as major players of the cancer-related inflammation. J Leukoc Biol. United States; 2009;86:1065–73.

120. Lankadasari MB, Mukhopadhyay P, Mohammed S, Harikumar KB. TAMing pancreatic cancer: combat with a double edged sword. Mol Cancer. England; 2019;18:48.

121. Weizman N, Krelin Y, Shabtay-Orbach A, Amit M, Binenbaum Y, Wong RJ, et al. Macrophages mediate gemcitabine resistance of pancreatic adenocarcinoma by upregulating cytidine deaminase. Oncogene. England; 2014;33:3812–9.

122. Liou G-Y, Döppler H, Necela B, Edenfield B, Zhang L, Dawson DW, et al. Mutant KRAS-induced expression of ICAM-1 in pancreatic acinar cells causes attraction of macrophages to expedite the formation of precancerous lesions. Cancer Discov. United States; 2015;5:52–63.

123. Sanford DE, Belt BA, Panni RZ, Mayer A, Deshpande AD, Carpenter D, et al. Inflammatory monocyte mobilization decreases patient survival in pancreatic cancer: a role for targeting the CCL2/CCR2 axis. Clin Cancer Res. United States; 2013;19:3404–15.

124. Kalbasi A, Komar C, Tooker GM, Liu M, Lee JW, Gladney WL, et al. Tumor-Derived CCL2 Mediates Resistance to Radiotherapy in Pancreatic Ductal Adenocarcinoma. Clin Cancer Res. United States; 2017;23:137–48.

125. Reid MD, Basturk O, Thirabanjasak D, Hruban RH, Klimstra DS, Bagci P, et al. Tumor-infiltrating neutrophils in pancreatic neoplasia. Mod Pathol. United States; 2011;24:1612–9.

126. Xiang Z-J, Hu T, Wang Y, Wang H, Xu L, Cui N. Neutrophil-lymphocyte ratio (NLR) was associated with prognosis and immunomodulatory in patients with pancreatic ductal adenocarcinoma (PDAC). Biosci Rep. England; 2020;40.

127. Zou J-M, Qin J, Li Y-C, Wang Y, Li D, Shu Y, et al. IL-35 induces N2 phenotype of neutrophils to promote tumor growth. Oncotarget. United States; 2017;8:33501–14.

128. Hirth M, Gandla J, Höper C, Gaida MM, Agarwal N, Simonetti M, et al. CXCL10 and CCL21 Promote Migration of Pancreatic Cancer Cells Toward Sensory Neurons and Neural Remodeling in Tumors in Mice, Associated With Pain in Patients. Gastroenterology. United States; 2020;159:665-681.e13.

129. Shaul ME, Fridlender ZG. Tumour-associated neutrophils in patients with cancer. Nat Rev Clin Oncol. England; 2019;16:601–20.

130. Mollinedo F. Neutrophil Degranulation, Plasticity, and Cancer Metastasis. Trends Immunol. England; 2019;40:228–42.

131. Fridlender ZG, Albelda SM. Tumor-associated neutrophils: friend or foe? Carcinogenesis. England; 2012;33:949–55.

132. Wislez M, Rabbe N, Marchal J, Milleron B, Crestani B, Mayaud C, et al. Hepatocyte growth factor production by neutrophils infiltrating bronchioloalveolar subtype pulmonary adenocarcinoma: role in tumor progression and death. Cancer Res. United States; 2003;63:1405–12.

133. Brandau S, Dumitru CA, Lang S. Protumor and antitumor functions of neutrophil granulocytes. Semin Immunopathol. Germany; 2013;35:163–76.

134. Shaul ME, Levy L, Sun J, Mishalian I, Singhal S, Kapoor V, et al. Tumor-associated neutrophils display a distinct N1 profile following TGFβ modulation: A transcriptomics analysis of pro- vs. antitumor TANs. Oncoimmunology. United States; 2016;5:e1232221.

135. Wang Y, Fang T, Huang L, Wang H, Zhang L, Wang Z, et al. Neutrophils infiltrating pancreatic ductal adenocarcinoma indicate higher malignancy and worse prognosis. Biochem Biophys Res Commun. United States; 2018;501:313–9.

136. Ardi VC, Kupriyanova TA, Deryugina EI, Quigley JP. Human neutrophils uniquely release TIMP-free MMP-9 to provide a potent catalytic stimulator of angiogenesis. Proc Natl Acad Sci U S A. United States; 2007;104:20262–7.

137. Munder M, Schneider H, Luckner C, Giese T, Langhans C-D, Fuentes JM, et al. Suppression of T-cell functions by human granulocyte arginase. Blood. United States; 2006;108:1627–34.

138. Zhang J, Xu X, Shi M, Chen Y, Yu D, Zhao C, et al. CD13(hi) Neutrophil-like myeloid-derived suppressor cells exert immune suppression through Arginase 1 expression in pancreatic ductal adenocarcinoma. Oncoimmunology. United States; 2017;6:e1258504.

139. Takesue S, Ohuchida K, Shinkawa T, Otsubo Y, Matsumoto S, Sagara A, et al. Neutrophil extracellular traps promote liver micrometastasis in pancreatic ductal adenocarcinoma via the activation of cancer-associated fibroblasts. Int J Oncol. Greece; 2020;56:596–605.

140. Zhang Y, Chandra V, Riquelme Sanchez E, Dutta P, Quesada PR, Rakoski A, et al. Interleukin-17-induced neutrophil extracellular traps mediate resistance to checkpoint blockade in pancreatic cancer. J Exp Med. United States; 2020;217.

141. Tao L, Zhang L, Peng Y, Tao M, Li L, Xiu D, et al. Neutrophils assist the metastasis of circulating tumor cells in pancreatic ductal adenocarcinoma: A new hypothesis and a new predictor for distant metastasis. Medicine (Baltimore). United States; 2016;95:e4932.

142. Hogendorf P, Durczyński A, Skulimowski A, Kumor A, Poznańska G, Strzelczyk J. Neutrophil Gelatinase-Associated Lipocalin (NGAL) concentration in urine is superior to CA19-9 and Ca 125 in differentiation of pancreatic mass: Preliminary report. Cancer Biomark. Netherlands; 2016;16:537–43.

143. Nielsen SR, Strøbech JE, Horton ER, Jackstadt R, Laitala A, Bravo MC, et al. Suppression of tumor-associated neutrophils by lorlatinib attenuates pancreatic cancer growth and improves treatment with immune checkpoint blockade. Nat Commun. England; 2021;12:3414.

144. Kim JM, Rasmussen JP, Rudensky AY. Regulatory T cells prevent catastrophic autoimmunity throughout the lifespan of mice. Nat Immunol. United States; 2007;8:191–7.

145. Bauer CA, Kim EY, Marangoni F, Carrizosa E, Claudio NM, Mempel TR. Dynamic Treg interactions with intratumoral APCs promote local CTL dysfunction. J Clin Invest. United States; 2014;124:2425–40.

146. Ghiringhelli F, Puig PE, Roux S, Parcellier A, Schmitt E, Solary E, et al. Tumor cells convert immature myeloid dendritic cells into TGF-beta-secreting cells inducing CD4+CD25+ regulatory T cell proliferation. J Exp Med. United States; 2005;202:919–29.

147. Scarlett UK, Rutkowski MR, Rauwerdink AM, Fields J, Escovar-Fadul X, Baird J, et al. Ovarian cancer progression is controlled by phenotypic changes in dendritic cells. J Exp Med. United States; 2012;209:495–506.

148. Frumento G, Rotondo R, Tonetti M, Damonte G, Benatti U, Ferrara GB. Tryptophan-derived catabolites are responsible for inhibition of T and natural killer cell proliferation induced by indoleamine 2,3-dioxygenase. J Exp Med. United States; 2002;196:459–68.

149. Sharma MD, Baban B, Chandler P, Hou D-Y, Singh N, Yagita H, et al. Plasmacytoid dendritic cells from mouse tumor-draining lymph nodes directly activate mature Tregs via indoleamine 2,3-dioxygenase. J Clin Invest. United States; 2007;117:2570–82.

150. Josefowicz SZ, Lu L-F, Rudensky AY. Regulatory T cells: mechanisms of differentiation and function. Annu Rev Immunol. United States; 2012;30:531–64.

151. Hiraoka N, Onozato K, Kosuge T, Hirohashi S. Prevalence of FOXP3+ regulatory T cells increases during the progression of pancreatic ductal adenocarcinoma and its premalignant lesions. Clin Cancer Res. United States; 2006;12:5423–34.

152. Liyanage UK, Moore TT, Joo H-G, Tanaka Y, Herrmann V, Doherty G, et al. Prevalence of regulatory T cells is increased in peripheral blood and tumor microenvironment of patients with pancreas or breast adenocarcinoma. J Immunol. United States; 2002;169:2756–61.

153. Jang J-E, Hajdu CH, Liot C, Miller G, Dustin ML, Bar-Sagi D. Crosstalk between Regulatory T Cells and Tumor-Associated Dendritic Cells Negates Anti-tumor Immunity in Pancreatic Cancer. Cell Rep. United States; 2017;20:558–71.

154. Cederbom L, Hall H, Ivars F. CD4+CD25+ regulatory T cells down-regulate co-stimulatory molecules on antigen-presenting cells. Eur J Immunol. Germany; 2000;30:1538–43.

155. Onishi Y, Fehervari Z, Yamaguchi T, Sakaguchi S. Foxp3+ natural regulatory T cells preferentially form aggregates on dendritic cells in vitro and actively inhibit their maturation. Proc Natl Acad Sci U S A. United States; 2008;105:10113–8.

156. Keenan BP, Saenger Y, Kafrouni MI, Leubner A, Lauer P, Maitra A, et al. A Listeria vaccine and depletion of T-regulatory cells activate immunity against early stage pancreatic intraepithelial neoplasms and prolong survival of mice. Gastroenterology. United States; 2014;146:1784-1794.e6.

157. Leao IC, Ganesan P, Armstrong TD, Jaffee EM. Effective depletion of regulatory T cells allows the recruitment of mesothelin-specific CD8 T cells to the antitumor immune response against a mesothelin-expressing mouse pancreatic adenocarcinoma. Clin Transl Sci. United States; 2008;1:228–39.

158. Chellappa S, Hugenschmidt H, Hagness M, Line PD, Labori KJ, Wiedswang G, et al. Regulatory T cells that co-express RORγt and FOXP3 are pro-inflammatory and immunosuppressive and expand in human pancreatic cancer. Oncoimmunology. United States; 2016;5:e1102828.

159. Zhang Y, Lazarus J, Steele NG, Yan W, Lee H-J, Nwosu ZC, et al. Regulatory T-cell Depletion Alters the Tumor Microenvironment and Accelerates Pancreatic Carcinogenesis. Cancer Discov. United States; 2020;10:422–39.

160. Emmrich J, Weber I, Nausch M, Sparmann G, Koch K, Seyfarth M, et al. Immunohistochemical characterization of the pancreatic cellular infiltrate in normal pancreas, chronic pancreatitis and pancreatic carcinoma. Digestion. Switzerland; 1998;59:192–8.

161. Farhood B, Najafi M, Mortezaee K. CD8(+) cytotoxic T lymphocytes in cancer immunotherapy: A review. J Cell Physiol. United States; 2019;234:8509–21.

162. Kallies A, Zehn D, Utzschneider DT. Precursor exhausted T cells: key to successful immunotherapy? Nat Rev Immunol. England; 2020;20:128–36.

163. Jiang Y, Chen M, Nie H, Yuan Y. PD-1 and PD-L1 in cancer immunotherapy: clinical implications and future considerations. Hum Vaccin Immunother. United States; 2019;15:1111–22.

164. McAllister F, Bailey JM, Alsina J, Nirschl CJ, Sharma R, Fan H, et al. Oncogenic Kras activates a hematopoietic-to-epithelial IL-17 signaling axis in preinvasive pancreatic neoplasia. Cancer Cell. United States; 2014;25:621–37.

165. Huber M, Lohoff M. IRF4 at the crossroads of effector T-cell fate decision. Eur J Immunol. Germany; 2014;44:1886–95.

166. Rincón M, Anguita J, Nakamura T, Fikrig E, Flavell RA. Interleukin (IL)-6 directs the differentiation of IL-4-producing CD4+ T cells. J Exp Med. United States; 1997;185:461–9.

167. De Monte L, Reni M, Tassi E, Clavenna D, Papa I, Recalde H, et al. Intratumor T helper type 2 cell infiltrate correlates with cancer-associated fibroblast thymic stromal lymphopoietin production and reduced survival in pancreatic cancer. J Exp Med. United States; 2011;208:469–78.

168. Piro G, Simionato F, Carbone C, Frizziero M, Malleo G, Zanini S, et al. A circulating T(H)2 cytokines profile predicts survival in patients with resectable pancreatic adenocarcinoma. Oncoimmunology. United States; 2017;6:e1322242.

169. Brunetto E, De Monte L, Balzano G, Camisa B, Laino V, Riba M, et al. The IL-1/IL-1 receptor axis and tumor cell released inflammasome adaptor ASC are key regulators of TSLP secretion by cancer associated fibroblasts in pancreatic cancer. J Immunother Cancer. England; 2019;7:45.

170. Folkman J. Tumor angiogenesis: therapeutic implications. N Engl J Med. United States; 1971;285:1182–6.

171. Folkman J. What is the evidence that tumors are angiogenesis dependent? J Natl Cancer Inst. United States; 1990;82:4–6.

172. Baeriswyl V, Christofori G. The angiogenic switch in carcinogenesis. Semin Cancer Biol. England; 2009;19:329–37.

173. Bry M, Kivelä R, Leppänen V-M, Alitalo K. Vascular endothelial growth factor-B in physiology and disease. Physiol Rev. United States; 2014;94:779–94.

174. Li S, Xu H-X, Wu C-T, Wang W-Q, Jin W, Gao H-L, et al. Angiogenesis in pancreatic cancer: current research status and clinical implications. Angiogenesis. Germany; 2019;22:15–36.

175. Potente M, Gerhardt H, Carmeliet P. Basic and therapeutic aspects of angiogenesis. Cell. United States; 2011;146:873–87.

176. Mentzer SJ, Konerding MA. Intussusceptive angiogenesis: expansion and remodeling of microvascular networks. Angiogenesis. Germany; 2014;17:499–509.

177. Budde MD, Gold E, Jordan EK, Frank JA. Differential microstructure and physiology of brain and bone metastases in a rat breast cancer model by diffusion and dynamic contrast enhanced MRI. Clin Exp Metastasis. Netherlands; 2012;29:51–62.

178. Yang J, Zhu D-M, Zhou X-G, Yin N, Zhang Y, Zhang Z-X, et al. HIF-2α promotes the formation of vasculogenic mimicry in pancreatic cancer by regulating the binding of Twist1 to the VE-cadherin promoter. Oncotarget. United States; 2017;8:47801–15.

179. Błogowski W, Bodnarczuk T, Starzyńska T. Concise Review: Pancreatic Cancer and Bone Marrow-Derived Stem Cells. Stem Cells Transl Med. England; 2016;5:938–45.

180. Vizio B, Novarino A, Giacobino A, Cristiano C, Prati A, Brondino G, et al. Pilot study to relate clinical outcome in pancreatic carcinoma and angiogenic plasma factors/circulating mature/progenitor endothelial cells: Preliminary results. Cancer Sci. England; 2010;101:2448–54.

181. Barău A, Ruiz-Sauri A, Valencia G, Gómez-Mateo MDC, Sabater L, Ferrandez A, et al. High microvessel density in pancreatic ductal adenocarcinoma is associated with high grade. Virchows Arch. Germany; 2013;462:541–6.

182. Komar G, Kauhanen S, Liukko K, Seppänen M, Kajander S, Ovaska J, et al. Decreased blood flow with increased metabolic activity: a novel sign of pancreatic tumor aggressiveness. Clin Cancer Res. United States; 2009;15:5511–7.

183. Van Cutsem E, Vervenne WL, Bennouna J, Humblet Y, Gill S, Van Laethem J-L, et al. Phase III trial of bevacizumab in combination with gemcitabine and erlotinib in patients with metastatic pancreatic cancer. J Clin Oncol. United States; 2009;27:2231–7.

184. Pàez-Ribes M, Allen E, Hudock J, Takeda T, Okuyama H, Viñals F, et al. Antiangiogenic therapy elicits malignant progression of tumors to increased local invasion and distant metastasis. Cancer Cell. United States; 2009;15:220–31.

185. Gioelli N, Maione F, Camillo C, Ghitti M, Valdembri D, Morello N, et al. A rationally designed NRP1-independent superagonist SEMA3A mutant is an effective anticancer agent. Sci Transl Med. United States; 2018;10:eaah4807.

186. Caporali A, Martello A, Miscianinov V, Maselli D, Vono R, Spinetti G. Contribution of pericyte paracrine regulation of the endothelium to angiogenesis. Pharmacol Ther. England; 2017;171:56–64.

187. Huang Y, Yuan J, Righi E, Kamoun WS, Ancukiewicz M, Nezivar J, et al. Vascular normalizing doses of antiangiogenic treatment reprogram the immunosuppressive tumor microenvironment and enhance immunotherapy. Proc Natl Acad Sci U S A. United States; 2012;109:17561–6.

188. Jain RK. Normalization of tumor vasculature: an emerging concept in antiangiogenic therapy. Science. United States; 2005;307:58–62.

189. Annese T, Tamma R, Ruggieri S, Ribatti D. Angiogenesis in Pancreatic Cancer: Pre-Clinical and Clinical Studies. Cancers (Basel). Switzerland; 2019;11.

190. Maione F, Capano S, Regano D, Zentilin L, Giacca M, Casanovas O, et al. Semaphorin 3A overcomes cancer hypoxia and metastatic dissemination induced by antiangiogenic treatment in mice. J Clin Invest. United States; 2012;122:1832–48.

191. Maione F, Molla F, Meda C, Latini R, Zentilin L, Giacca M, et al. Semaphorin 3A is an endogenous angiogenesis inhibitor that blocks tumor growth and normalizes tumor vasculature in transgenic mouse models. J Clin Invest. United States; 2009;119:3356–72.

192. Tian L, Goldstein A, Wang H, Ching Lo H, Sun Kim I, Welte T, et al. Mutual regulation of tumour vessel normalization and immunostimulatory reprogramming. Nature. England; 2017;544:250–4.

193. Kolodkin AL, Matthes DJ, Goodman CS. The semaphorin genes encode a family of transmembrane and secreted growth cone guidance molecules. Cell. United States; 1993;75:1389–99.

194. Janssen BJC, Malinauskas T, Weir GA, Cader MZ, Siebold C, Jones EY. Neuropilins lock secreted semaphorins onto plexins in a ternary signaling complex. Nat Struct Mol Biol. United States; 2012;19:1293–9.

195. Wen H, Lei Y, Eun S-Y, Ting JP-Y. Plexin-A4-semaphorin 3A signaling is required for Toll-like receptor- and sepsis-induced cytokine storm. J Exp Med. United States; 2010;207:2943–57.

196. Bouvrée K, Brunet I, Del Toro R, Gordon E, Prahst C, Cristofaro B, et al. Semaphorin3A, Neuropilin-1, and PlexinA1 are required for lymphatic valve formation. Circ Res. United States; 2012;111:437–45.

197. Kolodkin AL, Levengood DV, Rowe EG, Tai YT, Giger RJ, Ginty DD. Neuropilin is a semaphorin III receptor. Cell. United States; 1997;90:753–62.

198. Winberg ML, Noordermeer JN, Tamagnone L, Comoglio PM, Spriggs MK, Tessier-Lavigne M, et al. Plexin A is a neuronal semaphorin receptor that controls axon guidance. Cell. United States; 1998;95:903–16.

199. Bismuth G, Boumsell L. Controlling the immune system through semaphorins. Sci STKE. United States; 2002;2002:re4.

200. Suzuki K, Kumanogoh A, Kikutani H. Semaphorins and their receptors in immune cell interactions. Nat Immunol. United States; 2008;9:17–23.

201. Bielenberg DR, Pettaway CA, Takashima S, Klagsbrun M. Neuropilins in neoplasms: expression, regulation, and function. Exp Cell Res. United States; 2006;312:584–93.

202. Fard D, Tamagnone L. Semaphorins in health and disease. Cytokine Growth Factor Rev. 2021;57:55–63.

203. Komina AV, Palkina NV, Aksenenko MB, Lavrentev SN, Moshev AV, Savchenko AA, et al. Semaphorin-5A downregulation is associated with enhanced migration and invasion of BRAF-positive melanoma cells under vemurafenib treatment in melanomas with heterogeneous BRAF status. Melanoma Res. England; 2019;29:544–8.

204. Valentini E, Di Martile M, Del Bufalo D, D'Aguanno S. SEMAPHORINS and their receptors: focus on the crosstalk between melanoma and hypoxia. J Exp Clin Cancer Res. England; 2021;40:131.

205. Gurrapu S, Tamagnone L. Semaphorins as Regulators of Phenotypic Plasticity and Functional Reprogramming of Cancer Cells. Trends Mol Med. England; 2019;25:303–14.

206. Hu S, Zhu L. Semaphorins and Their Receptors: From Axonal Guidance to Atherosclerosis. Front Physiol. Switzerland; 2018;9:1236.

207. Capparuccia L, Tamagnone L. Semaphorin signaling in cancer cells and in cells of the tumor microenvironment--two sides of a coin. J Cell Sci. England; 2009;122:1723–36.

208. Takegahara N, Kumanogoh A, Kikutani H. Semaphorins: a new class of immunoregulatory molecules. Philos Trans R Soc Lond B Biol Sci. England; 2005;360:1673–80.

209. Tordjman R, Lepelletier Y, Lemarchandel V, Cambot M, Gaulard P, Hermine O, et al. A neuronal receptor, neuropilin-1, is essential for the initiation of the primary immune response. Nat Immunol. United States; 2002;3:477–82.

210. Liu L-N, Li X-M, Ye D-Q, Pan H-F. Emerging role of semaphorin-3A in autoimmune diseases. Inflammopharmacology. Switzerland; 2018;26:655–65.

211. Lepelletier Y, Moura IC, Hadj-Slimane R, Renand A, Fiorentino S, Baude C, et al. Immunosuppressive role of semaphorin-3A on T cell proliferation is mediated by inhibition of actin cytoskeleton reorganization. Eur J Immunol. Germany; 2006;36:1782–93.

212. Kiseleva EP, Rutto KV. Semaphorin 3A in the Immune System: Twenty Years of Study. Biochemistry (Mosc). United States; 2022;87:640–57.

213. Guo H-F, Vander Kooi CW. Neuropilin Functions as an Essential Cell Surface Receptor. J Biol Chem. United States; 2015;290:29120–6.

214. Casazza A, Laoui D, Wenes M, Rizzolio S, Bassani N, Mambretti M, et al. Impeding Macrophage Entry into Hypoxic Tumor Areas by Sema3A/Nrp1 Signaling Blockade Inhibits Angiogenesis and Restores Antitumor Immunity. Cancer Cell. 2013;24:695–709.

215. Acevedo LM, Barillas S, Weis SM, Göthert JR, Cheresh DA. Semaphorin 3A suppresses VEGF-mediated angiogenesis yet acts as a vascular permeability factor. Blood. United States; 2008;111:2674–80.

216. Cerani A, Tetreault N, Menard C, Lapalme E, Patel C, Sitaras N, et al. Neuron-Derived Semaphorin 3A Is an Early Inducer of Vascular Permeability in Diabetic Retinopathy via Neuropilin-1. Cell Metabolism. 2013;18:505–18.

217. Teesalu T, Sugahara KN, Kotamraju VR, Ruoslahti E. C-end rule peptides mediate neuropilin-1-dependent cell, vascular, and tissue penetration. Proceedings of the National Academy of Sciences. 2009;106:16157–62.

218. Alessandrì L, Cordero F, Beccuti M, Arigoni M, Olivero M, Romano G, et al. rCASC: reproducible classification analysis of single-cell sequencing data. Gigascience. United States; 2019;8.

219. Hou W, Ji Z, Ji H, Hicks SC. A systematic evaluation of single-cell RNA-sequencing imputation methods. Genome Biol. England; 2020;21:218.

220. Liu Y, Zhang J, Wang S, Zeng X, Zhang W. Are dropout imputation methods for scRNA-seq effective for scATAC-seq data? Brief Bioinform. England; 2022;23:bbab442.

221. Hao Y, Hao S, Andersen-Nissen E, Mauck WM 3rd, Zheng S, Butler A, et al. Integrated analysis of multimodal single-cell data. Cell. United States; 2021;184:3573-3587.e29.

222. Gilles M-E, Maione F, Cossutta M, Carpentier G, Caruana L, Di Maria S, et al. Nucleolin Targeting Impairs the Progression of Pancreatic Cancer and Promotes the Normalization of Tumor Vasculature. Cancer Res. United States; 2016;76:7181–93.

223. Costes SV, Daelemans D, Cho EH, Dobbin Z, Pavlakis G, Lockett S. Automatic and quantitative measurement of protein-protein colocalization in live cells. Biophys J. United States; 2004;86:3993–4003.

224. Peng J, Sun B-F, Chen C-Y, Zhou J-Y, Chen Y-S, Chen H, et al. Single-cell RNA-seq highlights intra-tumoral heterogeneity and malignant progression in pancreatic ductal adenocarcinoma. Cell Res. England; 2019;29:725–38.

225. Chen Y, Kim J, Yang S, Wang H, Wu C-J, Sugimoto H, et al. Type I collagen deletion in αSMA(+) myofibroblasts augments immune suppression and accelerates progression of pancreatic cancer. Cancer Cell. United States; 2021;39:548-565.e6.

226. Wang Y, Liang Y, Xu H, Zhang X, Mao T, Cui J, et al. Single-cell analysis of pancreatic ductal adenocarcinoma identifies a novel fibroblast subtype associated with poor prognosis but better immunotherapy response. Cell Discov. England; 2021;7:36.

227. Dominguez CX, Müller S, Keerthivasan S, Koeppen H, Hung J, Gierke S, et al. Single-Cell RNA Sequencing Reveals Stromal Evolution into LRRC15(+) Myofibroblasts as a Determinant of Patient Response to Cancer Immunotherapy. Cancer Discov. United States; 2020;10:232–53.

228. Huang H, Wang Z, Zhang Y, Pradhan RN, Ganguly D, Chandra R, et al. Mesothelial cell-derived antigen-presenting cancer-associated fibroblasts induce expansion of regulatory T cells in pancreatic cancer. Cancer Cell. United States; 2022;40:656-673.e7.

229. Shinkawa T, Ohuchida K, Nakamura M. Heterogeneity of Cancer-Associated Fibroblasts and the Tumor Immune Microenvironment in Pancreatic Cancer. Cancers (Basel). Switzerland; 2022;14.

230. Krishnamurty AT, Shyer JA, Thai M, Gandham V, Buechler MB, Yang YA, et al. LRRC15(+) myofibroblasts dictate the stromal setpoint to suppress tumour immunity. Nature. England; 2022;611:148–54.

231. Ando R, Sakai A, Iida T, Kataoka K, Mizutani Y, Enomoto A. Good and Bad Stroma in Pancreatic Cancer: Relevance of Functional States of Cancer-Associated Fibroblasts. Cancers (Basel). Switzerland; 2022;14.

232. Mizutani Y, Kobayashi H, Iida T, Asai N, Masamune A, Hara A, et al. Meflin-Positive Cancer-Associated Fibroblasts Inhibit Pancreatic Carcinogenesis. Cancer Res. United States; 2019;79:5367–81.

233. Hoang DV, Thuy LTT, Hai H, Hieu VN, Kimura K, Oikawa D, et al. Cytoglobin attenuates pancreatic cancer growth via scavenging reactive oxygen species. Oncogenesis. United States; 2022;11:23.

234. Phillips PA, McCarroll JA, Park S, Wu M-J, Pirola R, Korsten M, et al. Rat pancreatic stellate cells secrete matrix metalloproteinases: implications for extracellular matrix turnover. Gut. England; 2003;52:275–82.

235. Miyai Y, Sugiyama D, Hase T, Asai N, Taki T, Nishida K, et al. Meflin-positive cancer-associated fibroblasts enhance tumor response to immune checkpoint blockade. Life Sci Alliance. United States; 2022;5.

236. Iida T, Mizutani Y, Esaki N, Ponik SM, Burkel BM, Weng L, et al. Pharmacologic conversion of cancer-associated fibroblasts from a protumor phenotype to an antitumor phenotype improves the sensitivity of pancreatic cancer to chemotherapeutics. Oncogene. England; 2022;41:2764–77.

237. Steele NG, Biffi G, Kemp SB, Zhang Y, Drouillard D, Syu L, et al. Inhibition of Hedgehog Signaling Alters Fibroblast Composition in Pancreatic Cancer. Clin Cancer Res. United States; 2021;27:2023–37.

238. Sharma GP, Kosuru R, Lakshmikanthan S, Zheng S, Chen Y, Burns R, et al. Endothelial Rap1B mediates T-cell exclusion to promote tumor growth: a novel mechanism underlying vascular immunosuppression. Angiogenesis. Germany; 2022;

239. Ponzo M, Debesset A, Cossutta M, Chalabi-Dchar M, Houppe C, Pilon C, et al. Nucleolin Therapeutic Targeting Decreases Pancreatic Cancer Immunosuppression. Cancers (Basel). Switzerland; 2022;14.

240. Bengsch F, Knoblock DM, Liu A, McAllister F, Beatty GL. CTLA-4/CD80 pathway regulates T cell infiltration into pancreatic cancer. Cancer Immunol Immunother. Germany; 2017;66:1609–17.

241. Kole C, Charalampakis N, Tsakatikas S, Frountzas M, Apostolou K, Schizas D. Immunotherapy in Combination with Well-Established Treatment Strategies in Pancreatic Cancer: Current Insights. Cancer Manag Res. New Zealand; 2022;14:1043–61.

242. Datta M, Coussens LM, Nishikawa H, Hodi FS, Jain RK. Reprogramming the Tumor Microenvironment to Improve Immunotherapy: Emerging Strategies and Combination Therapies. Am Soc Clin Oncol Educ Book. United States; 2019;39:165–74.

243. Beatty GL, Chiorean EG, Fishman MP, Saboury B, Teitelbaum UR, Sun W, et al. CD40 agonists alter tumor stroma and show efficacy against pancreatic carcinoma in mice and humans. Science. United States; 2011;331:1612–6.

244. Chen W-B, Lenschow W, Tiede K, Fischer JW, Kalthoff H, Ungefroren H. Smad4/DPC4-dependent regulation of biglycan gene expression by transforming growth factor-beta in pancreatic tumor cells. J Biol Chem. United States; 2002;277:36118–28.

245. Vacca A, Scavelli C, Serini G, Di Pietro G, Cirulli T, Merchionne F, et al. Loss of inhibitory semaphorin 3A (SEMA3A) autocrine loops in bone marrow endothelial cells of patients with multiple myeloma. Blood. United States; 2006;108:1661–7.

246. Almahariq M, Tsalkova T, Mei FC, Chen H, Zhou J, Sastry SK, et al. A novel EPAC-specific inhibitor suppresses pancreatic cancer cell migration and invasion. Mol Pharmacol. United States; 2013;83:122–8.

247. TRPM8 inhibits endothelial cell migration via a non-channel function by trapping the small GTPase Rap1. United States; 2017.

248. Kelly KA, Allport JR, Yu AM, Sinh S, Sage EH, Gerszten RE, et al. SPARC is a VCAM-1 counter-ligand that mediates leukocyte transmigration. J Leukoc Biol. England; 2007;81:748–56.

249. Yamamoto M, Suzuki K, Okuno T, Ogata T, Takegahara N, Takamatsu H, et al. Plexin-A4 negatively regulates T lymphocyte responses. Int Immunol. England; 2008;20:413–20.

250. Podojil JR, Chiang M-Y, Ifergan I, Copeland R, Liu LN, Maloveste S, et al. B7-H4 Modulates Regulatory CD4(+) T Cell Induction and Function via Ligation of a Semaphorin 3a/Plexin A4/Neuropilin-1 Complex. J Immunol. United States; 2018;201:897–907.

251. Celus W, Oliveira AI, Rivis S, Van Acker HH, Landeloos E, Serneels J, et al. Plexin-A4 Mediates Cytotoxic T-cell Trafficking and Exclusion in Cancer. Cancer Immunol Res. United States; 2022;10:126–41.

252. Liu L, Huang X, Shi F, Song J, Guo C, Yang J, et al. Combination therapy for pancreatic cancer: anti-PD-(L)1-based strategy. J Exp Clin Cancer Res. England; 2022;41:56.

253. Winograd R, Byrne KT, Evans RA, Odorizzi PM, Meyer ARL, Bajor DL, et al. Induction of T-cell Immunity Overcomes Complete Resistance to PD-1 and CTLA-4 Blockade and Improves Survival in Pancreatic Carcinoma. Cancer Immunol Res. United States; 2015;3:399–411.

254. Walunas TL, Lenschow DJ, Bakker CY, Linsley PS, Freeman GJ, Green JM, et al. CTLA-4 can function as a negative regulator of T cell activation. Immunity. United States; 1994;1:405–13.

255. Luheshi NM, Coates-Ulrichsen J, Harper J, Mullins S, Sulikowski MG, Martin P, et al. Transformation of the tumour microenvironment by a CD40 agonist antibody correlates with improved responses to PD-L1 blockade in a mouse orthotopic pancreatic tumour model. Oncotarget. United States; 2016;7:18508–20.

256. Van Audenaerde JR, Marcq E, von Scheidt B, Davey AS, Oliver AJ, De Waele J, et al. Novel combination immunotherapy for pancreatic cancer: potent anti-tumor effects with CD40 agonist and interleukin-15 treatment. Clin Transl Immunology. Australia; 2020;9:e1165.